Locus coeruleus modulates locomotor activity via the medial septum and the diagonal band of Broca

Dissertation

zur

Erlangung des Doktorgrades (Dr. rer. nat.)

der

Mathematisch-Naturwissenschaftlichen Fakultät

der

Rheinischen Friedrich-Wilhelms-Universität Bonn

vorgelegt von

Felix Ludwig

aus

Neuss

Bonn 2020

Angefertigt mit Genehmigung der Mathematisch-Naturwissenschaftlichen Fakultät der Rheinischen Friedrich-Wilhelms-Universität Bonn

1. Gutachter: Prof. Dr. Stefan Remy

2. Gutachter: Prof. Dr. Walter Witke

Tag der Promotion: 18.08.2020

Erscheinungsjahr: 2020

Acknowledgment

Firstly, I would like to express my sincere gratitude to my advisor Prof. Dr. Remy for the continuous support of my Ph.D. study. Besides my advisor, I would like to thank the rest of my thesis committee: Dr. Fuhrmann and Dr. Wittke, for their insightful comments and encouragement.

My sincere thanks also goes to Prof. Dr. Susanne Schoch-McGovern who provided me the viral vectors used in this thesis.

Thanks to my fellow labmates, especially Dr. Oliver Barnstedt and Dr. Liudmila Sosulina, who helped me a lot in the preparation of this dissertation. I thank the AG Remy and the AG Fuhrmann for the stimulating discussions, for the sleepless nights we were working together, and for all the fun we have had in the last years.

Last but not least, I would like to thank my family, especially my wife Svenja and our kids, for supporting me spiritually throughout writing this thesis and my life in general.

Abstract

The locus coeruleus (LC) is positioned in the brainstem and one of the main sources of norepinephrine in the brain. With its projections throughout the whole brain, the LC plays an important role in regulating the general level of arousal and in motivation. With the present study I have identified specific anatomical and functional connectivity patterns between the LC and cell populations in the medial septum diagonal band (MSDB). The direct activation of tyrosine hydroxylase positive neurons in LC has been shown to induce general locomotor arousal and changes in the hippocampal theta activity (Carter et al. 2010). It was shown, that the MSDB is integrated into locomotor activity and controls hippocampal locomotion dependent theta oscillation (Fuhrmann et al. 2015). In this study LC afferent fibers in the MSDB get activated optogenetically in order to investigate if noradrenergic input modulates MSDB activity and alters running behavior. Histology of Th-Cre mice with EYFP Injections in the LC confirms projections to the MSDB area. The results of this study indicate that optogenetic stimulation of noradrenergic locus coeruleus afferents in MSDB leads to increased running behavior in terms of running duration and running initiations but not velocity. Follow-up slice preparations of MSDB placed on a multi electrode array can be used to monitor spontaneous in-vivo like network and single unit activity. 15% of these units increase their firing when noradrenergic afferents are stimulated. Also, 30% of all recorded Units are theta modulated, but no effect on theta modulation could be observed. The two dimensional structure of the MEA allows to further distinguish between dorsal and ventral distributed unit populations within the MSDB. Differences in firing frequency and burst probability along the coronal section of the MSDB indicate a heterogeneous LC input with a majority of noradrenalin sensitive cells in the dorsal MS, rather than the DB.

Table of Contents

1 Introduction

1.1 Arousal and behavior

During the course of a day, all living organisms with a nervous system are confronted with varying situations across the spectrum of arousal. Greater degrees of generalized central nervous system (CNS) arousal result in greater responsiveness to sensory stimuli in all sensory modalities; increased motor activity; and higher emotional reactivity (Pfaff et al. 2008). From situations of extreme stress to phases of relaxation and regeneration, the brain adaptively modulates the resulting behavior in response to these arousal related changes. The most prominent system for modulating the level of arousal in the brain is the noradrenergic system (Totah et al. 2018). It encompasses a variety of central nuclei located in the brainstem, including one of the smallest nuclei in the brain, the locus coeruleus (LC) (Purves et al. 2012). Norepinephrine (NE; also known as noradrenaline)-containing axons originating from the LC are widely distributed throughout the CNS, suggesting a prominent role of this neurotransmitter in CNS function and behavior (Kandel et al. 2013).

The LC is closely connected to the ascending reticular activating system, a system of netlike clusters of neurons, scattered in the tegmental area of the brainstem (Purves et al. 2012). Its nuclei can be divided into two functional groups: those with modulatory functions and those with premotor functions. The LC, and serotonergic neurons of the raphe nuclei, form an antagonistic neuromodulatory system with long-range projections throughout the brain (Pudovkina et al. 2002). Its proposed purpose is to modulate the conscious state of the brain, including sleep and wakefulness. Also, pain modulation, cardiovascular control and habituation to repetitive stimuli are thought to be mediated by the nuclei of the reticular formation (Horn 2005).

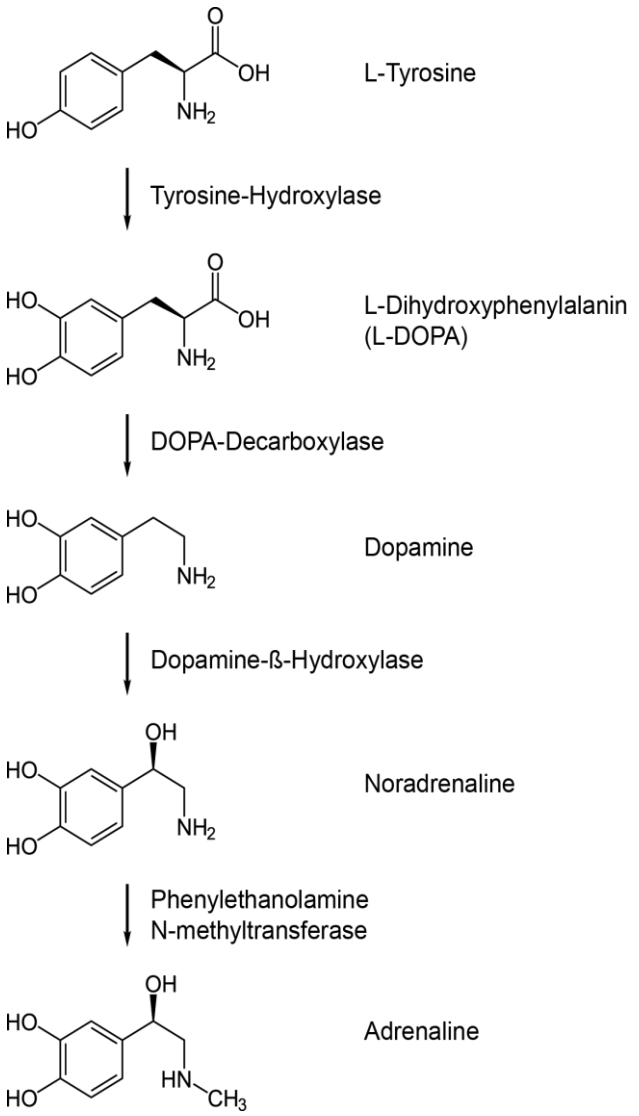

Figure 1 Catecholamine Synthesis
Biochemical pathway to produce dopamine, noradrenaline, and adrenaline.

Experiments using pharmacological modulation showed that LC and the noradrenergic system are involved in the regulation of global arousal. The central administration of noradrenergic antagonists caused substantial sedative effects (Sarro et al. 1987; Berridge and Morris 2000), whereas norepinephrine injected directly in the ventricles promoted wakefulness (Flicker and Geyer 1982; Segal and Mandell 1970). Also, direct optogenetic manipulations of LC with inhibitory opsins led to significant reductions in wake episodes, indicating that LC is necessary for maintaining normal durations of wakefulness (Carter et al. 2010). A direct activation of LC neurons using ChR2 resulted not only in an immediate sleep to wake transition, but also a significant increase in locomotor activity (Carter et al. 2010). Taken together, these results

suggest that the locus coeruleus is finely-tuned to influence wakefulness and behaviors such as locomotion.

1.2 The noradrenergic system

Discovered in the central nervous system by the swedish physiologist Ulf von Euler in the 1940s (Euler 1946), NE was one of the first neurotransmitters to be identified. Yet, only later experiments of Dahlström and Fuxe (1964) identified the LC as the main source of NE and one of the most extensively projecting nuclei in the brain. Although the nucleus is easy to identify in histological preparations by its unusual pigmentation, little was known about its composition until Falck and Hillarp (1959) developed an immunolabeling technique in 1964 that was specific to dopamine-ß-hydroxylase. Dopamine ß-hydroxylase is an enzyme responsible for converting dopamine to NE as part of the catecholamine biosynthesis. NE, in turn, gets further processed to epinephrine by the enzyme phenylethanolamine N-methyltransferase (Kandel et al. 2013). Immunolabeling dopamine-ß-hydroxylase allows for the precise detection of monoamines, including NE^+ neurons and their extensive axonal projections. The newly developed histological procedures by Falck and Hillarp initially supported the long-held assumption that the LC is a rather homogeneous structure, composed exclusively of NE+ neurons.

1.2.1 Locus coeruleus

The LC is a compact cluster of NE-containing neurons, located adjacent to the fourth ventricle in the pontine brainstem. It is composed of a small number of neurons: approximately 1600 in rodents, and 10,000–15,000 in human, which project broadly throughout the brain, from spinal cord to neocortex (Berridge and Waterhouse 2003). In contrast to early assumptions about the LC's cellular homogeneity, recent studies showed that the LC is a heterogeneous structure with cells of different sizes, projections, electrophysiological properties, and equipped with varying sets of membrane proteins and neurotransmitters (Uematsu et al. 2017).

At least two types of NE^+ cells have been observed within the LC: large multipolar cells (~35 µm) and smaller fusiform cells (~20 µm) (Grzanna and Molliver 1980). Although both cell types are spread throughout the LC, their distribution is biased. Multipolar cells are located more ventrally within the LC, whereas the smaller fusiform cells are located more dorsally (Swanson 1976).

Physiological recordings of the locus coeruleus demonstrated that neurons fire tonically from 1–3 Hz during wakefulness (Aston-Jones and Bloom 1981) as well as phasically in short bursts (500 ms) of 8–10 Hz during the presentation of salient stimuli (Foote et al. 1980). In line with its heterogeneous cell composition, discharge activity also varied substantially among LC neurons. Studies in anesthetized rats showed that simultaneously recorded pairs of LC neurons did not necessarily exhibit synchronized activity for either “tonic” spontaneous discharge or foot shock driven “phasic” discharge. Instead, subsets of neurons with similar efferent forebrain projections showed sparse and dynamically correlated activity over short periods. Studies suggest that gap junctions may be responsible for such ensemble activity (Aston-Jones and Cohen 2005). Depending on their projection areas, these electrophysiologically coupled LC neurons are capable of upregulating NE concentrations in some forebrain regions while simultaneously downregulating NE in other regions, over a timescale of 2 to 10 s (Totah et al. 2018).

In addition to morphological and electrophysiological differences, LC neurons differ in the types of neuropeptides they release as co-transmitters along with NE. The most abundant examples are galanin (Gal), which is expressed by up to 80% of LC neurons, and Neuropeptide Y (NPY, ~20% of all LC neurons) (Holets et al. 1988). The release of Gal and NPY in the brain modulates many behaviors, such as wake/sleep states, nociception, feeding, and parental behavior (Wu et al. 2014). The functional relevance of norepinephrine and neuropeptide co-release from LC neurons is virtually uncharacterized, as are the projections of NE^+/Gal^+ and NE^+/ NPY^+ axons throughout the brain. However, neuropeptide co-release could in principle modify the effect of NE release at specific output sites (Tsuda et al. 1989).

1.2.2 Functional properties of noradrenergic projections

Efferent projections of the LC exit the nucleus in three bundled pathways: The dorsal noradrenergic bundle, the cerebellar pathway and the descending pathway (Szabadi 2013). The dorsal bundle targets nuclei in the midbrain, thalamus and the entire limbic system, including the septal nuclei, the hippocampal system and the amygdala. Also, all cortical areas receive noradrenergic input via this ascending track (see Figure 2). The cerebellar pathway projects to the cerebellar cortex and the underlying nuclei. With a direct connection to motor nuclei in the brainstem and motor neurons in the spinal cord, the descending pathway provides direct noradrenergic modulation of locomotor behavior on an executive level (Goulding 2009).

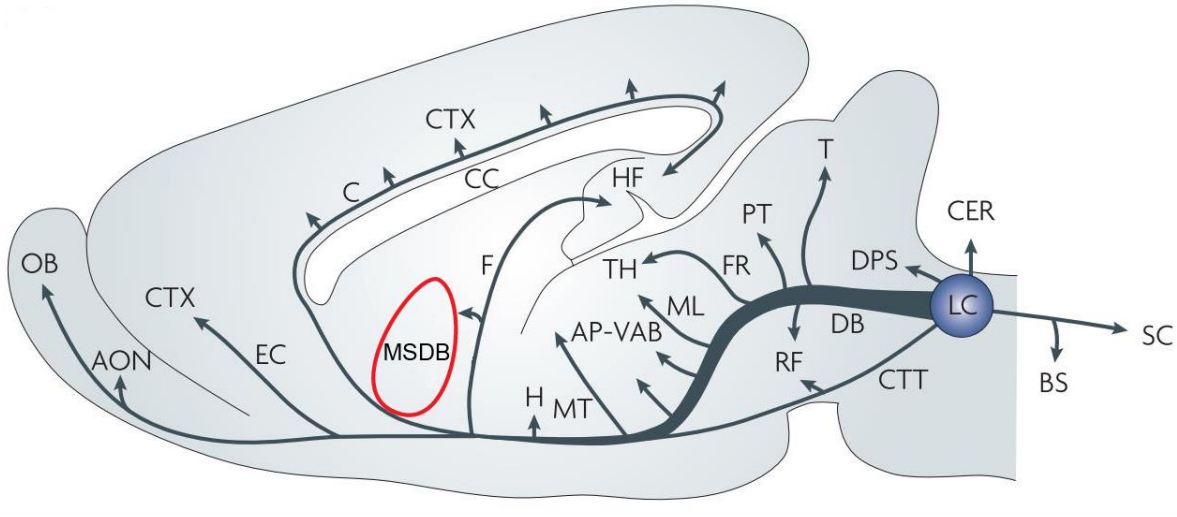

Figure 2 **LC projections**
Noradrenergic locus coeruleus (LC), with terminals in diverse remote brain regions, including the forebrain, the brainstem, the cerebellum, the entire cerebral cortex, including the frontal cortex and all sensory regions. The LC also sends projections to thalamic nuclei and the limbic system, including the amygdala, the hippocampus (HF) and the septal area (MSDB). The major output pathway of the MSDB region, the fornix, also carries noradrenergic projections towards the HF. The only major region that does not receive input from the LC is the area that contains the basal ganglia (modified from Sara (2009)).

The LC projects extensively to virtually all brain regions with the exception of the striatum. Yet it remains unclear how the LC, a small, seemingly homogeneous structure, responds to diverse sensory stimuli and modulates neuronal activity in distinct brain regions, with a variety of behavioral consequences. Early studies provided evidence for an efferent topography within the LC, suggesting a spatial organization of LC cells with respect to their terminal field targets (Mason and Fibiger 1979). LC neurons form small functional clusters and send axon collaterals to multiple targets that process the same sensory information (Schwarz et al. 2015). Because of their collateral projections, the discharge of LC neurons resulted in an almost simultaneous release of NE at two or possibly more sites along the ascending path. As a result of this anatomical differentiation, subsets of LC neurons could exert coordinating influences on distinct behavior in functionally related brain areas (Simpson et al. 1997).

In line with more recent studies on functional specializations of LC neuronal subgroups it was shown that also anatomical, molecular and physiological properties of distinct LC subgroups vary according to their terminal field projection (Chandler 2016). In addition, LC neuron populations respond differently according to the somatosensory input they are receiving, e.g. firing rates of LC neurons are heterogeneous and

patterned, in response to discrete and moderate cues, whereas more intense and aversive stimuli result in a unified co-activation of distinct cell populations with specific anatomical connectivity (Uematsu et al. 2017). The ability of LC neurons to switch between a global modulatory mode versus a targeted modulation of specific brain regions allows the LC to flexibly mediate general arousal as well as more precise control in response to dynamic situations requiring adaptive behavior (Uematsu et al. 2017). Mapping the LC neuron population with respect to their functional assignments revealed functionally distinct cell modules with specific anatomical connectivity. These functional connections can be traced back to intra-LC mechanisms such as gap junctions, recurrent collaterals, inhibitory feedback of released NE, or other effects. There could also be peri-LC interactions shown between extended LC dendrites and a pool of GABA neurons known to be located just outside the LC acting as an inhibitory interneuron population with regulatory influence on LC activity (Aston-Jones et al. 2004).

1.2.3 Adrenergic receptors

Similar to other neurotransmitter systems, NE acts at multiple receptors in target tissues. Traditionally, three noradrenergic receptor (AR) types with three subtypes each have been recognized: Three α_1 ARs (α_1a, α_1b, and α_1d), three α_2 ARs (α_2a, α_2b, and α_2c), and three ß ARs (ß1, ß2, and ß3) (Berridge and Waterhouse 2003). α_1 and ß receptors are thought to exist primarily at postsynaptic sites, whereas α_2 receptors exist both pre- and postsynaptically (Schwarz and Luo 2015). ARs are G protein–coupled receptors that signal through diverse downstream effector proteins to alter neurotransmission, cell excitability, and gene transcription.

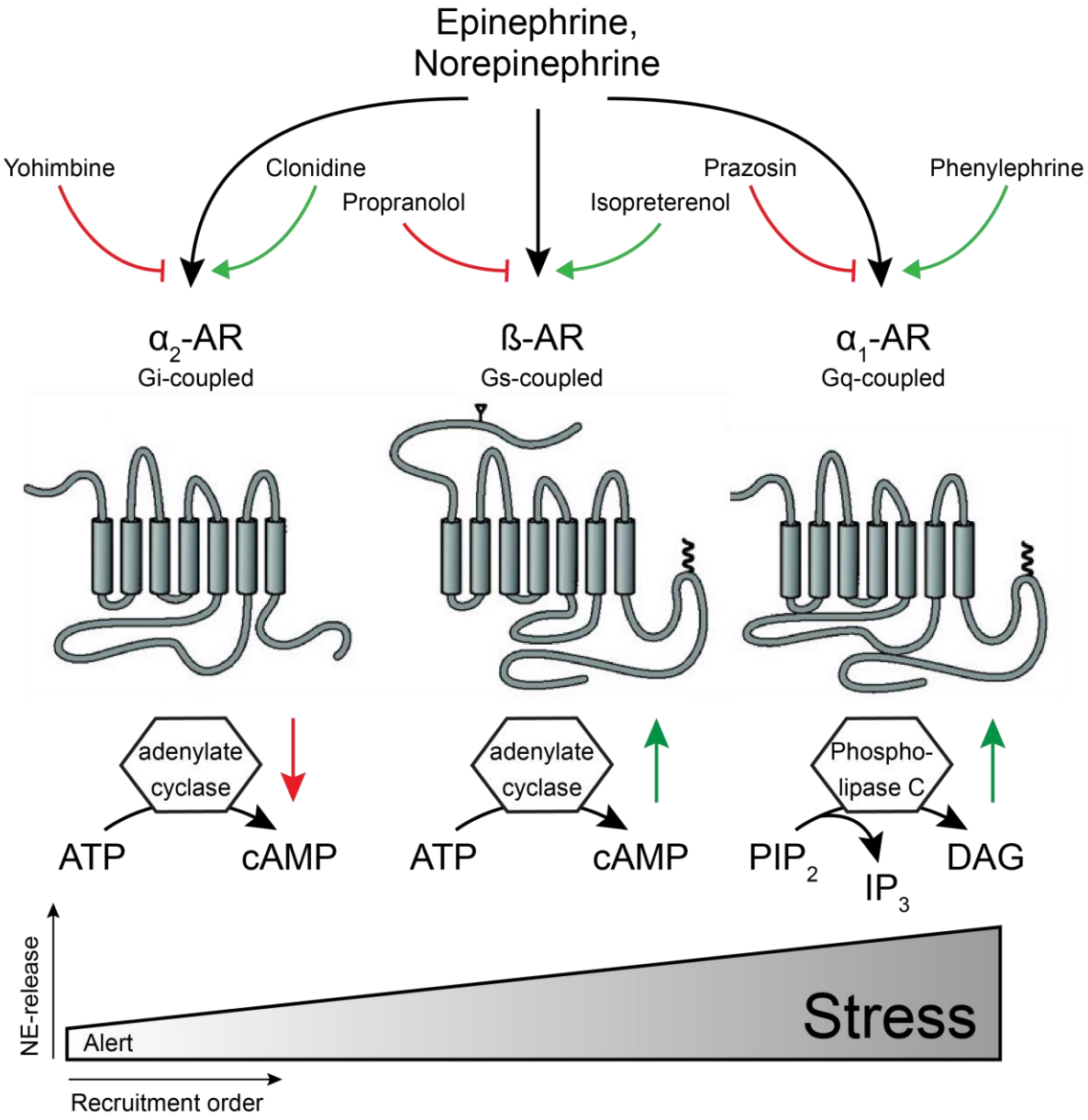

Figure 3 **Adrenergic receptors**
Protein Structure of α1, α2 and β adrenergic receptors and their G-protein coupling. Red arrows mark the most common pharmacological antagonists, while green arrows mark pharmacological agonists. The lower part shows the sequence of activation of ARs with increasing NE concentrations as a result of increased stress. (modified from Ramos and Arnsten (2007) and Dorn (2010)).

α_1 ARs are $G\alpha_q$ coupled, and their activation stimulates phospholipase C activity to cleave phosphatidylinositol 4,5-biphosphate (PIP_2) and increase inositol triphosphate (IP_3) and diacylglycerol (DAG), causing an increase of intracellular calcium and activation of protein kinase C (Schwarz and Luo 2015). ß ARs are typically $G\alpha_s$-coupled and activate protein kinase A (PKA) via stimulation of adenylate cyclase activity and cyclic adenosine monophosphate (cAMP) production (Schmidt and

Weinshenker 2014). In addition, ß ARs can switch coupling from $G\alpha_s$ to $G\alpha_i$ via PKA-mediated phosphorylation of the receptor, leading to a protein kinase pathway activation (Daaka et al. 1997). Since α_1 and ß receptors are located on the same cell, they interact through parallel actions on second messenger systems (e.g. IP_3 / DAG vs. cAMP), influencing the membrane potential, which ultimately results in an increase of excitability. α_2 ARs are $G\alpha_i$-coupled and function as inhibitory autoreceptors on noradrenergic neurons, although both pre- and postsynaptic α_2 AR heteroreceptors on NE target neurons are also abundant in the brain. Activation of these receptors decreases PKA activation by suppressing cAMP production by adenylate cyclase.

Noradrenergic receptors have different affinities for NE. Noradrenergic receptor family α_2 has the highest affinity to NE (K_D ~50 nM), followed by α1 ARs (K_D ~300 nM), and β ARs (K_D ~0.7–0.8 µM). The downstream effects of LC activity are dependent on the amount of NE release in any given behavioral situation. In situations of stress, such as during fight or flight, first α1 receptors are activated, followed by β ARs (see Figure 3). The focus of the overall brain activity allocation moves from areas responsible for higher cognitive processes to increased sensory performance and motor involvement (Ramos and Arnsten 2007; Atzori et al. 2016).

Table 1 Adrenergic receptor characteristics (adapted from Delaville et al. (2011))

Receptor subtype	G protein	Description	Effects
α1	G_q	● Postsynaptic ● Throughout the brain (incl. cortex, thalamus, basal forebrain)	● Excitability increased
α2	$G_{i/o}$	● Presynaptic ● On NAergic and non NAergic terminals	● Spontaneous firing and excitability increased ● Reduced neurotransmitter release
ß	G_s/G_i	● Postsynaptic in cerebellum, cortex, HC, midbrain, peripheral NS	● AC activation increases cAMP production ● LTP induction

The distribution and second messenger coupling of the receptor subtypes vary within and across brain regions. ß receptors appear to be more broadly distributed across neocortex laminae and are coupled to the G_s/cAMP second messenger system. α_1 and α_2 receptors, on the other hand, are concentrated in the superficial layers and are coupled to the PIP_2 and G_i/cAMP systems (Dohlman et al. 1991). Although NE is the most frequent neurotransmitter acting on adrenergic receptors, its processed form epinephrine actually activates α_1 receptors with the highest affinity (Morrow and

Creese 1986). Yet because epinephrine levels in the brain are very low (Mefford 1988), it is likely that NE mediates most of the effects associated with adrenergic receptor activation (although some evidence for epinephrine regulation of motor activity exists (Stone et al. 2003)). Adding to the complexity of LC action, LC-NE axons possess both, traditional synaptic release sites and volume / extra synaptic release sites that are not adjacent to postsynaptic junctions. The distance between a NE release site and a post-synaptic receptors likely has an impact on the response of this receptor to NE release (Zoli et al. 1998). Thus, variations in the spatial relationships between release sites and receptors may be one reason for functionally-specific, distinct patterns of LC discharge activity in different brain regions.

In line with its opposing physiological roles, a1 and α2 ARs also play antagonistic roles in the modulation of behavior. The blockade of α_1 receptors, for example, decreases the acute locomotor response to stimulants like amphetamines, whereas antagonizing α_2 receptors increases it. Studies have shown that α_1 adrenergic receptors antagonists such as prazosin, terazosin, and WB-4101 decrease drug-induced motor activity and behavioral sensitization, but do not impair basal activity (Snoddy and Tessel 1985; Alsene et al. 2010). On a single cell level the modulatory effect of NE affects information integration in a way that spontaneous firing rates of cells get suppressed to a greater extent than stimulus-evoked discharges, thus yielding a net increase in “signal to noise” ratio (Segal and Bloom 1976). Findings like this supported the idea that a prominent physiological function of central NE might be to enhance the efficacy of both excitatory and inhibitory synaptic transmission (Moises et al. 1983).

1.3 Projections from LC to the basal forebrain

Injecting radioisotopes into the LC, Pickel et al. (1974) discovered extensive projections to the forebrain, cerebellum, brainstem, and spinal cord. Additional studies indicate that noradrenergic efferents act within an extended region of the medial basal forebrain to modulate behavioral state (Berridge and Foote 1996; Berridge and Waterhouse 2003; Berridge et al. 2003). Thus, the basal forebrain (BF) belongs to an ascending arousal controlling system, along with the LC, the parabrachial nucleus, and the raphe nucleus.

The BF encompasses the general region of the medial septal area (MSA; including the medial septum, the diagonal band of Broca and the nucleus basalis) and the general region of the medial preoptic area (MPOA; including the medial preoptic area proper

and the medial preoptic nucleus). España and Berridge (2006) used Fluoro-Gold to retrogradely label NE cells according to their efferent projections. They revealed a topographical organization of MSDB efferents within the LC. Retrogradely labeled cells targeting MSDB were observed primarily ipsilaterally within the LC (83.9 ± 1.9% ipsilateral vs. 16.1 ± 1.9% contralateral). In rostrocaudal orientation, retrograde labeling was concentrated more to the rostral (38.4 ± 4.8%) and central portions (main body; 41.6 ± 3.3%) of the LC, whereas dorsoventrally, the most consistent and densest labeling was observed within the dorsal (45.4 ± 4.9%) and central thirds (33.3 ± 3.4%) of the LC (España and Berridge 2006). Across all NE^+ neurons targeting the MSDB that were retrogradely labeled in these studies, approximately 50% were located within the LC. Other noradrenergic nuclei, like the noradrenergic cell group A1/C1 provide substantially less input to the MSA (23.6%) (España and Berridge 2006).

1.3.1 Medial septum and diagonal band of Broca

In the center of the BF, the general region of the MSDB splits up into the medial septum, the vertical limb of the diagonal band of Broca, the islands of Calleja, and relatively small portions of the lateral preoptic area. This part of the BF receives extensive inputs from regions like the hypothalamus and the raphe nucleus and forwards integrated information to higher cognitive regions. Major output pathway is the dorsal fimbria fornix, targeting the hypothalamus in a feedback loop, as well as the habenular nuclei and, importantly, the hippocampal formation (HCF). The vertical limb of the diagonal band of Broca is extensively connected to the HCF and the cingulate cortex. Also, surrounding and ventral nuclei receive efferent projections from the MSDB, namely the lateral septum and the ventral tegmental area.

The BF contains three largely non-overlapping groups of neurons which can be distinguished based on their neurotransmitter phenotype i.e. cholinergic, GABAergic and glutamatergic neurons. Although cholinergic neurons represent a minority of BF neurons (10–20%, depending on the subregion) (Zaborszky et al. 2012), they have been largely in the center of research because of their broad projections to the hippocampus, synapsing onto pyramidal cells, dentate granule cells, and inhibitory interneurons. Cholinergic neurons can be identified via their characteristic synthesis enzyme choline acetyltransferase (ChAT) and connect within the medial septum to GABAergic interneurons. GABAergic interneurons represent the numerically largest group of basal forebrain neurons and can be divided into several subgroups. Stereological estimates in rats suggest there are ~5 times more GABAergic than

cholinergic neurons (Gritti et al. 2006). Most are small or medium-sized (<20 µm) neurons but ~12% are large-sized (>20 µm) projection neurons (McKenna et al. 2013). Those particularly large and parvalbumin (PV)-expressing GABAergic neurons make up only 7% of all GABAergic neurons in the basal forebrain (McKenna et al. 2013). Nevertheless, they are functionally important in controlling cortical local field potential (LFP) oscillations. Glutamatergic neurons represent the smallest of the three major groups of BF neurons. Most contain the vesicular glutamate transporter, subtype 2 (VGluT2). VGluT2$^+$ neurons comprise ~5% of cortically projecting neurons in the BF (Hur and Zaborszky 2005). Tracing experiments suggest that BF VGluT2$^+$ neurons have relatively weak projections to cortex but within the MS glutamatergic neurons provide prominent excitatory inputs to a majority of local GABAergic and a minority of septal cholinergic neurons (Hur and Zaborszky 2005).

1.3.2 Afferents to hippocampus and theta modulation during movement

The hippocampal formation is one of the central brain regions involved in memory processing, navigation and integrating sensory information. Consisting of the hippocampus proper, the adjacent subiculum and the entorhinal cortex, the hippocampal formation has been the focus of several studies investigating the pathogenesis of degenerative diseases like Alzheimer's and Parkinson's disease (Trillo et al. 2013). These diseases go along with disorientation and locomotor deficits. One characteristic trait of the hippocampus are rhythmic oscillations in the LFP (Buzsáki 1986). EEG measurements show such activity during locomotor behavior and goal orientated manipulations of the environment. Theta band oscillations (4-12 Hz) can be observed during REM sleep. These oscillations represent a brain state specialized for processing navigation-related input (Buzsáki 2002). The MSDB was identified to serve as a pacemaker for theta rhythmicity in the hippocampus (Meibach and Siegel 1977; Holsheimer et al. 1982; Buzsáki et al. 1983). The pharmacological inactivation of the MSDB leads to an elimination of theta rhythmicity in hippocampal LFP (McNaughton et al. 2006).

All three main cell types of the septal formation – GABAergic (Köhler et al. 1984), cholinergic (Lewis and Shute 1967), and glutamatergic neurons (Sotty et al. 2003) – project to the hippocampus, but recent studies have highlighted the role of glutamatergic neurons in particular. With only 2.6 ± 0.2% the number of MSDB glutamatergic neurons projecting to the hippocampus is comparatively low (Robinson et al. 2016). However, it was observed that optogenetic activation of MSDB VGluT2$^+$ neurons was able to drive endogenous hippocampal theta rhythm (Fuhrmann et al.

2015), whereas stimulation of fibers projecting directly to the hippocampus through the fornix had no effect on hippocampal rhythmicity. These results showed that glutamatergic neurons can drive rhythms through intraseptal connections, activating both GABAergic and cholinergic neurons, which in turn modulate hippocampal network activity (Robinson et al. 2016).

Fuhrmann et al. (2015) showed in experiments on voluntary movement, that the septo-hippocampal network is involved in modulating locomotion speed. In doing so, interneurons in the hippocampal formation integrate speed dependent input from septal VGluT2+ neurons. Fulfilling both tasks, driving hippocampal theta and forwarding speed information, septal VGluT2+ neurons couple locomotor behavior and speed dependent theta modulation. Theta oscillations in the hippocampus and activity of VGluT2+ and PV+ neurons in MSDB can even be used to predict locomotor behavior (Hannes 2017). Several hundred milliseconds before onset of locomotion the activity of VGluT2+ and PV+ neurons in MSDB and theta oscillations in the hippocampal field potential increase, lending another piece of evidence for the functional connection between MSDB controlled theta and locomotor behavior.

1.3.3 Modulating efferents from locus coeruleus towards the MSDB

Noradrenergic efferents influence behavioral and EEG activity states within an extended region of the medial BF encompassing the MSA and the MPOA through actions at ß and/or α_1 ARs. In the MSDB, NE released from LC axonal projections exerts wake-promoting actions (Berridge and Waterhouse 2003). The release of norepinephrine from LC terminals in the BF simultaneously activates cholinergic neurons that express α_1 and ß ARs (Berridge et al. 2003), and inhibits GABAergic neurons, which express α_2 ARs (Manns et al. 2003). In this way, LC activation modulates both cholinergic and GABAergic neurons in opposing manners, ultimately promoting arousal.

1.4 Central hypothesis

The LC is the center of a widespread modulatory network with projections into nearly all brain regions. These projections are capable of influencing the general activity in functionally connected regions as well as modulating the single unit firing properties in specific nuclei. With efferents to behaviorally relevant regions like the MSDB, the LC influences the integration of sensory information and the modulation of behavioral responses to given situations. However, the remaining question in the understanding

of the LC-NE system is how its organization, diversity of firing modes, and variety of projections all generate different behavioral outcomes. The MSDB and its projections to the HCF are a modulatory system for distinct behavioral patterns itself (Anaclet et al. 2015; Zant et al. 2016; Herman et al. 2016). Inhibitory GABAergic and excitatory cholinergic neurons projecting to Cornu ammonis region 1 (CA1) hippocampal pyramidal neurons set the pace for oscillatory theta LFP in the HCF (Buzsáki 2002). In addition, glutamatergic neurons in the MS modulate HCF activity in a speed-dependent manner (Fuhrmann et al. 2015). Activating this MSDB-HC microcircuit optogenetically even induces locomotion, indicating not only a modulatory, but also an active role in the generation of behavior (Fuhrmann et al. 2015).

The central hypothesis of this study builds up on findings by Carter et al. (2010) who found that the direct optogenetic stimulation of LC results in increased locomotor behavior. In addition, I refer to the studies of Berridge and Waterhouse (2003), where pharmacological modulation of the MSDB triggers sleep to wake transition and movement. Together with the newly discovered role of glutamatergic neurons in MSDB on modulating running speed (Fuhrmann et al. 2015), this thesis is investigating the influence of LC on locomotor behavior, executed via long range MSDB projections. I hypothesize that this functional connection is sufficient to evoke locomotor behavior in mice. The response of the MSDB neuronal network was thus investigated on three levels:

1. Intact, physiological network responses recorded in vivo.
2. Extracellular recordings from functional networks in acute brain slice preparations.
3. Single cell observations using current clamp recordings in vitro.

On all three levels, the systems were treated with pharmacological modulatory drugs to investigate if the effects on locomotor behavior are caused by the local release of NE from LC axon terminals.

2 Methods

2.1 Transgenic mouse lines

All *in vivo* experiments and microelectrode array (MEA) recordings were conducted with the genetically modified mouse line B6.Cg-7630403G23Rik$^{Tg(Th\text{-}cre)1Tmd}$/J (in short, TH1-Cre), purchased at Jackson laboratory (Stock No: 008601). TH1-Cre mice express the protein cre-recombinase under the tyrosine hydroxylase 1 promotor. Tyrosine hydroxylase is an enzyme catalyzing the conversion of the amino acid L-tyrosine to L-DOPA in the catecholamine biosynthesis (). The TH1-Cre mouse line was used to target exclusively catecholaminergic neurons and study noradrenergic cell function.

For patch clamp experiments, Slc17a6 tm2(cre)Lowl /J (in short, VGluT2-Cre) mice, purchased at Jackson laboratory (Stock No: 016963) were used. In these mice, cre recombinase is expressed under the promoter of the sodium-dependent inorganic phosphate cotransporter member 6. The VGluT2-Cre mouse line was used to label glutamatergic neurons in MSDB with red fluorescent tdTomato.

Mice of both sexes aged between 8 and 15 weeks were used. All mice were group-housed with a 12 h day-night light cycle at 21 °C, with food and water provided ad libitum. All experiments have been previously approved by local authorities, covered by the animal protocol 81-02.04.2017 A426.

2.2 Viral vectors

In order to express ChR2 in noradrenergic neurons the Cre-Lox recombination system was used (McLellan et al. 2017; Sternberg and Hamilton 1981; McLellan et al. 2017). This system combines the cell specificity of genetically modified mouse lines with the transfection system of adeno-associated virus (AAV) type 2. All AAVs are non-pathogenic for humans. Combined with precise stereotactic injection, it is possible to target a specific cell population in a confined area to express a cargo protein of choice.

In this case, channelrhodopsin 2 (ChR2) (Nagel et al. 2003) was exclusively expressed in noradrenergic cells of the locus coeruleus (LC). The AAV carries a single stranded DNA vector coding for the protein structure of ChR2 and a fluorescent tag (enhanced yellow fluorescent protein, EYFP) flanked by designated cleaving sites (loxP sites). The coding sequence for the cargo protein is inverted, preventing the vector from

being translated. In the target cells expressing the Cre-recombinase, the enzyme cuts at both loxP sites, and a second protein, the DNA ligase, rejoins the fragmented vector in an inverted orientation. In this way, the open reading frame is corrected, enabling the cargo protein to be transcribed. The expression in the target cells is driven by an EF1a-Promotor and a posttranscriptional protein (WPRE) to enhance and prolong protein expression. The virus was kindly provided by Dr. Susanne Schoch (see Figure 4).

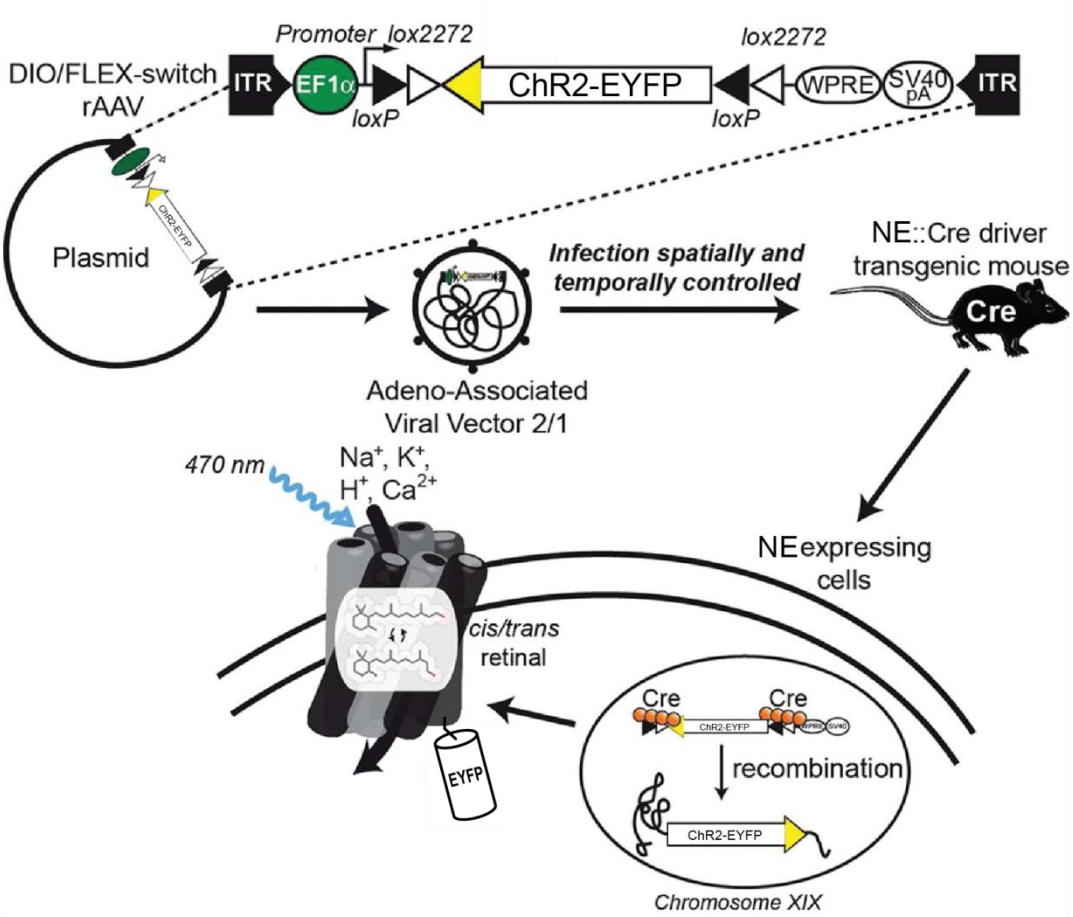

Figure 4 **Cre-Lox-P viral delivery system**
Structure of viral vector carrying ChR2-EYFP construct and Cre-dependent expression in NE-Cre driver mouse line. Modified from Urban et al. (2012).

2.3 Surgeries

Mice were anesthetized by intraperitoneal injection of ketamine (0.13 mg/g body weight) and xylazine (0.01 mg/g body weight). In addition, buprenorphine (0.05 µg/g body weight), carprofen (5 µg/g body weight) and cefotaxime (0.2 µg/g body weight) were administered to prevent the mouse from experiencing pain or developing inflammations. In the case of incomplete anesthesia, additional anesthetics with up to

50 % dose were given. Surgeries were performed once animals turned unresponsive to stimuli such as tail pinch. Mice were placed on a heat pad to maintain body temperature, and fixed in a stereotactic frame (MA-6N, Narishige, Tokyo, Japan) including ear bars and a nose clamp. After the surgery, additional buprenorphine (0.05 µg/g body weight) was administered three times a day for three consecutive days.

2.4 Stereotactic injections

In order to express ChR2 in noradrenergic cells, an AAV was stereotactically bilaterally injected into LC. After anesthetizing the animal and fixing it in the stereotactic frame, the skin on top of the skull was opened. To adjust the injection setup, the skull was moved in a horizontal position with bregma and lambda on the same horizontal plane. The precision infusion cannula (34G cannula Hamilton syringe, World Precision instruments, Berlin, Germany) was zeroed on lambda by finding the crossing of visualized lines that most closely approximate the sutures in situ. Following the stereotactic coordinates taken from the mouse atlas (-800 µm rostral-caudal; ±800 µm bilateral; -3200 µm dorsal-ventral ; Franklin & Paxinos "The mouse Brain in stereotaxic coordinates, Third Edition, Academic Press), the cannula was carefully guided to the injection site.

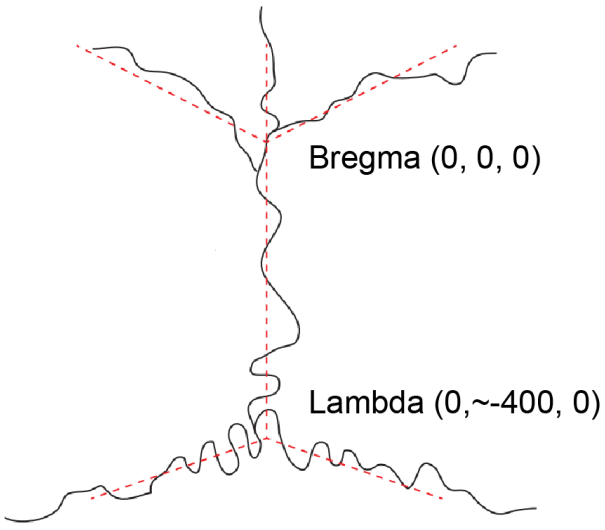

Figure 5 **Mouse skull sutures**
Identification of bregma and lambda by extending the skull sutures.

A small hole covering the diameter of the cannula, was drilled into the skull using a dental drill (Drill, Foredom Electric), and the injection needle was slowly forwarded to its final position. Using an UltraMicroPump (World Precision Instruments, Germany), 1 µl of virus at a rate of 0.1 µl/min were injected into the tissue, followed by a 10 min pause to let the virus diffuse into the tissue before removing the needle. The craniotomy was sealed with dental acrylic (Cyano-Veneer fast; Heinrich Schein Dental

Depot, Munich, Germany) and the skin was sewed with absorbable sutures (Vicryl Plus, Johnson & Johnson Medical GmbH, Norderstedt, Germany).

2.5 Hybrid fiber and LFP electrode placement

After four weeks a hybrid optic and fluid cannula (OFC 400/430- 0.37 5 mm SM3 FLT ST166 0.1 mm, Doric Lenses, Quebec, Canada) was implanted right above the MSDB in a second surgery (see Figure 6). The preparations correspond to those in the stereotactic injection. In addition LFP electrodes were placed in the CA1 layer of the hippocampus bilaterally.

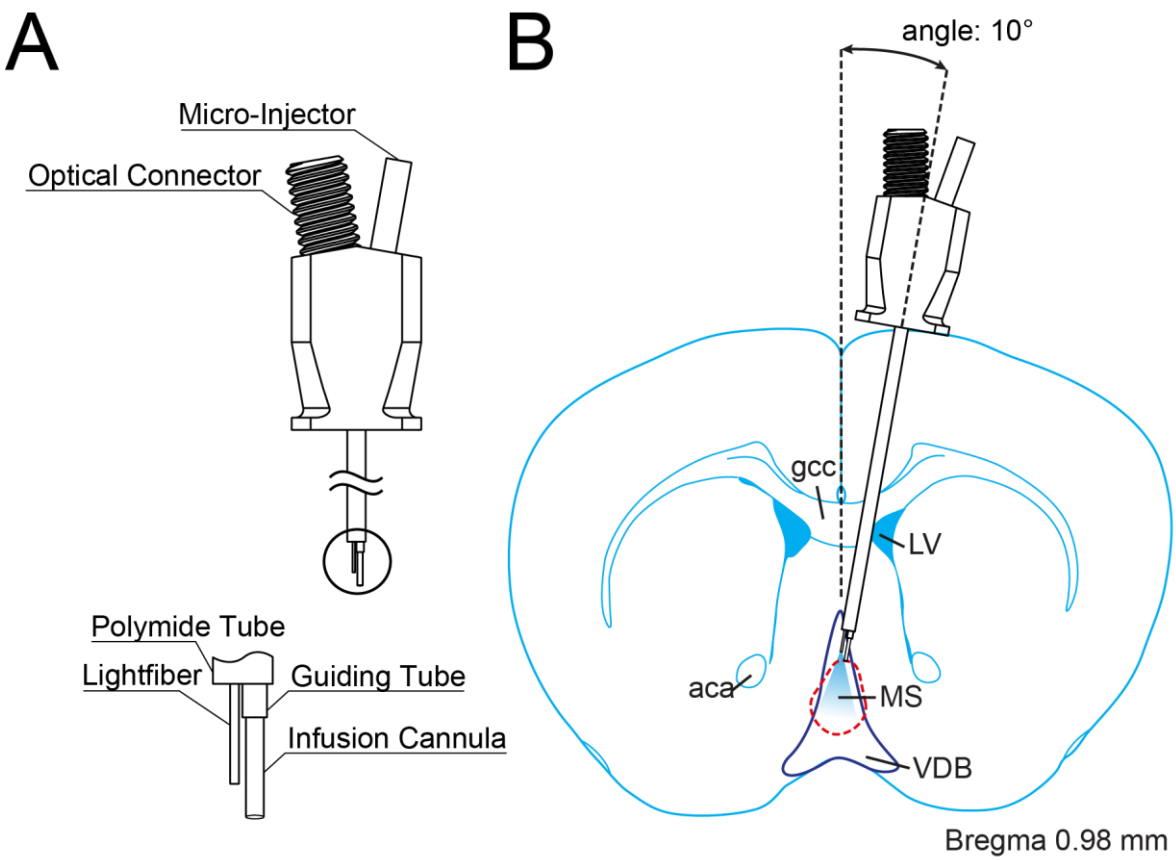

Figure 6 **Scheme of hybrid fiber placement in the MSDB**
A. Hybrid fiber consisting of a light fiber coupled to a 473nm laser and an infusion cannula connected to an infusion syringe. **B.** The hybrid fiber is placed with a 10° angle above the MSDB.

Anesthesia and preparation of the mice were performed similarly to the stereotactic injection. In order to achieve a clean surgical field, the scalp and the periosteum were removed. A solid basis was created by treating the skull bone with phosphoric acid (Phosphoric Acid Gel Etchant 37.5%, Kerr Italia, Italy), and covering it with a volatile primer solution (OptiBond FL Prime, Kerr Italia, Italy) and adhesive glue (OptiBond FL

Adhesive, Kerr Italia, Italy). Once the glue was cured with UV light, a craniotomy was added above the MSDB and the hybrid fiber was pushed slowly to its final position above the MSDB. To prevent damage to large blood vessels, the MSDB was approached from a 10° medial-lateral angle (+1000 µm rostral-caudal; +750 µm lateral; -4400 µm dorsal-ventral). Two more craniotomies were added bilaterally above the HC CA1 region (+2300 µm rostral-caudal; +2000 µm lateral; -1200 µm dorsal-ventral) and monopolar LFP tungsten electrodes (W558511, Advent Research Materials, Oxford, England) were inserted. A ground and a reference electrode were added in the cerebellar region. The tungsten wires and a metal bar for the head fixation were fixed with a light-curable composite (Gradia Direct Flo, GC Corporation, Japan) onto the skull (see Figure 7). After the surgery, the analgesic buprenorphine (0.05 mg/kg) was administered three times daily for three days according to the animal protocol.

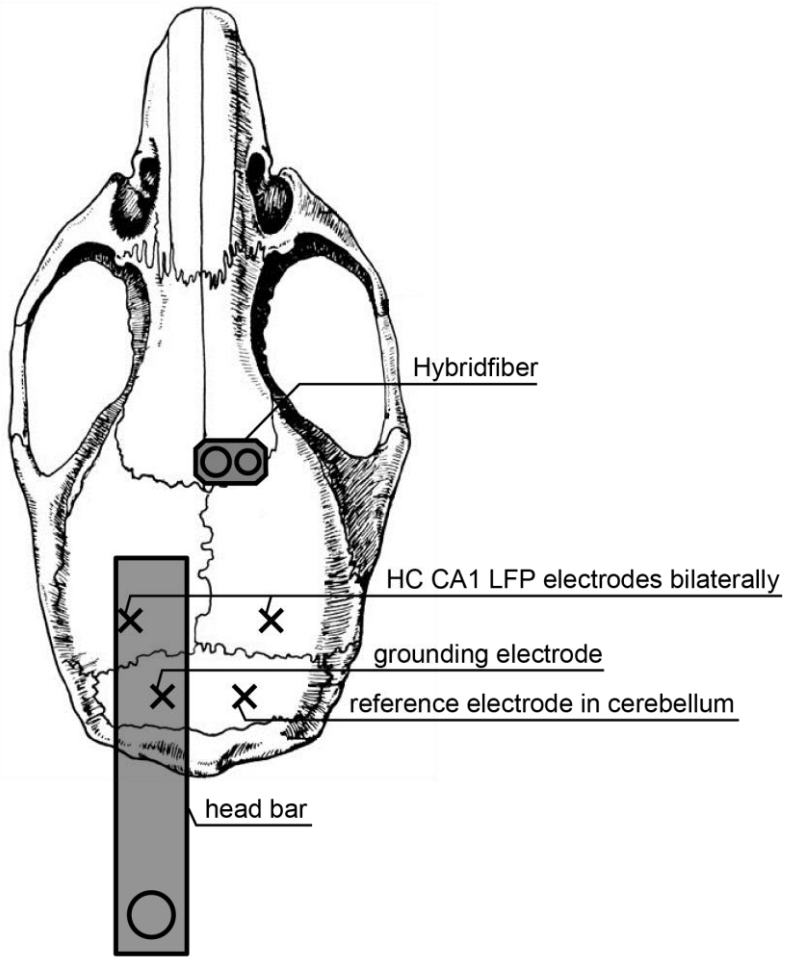

Figure 7 Mouse skull with hybrid fiber, LFP electrode and head bar positioning.
A hybrid fiber, including a light fiber and an infusion cannula, was implanted in close proximity to the MSDB. Two LFP electrodes were implanted in layer CA1 of the hippocampus bilaterally. A reference electrode was placed in the cerebellum and the grounding electrode in the CF.

2.6 Treadmill

For *in vivo* experiments a custom built linear treadmill was used with a 7 cm wide and 2 m long belt placed in a dark and noise-reduced environment built from Luigs & Neumann elements (Luigs & Neumann, Ratingen, Germany). The position of mice on the linear treadmill was tracked via an optical computer mouse, measuring the rotation of the treadmill cylinder. The mice were head fixed with a screw fixing the metal head bar with an adjustable arm above the belt. Light fiber, infusion cannula and LFP wiring were connected accordingly. Hippocampal field potentials were recorded at 10 kHz through an EXT-02F extracellular amplifier (NPI, Germany) and an ITC-18 board (NPI, Germany), operated with Igor Pro software (Wavemetrics, Oregon, USA). Electrical signals were filtered with a 3 Hz high-pass and a 500 Hz low-pass filter. Amplitudes were amplified 500-fold. Every mouse was habituated to physical handling by the experimenter and head restraining on the setup starting one week prior to experiments. All mice showed voluntary running behavior on the treadmill.

2.7 Optogenetic stimulation

Light stimulation was performed with a 473 nm diode laser (LuxX 473-80, Omicron-Laserage, Rodgau-Dudenhofen, Germany) coupled to the implanted fiber-optic cannula with a fiber-optic cord (MFP 400/430/1100-0.37 1m FC-CM3(P), Doric Lenses, Quebec, Canada). The light intensity was adjusted to 20 mW at the tip of the light fiber. During experiments, a 10 min light stimulation pattern was used in 6 repetitions, alternating 5 min phases of 3 Hz and 3 ms Light pulses with 5 min of no stimulation (see Figure 8). In experiments including drug application, the light stimulation phases alternated with phases of drug infusion. As light stimulation control, a fiber-coupled 561 nm laser (OBIS 561 LS, Coherent, Santa Clara, USA) was used.

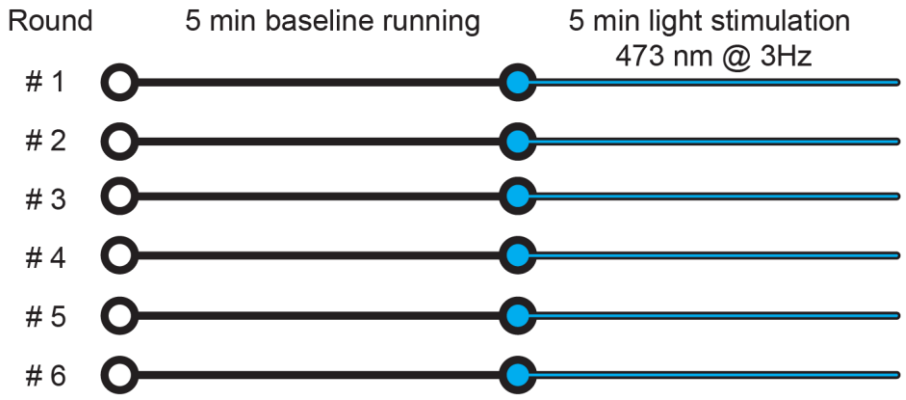

Figure 8 **Light stimulation scheme for in vivo experiments on the linear treadmill**
Light stimulation scheme with 6 consecutive trials consisting of 5 minutes baseline recording followed by 5 minute 3 Hz light simulation with 473nm.

2.8 Pharmacology

The hybrid fiber infusion cannula was used to apply noradrenergic agonists and antagonists as well as ACSF for sham applications (see Table 2).The basal forebrain, including the MSDB area, receives extensive input from the LC. NE released from noradrenergic axon terminals activated wakefulness-promoting cholinergic neurons, via the stimulation of excitatory α_1 and β ARs (Berridge and Waterhouse 2003), whereas it suppressed the activity of sleep-promoting GABAergic neurons, via the stimulation of inhibitory α_2 ARs (Manns et al. 2003). In order to suppress the NE input, prazosin and propranolol were applied to block α_1 and ß AR activity. Clonidine, an α_2 receptor agonist was applied in order to achieve presynaptic inhibition via α_2 action on presynaptic receptors. All chemicals were purchased at Tocris Bioscience, Bristol UK and dissolved in ACSF.

Table 2 NE agonists and antagonists used in in vivo linear treadmill experiments

Drug	Effect	Conc.	Reference	Vendor
Prazosin	α_1 antagonist	2 µM	(Pudovkina and Westerink 2005)	Tocris Cat. No. 0624
Clonidine	α_2 agonist	10 µM	(Saad et al. 2002)	Tocris Cat. No. 0690
Propranolol	ß antagonist	10 µM	(Scotti et al. 2011)	Tocris Cat. No. 0624

In vivo infusion rate was 0.1 µl/s (0.5 µl in total), controlled by an UltraMicroPump (World Precision Instruments, Germany). The administration followed an alternating scheme with the light stimulation (see Figure 9).

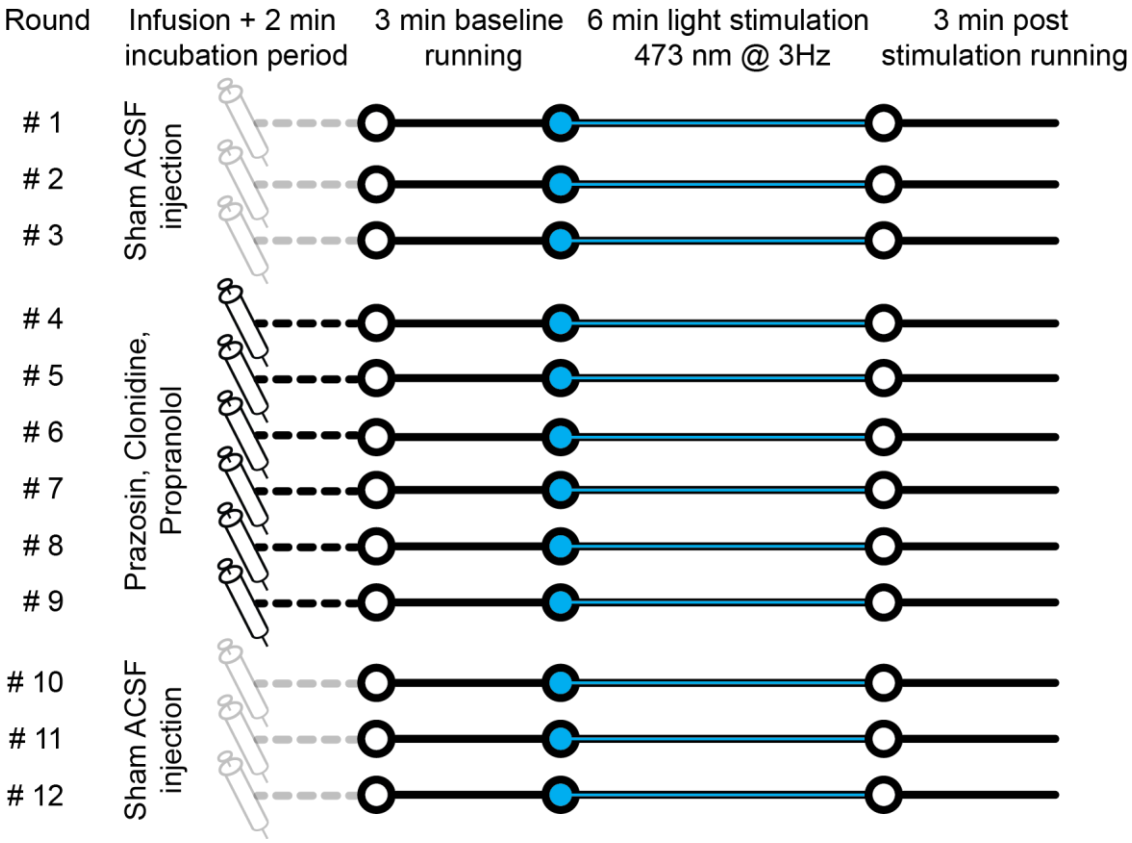

Figure 9 **Infusion scheme for in vivo treadmill experiments.**
For the experiment, a mouse was head fixed on a linear treadmill with an implanted hybrid fiber consisting of a light fiber and an infusion cannula. For three rounds, ACSF was administered as a sham control, then baseline running was recorded for 3 minutes, followed by a 6 minute period of light stimulation and again 3 minutes without stimulation. Prior to round 4, NE agonists and antagonists were administered, followed by a 2 minute incubation period. Then, baseline running and running with light stimulation was recorded as before. In total, 6 rounds of drug application were performed. Round 10 to 12 follow the initial scheme with ACSF sham infusion.

2.9 Slice preparation and storage in interface chamber

Mice were deeply anesthetized with isoflurane to a depth at which no reaction to painful stimuli such as tail pinch could be observed. After decapitation, the brain was removed quickly and sliced in coronal slices (500 µm) containing the MSDB. For slicing, a Leica VT-1200S vibratome (Leica Microsystems, Wetzlar, Germany) filled with ice-cold sucrose solution containing (mM): 60 NaCl, 100 sucrose, 2.5 KCl, 1.25 NaH_2PO_4, 26 $NaHCO_3$, 1 $CaCl_2$, 5 $MgCl_2$, 20 glucose, oxygenated with 95% O_2 and 5% CO_2 was used. After cutting, the slices were transferred to an interface chamber (Brain Slice Chamber System with Haas Top, Warner Instruments, Hamden USA; (Haas et al. 1979)) containing warm artificial cerebrospinal fluid (ACSF) for recovery (mM): 119 NaCl, 2.5 KCl, 1.3 $MgCl_2$, 2.5 $CaCl_2$, 10 glucose, 1.0 NaH_2PO_4, 26 $NaHCO_3$, gassed with carbogen (95% O_2 / 5% CO_2; pH 7.4 at 37 °C; 290–310 mosmol/l). The interface chamber provided the slices with optimal oxygenation by creating a laminar flow of pre heated ACSF above and underneath the slices.

2.10 Microelectrode array

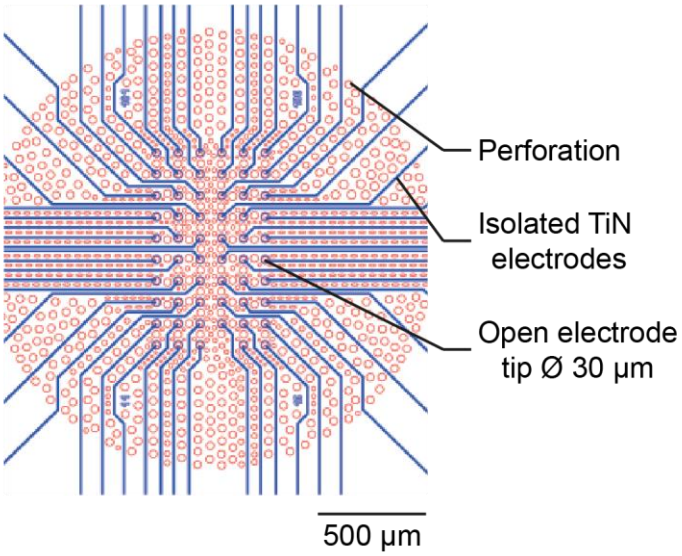

Figure 10 Multielectrode array
Blue lines depict the isolated TiN electrodes, each ending in a recording site with an open tip. The perforation is shown in orange.

For extracellular in vitro slice recordings a MEA 2100-60-System (MultiChannel-Systems, Reutlingen, Germany) including an Interface Board 3.0 multiboard was used. The head stage was equipped with a perfusion element to be used with perforated MEA-chips. For the recordings 60pMEA100/30iR-Ti with TiN electrodes were used. The 60 electrodes are arranged in a 6x10 grid, with an electrode spacing of 100 µm and an electrode diameter of 30 µm (see Figure 10). ACSF temperature was controlled and set to 35 °C with a PH01-inline heating element and the TC01 controlling unit (MultiChannel-Systems, Reutlingen, Germany). In order to secure the slice on the MEA, improve the connection to the electrodes, and to increase the vertical ACSF supply through the tissue, the lower circuit of the perfusion

element was connected to a constant vacuum pump, set to a negative pressure of 1.5 mbar. The software that was used for data acquisition was Multi Channel Suite (MultiChannel-Systems, Reutlingen, Germany). Data was sampled at a sampling rate of 20 kHz.

To stimulate ChR2 in the slice optogenetically, a light fiber was placed above the slice in a distance of approx. 0.5 cm connected to a 473 nm diode laser (LuxX 473-80, Omicron-Laserage, Rodgau-Dudenhofen, Germany). The light stimulation pattern was controlled by a custom-written Igor script and forwarded to the MEA acquisition software to synchronize the slice recording and the light stimulation trigger (see Figure 11).

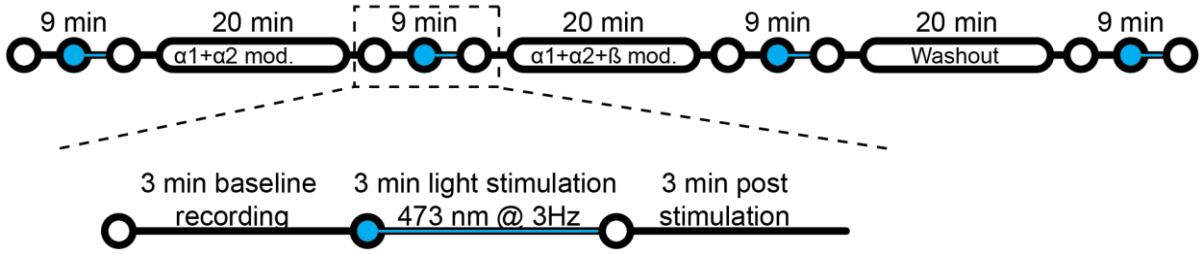

Figure 11 MEA light stimulation scheme
The experiment consisted of four recording sessions, 9 min each, with 3 min baseline recording, 3 min light stimulation and 3 min post stimulation. In between, NE modulatory drugs (prazosin, clonidine and propranolol) were added to the ACSF supply. In the end a 20 min washout phase was performed, followed by a recording session, including light stimulation.

Noradrenergic agonists and antagonists were applied directly to the ACSF supply of the MEA-chamber. The concentrations are identical to those used in vivo (see Table 2). After changing to a noradrenergic agonist/antagonists, all recordings were paused for a 20 min wash-in phase.

2.11 Patch clamp

In order to investigate the influence of noradrenergic modulation on single cell properties, the MSDB of VGluT2-Cre transgenic mice was transduced with AAV carrying a floxed version of red fluorescent protein tdTomato. In addition, a second virus carrying the coding information for ChR2-EYFP in an unfloxed version was injected bilaterally into the LC. After three weeks of incubation, coronal slices (300 µm thickness) of the medial septum were prepared with a Leica VT-1200S vibratome (Leica Microsystems, Wetzlar, Germany) in ice-cold sucrose solution containing (mM):

60 NaCl, 100 sucrose, 2.5 KCl, 1.25 NaH_2PO_4, 26 $NaHCO_3$, 1 $CaCl_2$, 5 $MgCl_2$, 20 glucose, oxygenated with 95% O_2 and 5% CO_2. After recovery for at least 30 min at 35 °C, slices were transferred into standard ACSF with the following composition (mM): 125 NaCl, 3 KCl, 1.25 NaH_2PO_4, 26 $NaHCO_3$, 2.6 $CaCl_2$, 1.3 $MgCl_2$, 15 glucose) at room temperature. Recordings were obtained from red fluorescent neurons visualized by infrared DIC and fluorescence microscopy for tdTomato identification (SliceScope, Scientifica, East Sussex, UK; BX-RFA, Olympus, Hamburg, Germany). Whole-cell current-clamp recordings were performed using a Dagan BVC-700A amplifier (Minneapolis, USA) and digitalized at 50 kHz or higher sampling rates using an ITC-18 interface board (HEKA) controlled by IgorPro 6.2 software (WaveMetrics, Portland, USA). The recording pipettes with a resistance of 4-6 MΩ were filled with standard intracellular solution containing (mM): 140 K-gluconate, 7 KCl, 5 HEPES-acid, 0.5 $MgCl_2$, 5 phosphocreatine, 0.16 EGTA. All recordings were performed at 34 °C without correction for liquid junction potentials.

2.12 Analysis

2.12.1 Analysis of locomotion

To investigate running behavior, a linear treadmill with a 2 m belt was used. The movement of the belt was detected with an optical mouse measuring the rotation of the belt. The detected position signal was further analyzed using custom-written Matlab scripts (Matlab 2013b, MathWorks, Natick, USA). Before further analysis, the running traces were smoothed, using a boxcar filter over 40 ms. Velocities below 0.1 cm/sec were defined as resting. Locomotion was defined as movement faster than 4 cm/sec. From the running traces and the time course of the experiment, the average velocity in cm/sec, the average running velocity, excluding the resting phases, the average running duration in % of time spent running, and the number of running initiations per minute were calculated. Movement phases of at least 1 sec duration were considered running phases. These parameters were calculated for both baseline phases and phases with stimulation.

2.12.2 Local field potential recordings

Local field potentials were recorded from CA1 with implanted electrodes in both hippocampi. Movement artefacts above 8 standard deviations (SD) were cut from the recording. LFP spectra were created using a Morlet wavelet transformation algorithm in Matlab 2013b (MathWorks, Natick, USA). Theta oscillations were defined as

frequencies between 4 to 12 Hz, and separated into 1 Hz bands. From the LFP spectrum, the prominent frequency band in the theta range and the maximum power at this peak was calculated. Peak frequency and maximum theta power was compared between running and resting phases in stimulated and unstimulated conditions.

2.12.3 Microelectrode array

Extracellular recordings from whole brain slices were performed on a microelectrode array with 25 kHz sampling rate. In order to follow single units over several recordings, all raw data from consecutive recordings were translated into binary data and merged. The merged file was further analyzed with Matlab 2013b (MathWorks, Natick, USA) and an open-access unit detection and sorting algorithm ("Kilosort", https://github.com/cortex-lab/KiloSort, Pachitariu et al. (2016)). For the detection, spikes with an amplitude of 5 SD above baseline were isolated for every electrode. By comparing the spike timing, localization on the MEA, and the spike waveform, spikes were sorted into single units. All units were validated manually, dismissing artefacts and units with less than 50 spikes in total. During every experiment, the placement of the septal slice on the MEA chip was documented. Comparing the placement of the electrodes with the Allen Brain Atlas (Lein et al. 2007), the precise location from which extracellular recordings were gathered in 14 experiments could be reconstructed. The mean firing frequency for every unit was calculated with and without stimulation and before vs. during pharmacological modulation.

2.12.4 Patch clamp

In order to validate noradrenergic input on a single cell level, patch clamp experiments were performed with spare slices of MEA experiments. For all cells, characteristic response patterns to −200 pA and +500 pA current injections were recorded. Furthermore, the response to NE release due to optogenetic fiber stimulation was recorded. The maximum depolarization in response to the stimulus was compared between control and NE modulated conditions.

2.12.5 Statistical analysis

Statistical analysis of the data was performed using GraphPad Prism 7 software (GraphPad Prism version 7.00 for Windows, GraphPad Software, La Jolla California USA). All data was first checked for Gaussian distribution with a Kolmogorov-Smirnov test. Normally distributed data was tested for significant differences with the paired or unpaired two-tailed Student's t-test. Heterogeneously distributed related and

independent samples were tested with a non-parametric related-samples Wilcoxon signed rank test and Mann-Whitney U test, respectively. Significance levels were defined as $p<0.05$ = *, $p<0.01$ = **, $p<0.001$ = ***, and $p<0.0001$ = ****.

3 Results

3.1 LC fiber stimulation in MSDB increases locomotor behavior

3.1.1 Baseline running

In order to evaluate baseline running properties, voluntary movement of 12 mice was recorded in 6 experiments per mice, 10 min each on consecutive days. The running behavior was measured on a linear treadmill, allowing the precise recording of linear movement (see Figure 12A). Immobility or resting was defined as every time point with a velocity slower than 0.1 cm/sec and running was defined as movement longer than 1 sec with a speed of at least 2 cm/sec. For the setup, a belt of 2 m length was used in combination with an optical mouse that scans the rotation of the belt (described in Fuhrmann et al. (2015)). To minimize sensory distractions from external stimuli (acoustic or visual), the setup was covered by a closed box.

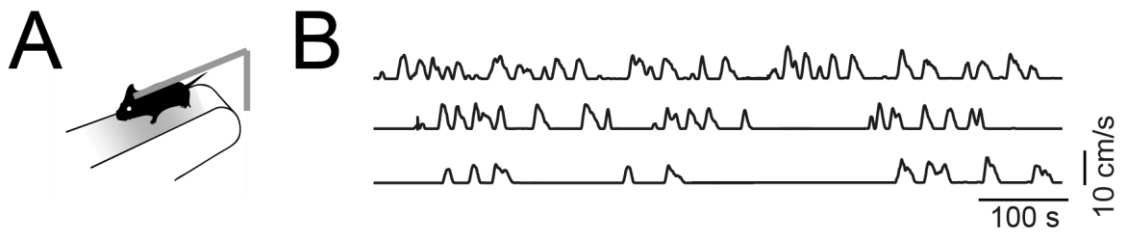

Figure 12 Baseline running on a linear treadmill
A. shows a sketch of the linear treadmill setup with a mouse head-fixed on the belt. The setup was built sound and light proof to reduce sensory distractions. All mice were well habituated to the setup and showed voluntary running behavior. In **B.** an example running trace of one mouse with three consecutive laps is shown. All mice showed characteristic phasic running behavior, with short bursts of movement alternating with resting phases.

All mice were well habituated to the head fixation on the treadmill and showed voluntary running behavior (see example in Figure 12B) with an average velocity of 4.79 ± 1.27 cm/sec, excluding resting phases (mean ± SD; N = 12 mice; see Figure 13A). With resting and slow movement phases included the average velocity over the course of the 10 minute experiment was 0.87 ± 1.07 cm/sec (mean ± SD; N = 12 mice; see Figure 13B). All mice showed characteristic phasic running behavior with 22.86 ± 13.22 running initiations per minute on average (mean ± SD; N = 12 mice; see Figure 13D). Overall, the mice spent an average of 13.5 ± 10.25 % of the total duration of the experiment running (mean ± SD; N=12 mice; see Figure 13C).

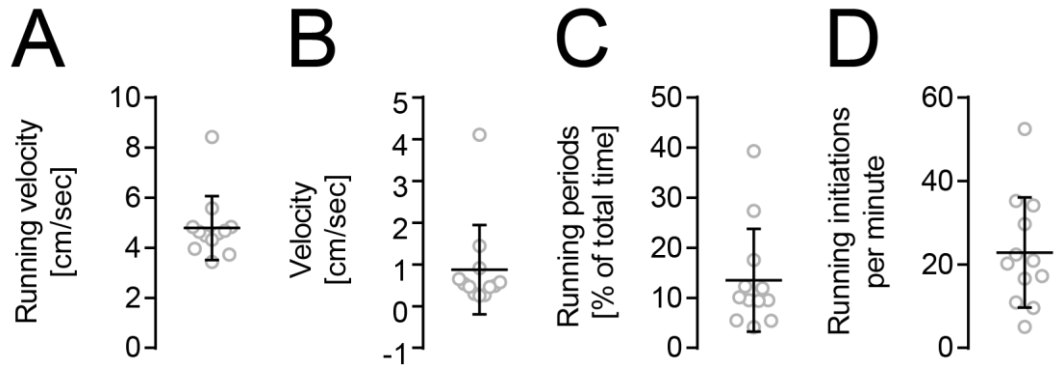

Figure 13 Baseline running analysis.
Running was defined as linear movement with a speed of at least 2 cm/sec. Resting was defined as velocities slower than 0.1 cm/sec. **A.** Running velocity [cm/sec] shows the running speed during phases of movement, excluding resting phases. **B.** For the overall velocity [cm/sec] the average speed of complete recordings, including movement and resting phases was taken into account. **C.** The running duration [% of total time] calculates from the total duration of running phases versus the overall duration of the experiment. **D.** Running initiations per minute depicts the phasic nature of the movement and counts all onsets of running phases during the experiment. (Individual mouse data are presented in gray, n=12 mice, mean values ± SD).

3.1.2 Effect of optogenetic LC fiber stimulation in MSDB on running behavior

In 6 experiments 12 TH1-Cre mice were used to investigate the effects of LC-axon terminal excitation within the MSDB on running behavior. 4-8 weeks before the experiments, all mice received bilateral stereotactic AAV virus injections into LC, carrying floxed ChR2. In addition, LFP electrodes were placed bilaterally in hippocampal CA1. Furthermore, a light fiber was placed above the MSDB in order to stimulate ChR2 in the MSDB. After 2 weeks of expression and habituation to the setup, all mice showed voluntary running behavior, while being head-fixed on the linear treadmill (see Figure 14A). The light fiber was coupled to a 473 nm laser with 20 mW power, providing 3 Hz stimulation with 3 ms pulses.

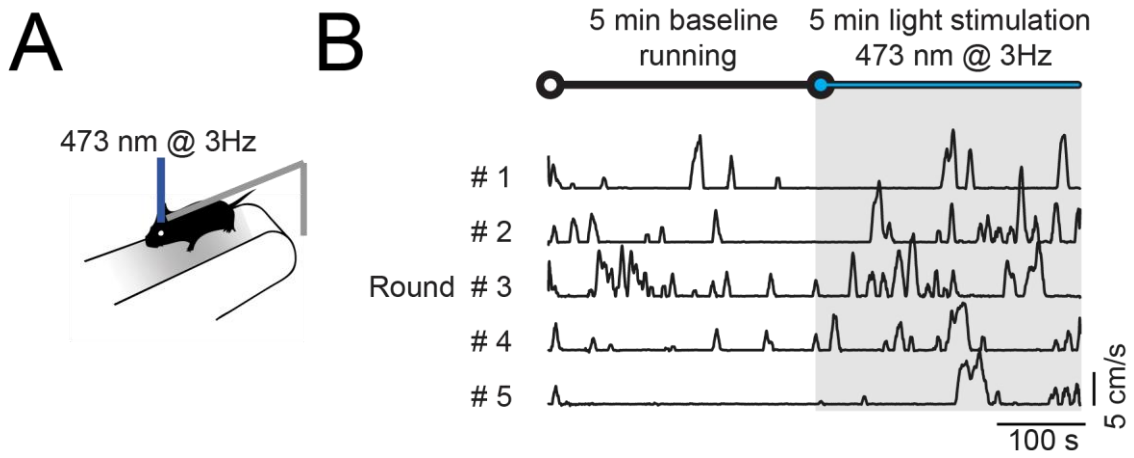

Figure 14 Optogenetic MSDB stimulation on the treadmill and exemplary running traces.
A. Scheme of the linear treadmill setup with a mouse head fixed and a lightfiber implanted above the MSDB. **B.** Five consecutive running traces from one exemplary experiment, showing increased running behavior when 3 Hz light stimulation was applied.

For the analysis of voluntary versus stimulated running, running velocity, overall velocity, running duration and running initiations per minute were averaged for 6 experiments per mice (see individual data in Appendix figure 1 and Appendix figure 2). The D'Agostino-Pearson normality test showed a nonparametric distribution of all measurements. Therefore, average values were compared using the Wilcoxon matched-pairs signed rank test.

Stimulating LC axon terminals in MSDB resulted in an overall increase of locomotor behavior compared to unstimulated conditions (see example in Figure 14B). The number of running initiations per minute (see Figure 15D; n=12, $\mu_{baseline}$=22.8 ± 13.22 [running initiations/min], $\mu_{stimulation}$=30.8 ± 11.37 [running initiations/min], p=0.0068) and the overall duration spent running (see Figure 15C; n=12, $\mu_{baseline}$=13.5 ± 10.25 [% total time], $\mu_{stimulation}$=17.75 ± 8.99 [% total time], p=0.0210) were significantly increased. Following the overall speed during the experiment, this results in an increased overall velocity (see Figure 15B; n=12, $\mu_{baseline}$=0.87 ± 1.07 [cm/sec], $\mu_{stimulation}$=1.12 ± 1.07 [cm/sec], p=0.0269). Although excluding all resting phases, the running velocity was not significantly changed (see Figure 15A; n=12, $\mu_{baseline}$=4.79 ± 1.26 [cm/sec], $\mu_{stimulation}$=5.04 ± 1.33 [cm/sec], p=0.2036). These data show that optogenetic stimulation of LC->MSDB projections leads to increased running behavior, without influencing the speed during running.

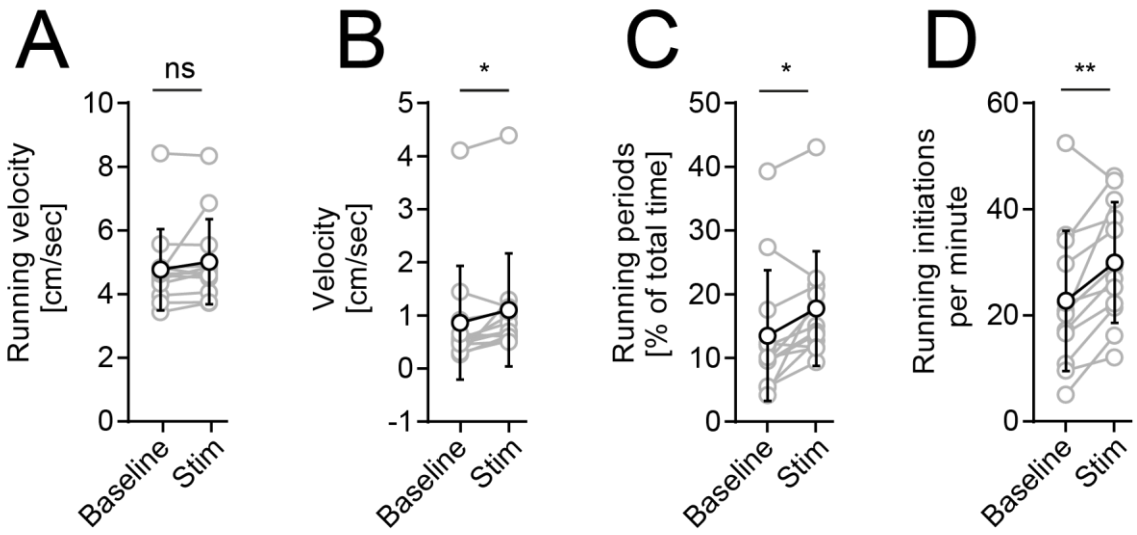

Figure 15 Stimulated running analysis.
A. Running velocity at baseline vs. rest. For the analysis of running velocity, the running speed during all phases of movement without resting phases was included. **B.** Overall velocity at baseline vs. rest, including all movement and resting phases. **C.** Percent of running periods at baseline vs. rest. Running periods were calculated from the total duration of running phases divided by the overall duration of the experiment. **D.** Number of running initiations per minute at baseline vs. rest. Running onsets faster than 4 cm/sec and longer than 1 sec were considered running initiations. (All statistical comparisons were performed with the Wilcoxon matched-pairs signed rank test. Each gray line depicts one mouse with 6 averaged experiments. Black line = mean values ± SD.)

3.1.3 Yellow laser control

To rule out that the placement of a light fiber and the illumination of neuronal tissue with potential heating effects due to illumination was causing any changes to the physiological functionality of the systems studied, a yellow laser control was performed. To do so, a laser with the emission wavelength of 561 nm was coupled to the light fiber implanted and the stimulated running experiments were conducted as before. Light with a wavelength of 561 nm exceeds the absorption spectrum of ChR2 and is therefore not functional for causing structural changes of the retinal within the ChR2-protein. The emitted light intensity was tuned to 20 mW, matching the light intensity of the 473 nm laser used in the experiments.

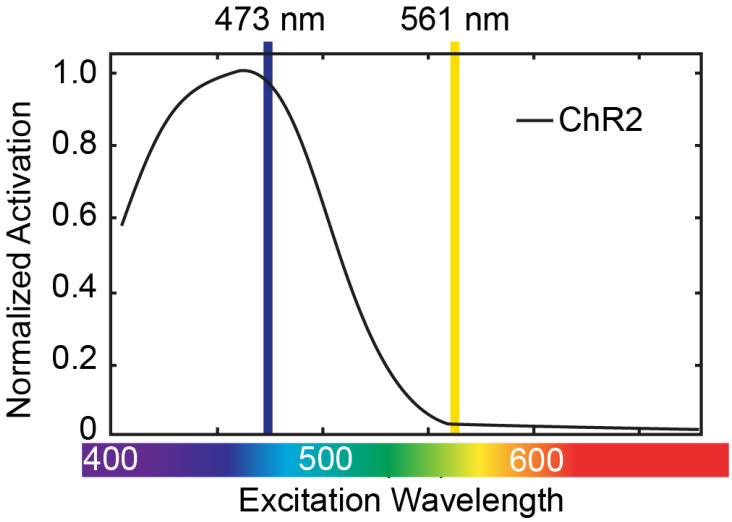

Figure 16 Absorption spectrum of ChR2
Adapted from EuroPhotonics March 2015; www.photonics.com

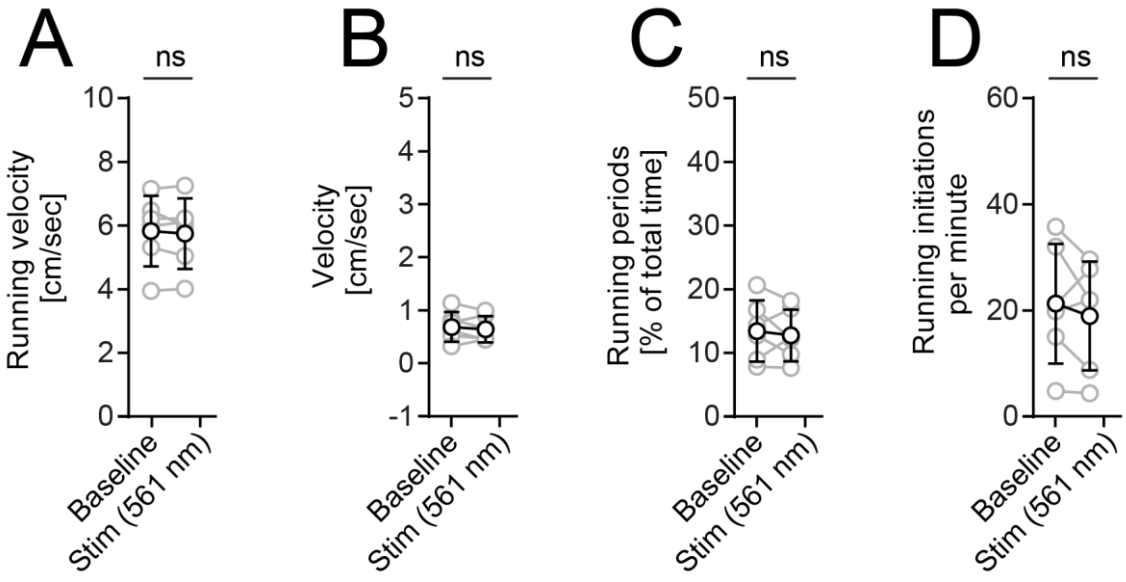

Figure 17 Voluntary running analysis with 561 nm yellow control laser stimulation. In **A.**, the running velocity [cm/sec] of baseline running, excluding all resting phases (> 4 cm/sec), is compared with yellow laser (561 nm) stimulated running. **B.** shows the overall running velocity for baseline vs. stimulated running. **C.** sums up the share of running periods in % of the total time for baseline and stimulated running. In **D.**, the running initiations per minute are shown for baseline vs. yellow laser stimulation. (All statistical comparisons were performed with the Wilcoxon matched-pairs signed rank test. Each gray line depicts one mouse with 6 averaged experiments. Black line = mean values ± SD.)

All measurements collected during baseline conditions matched those collected in experiments using the blue laser for optogenetic stimulation (see Figure 15). Unlike the blue laser stimulation, yellow laser light stimulation did not induce any significant effects on any of the four calculated running parameters (see Figure 17).

3.1.4 LPF & theta oscillations during rest and locomotion

Any excitable membrane — whether it is a spine, dendrite, soma, axon or axon terminal — and any type of transmembrane current contributes to the LFP. All transmembrane currents, irrespective of their origin, lead to an intracellular as well as an extracellular voltage deflection. The characteristics of the LFP waveform, such as the amplitude and frequency, depend on the proportional contribution of the multiple sources and various properties of the brain tissue (Buzsáki et al. 2012). During the transition from resting states to moving states, changes in the LFP in CA1 stratum pyramidale could be observed (Buzsáki 1986). This layered structure has been shown to typically oscillate at theta frequencies between 4-12 Hz in mice (Whishaw and Vanderwolf 1973). Changes in the oscillatory activity represent changes in the population activity and thus changes to the systems mode, e.g. transition from rest to run. In this study, LFP changes were measured during all *in vivo* linear treadmill experiments using electrodes placed in CA1 stratum pyramidale. LFP oscillations, measured on the treadmill confirmed the presence of rhythmic slow activity during episodes of voluntary movements, while mice were optogenetically stimulated and while they were not (see example in Figure 18). In addition to the frequency shift, the LFP power also increased during movement (see example in Figure 18C).

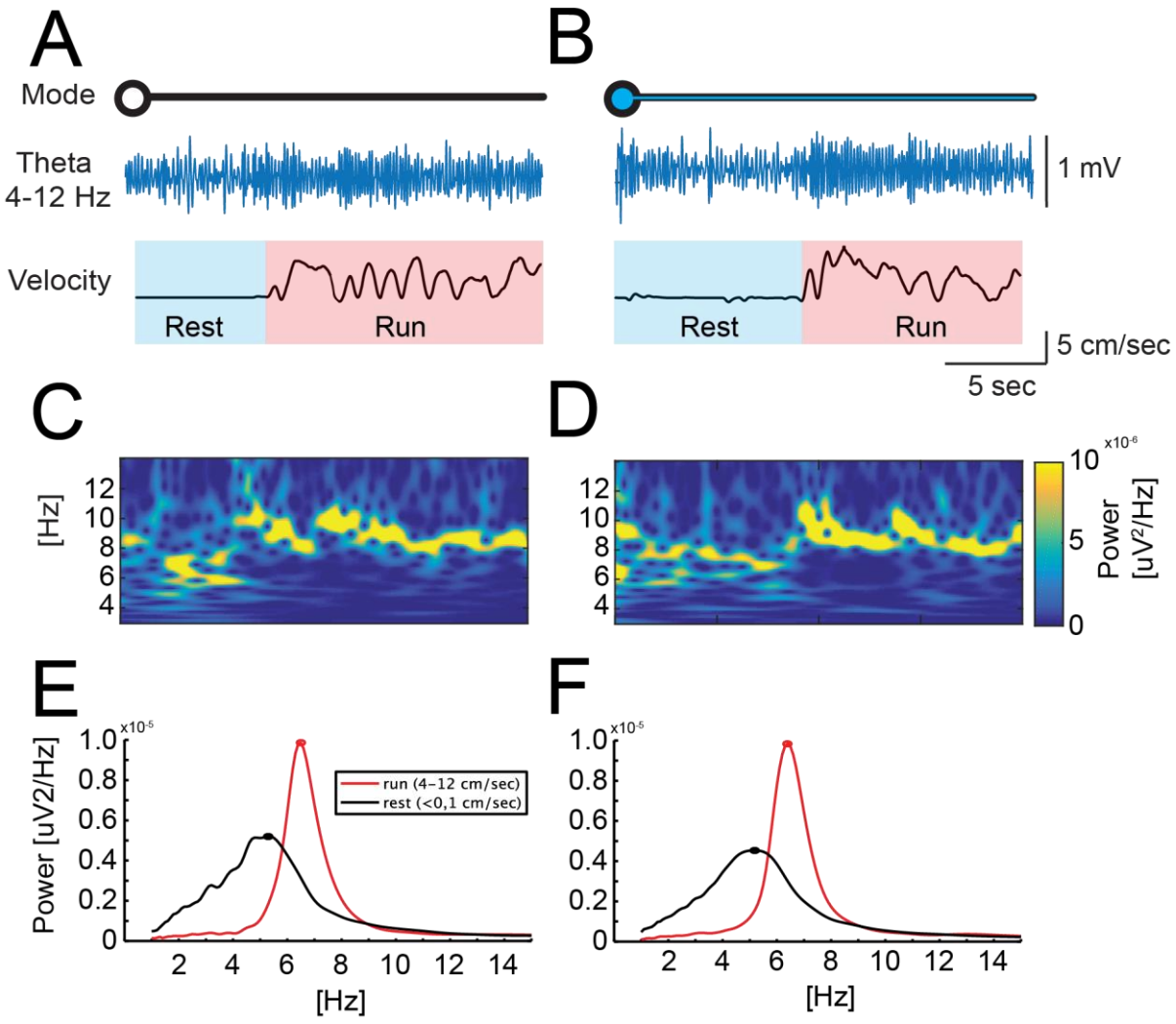

Figure 18 **Example LFP theta oscillations, with and without optogenetic stimulation of LC fibers in MSDB.**
A. shows exemplary local field potential recordings, derived from electrodes placed in CA1 stratum pyramidale of the hippocampus. Below, the correspondent velocity trace with resting and movement phases is shown. **B.** shows an LFP signal from the same recording site during optogenetic stimulation of LC fibers in MSDB. **C.** Power spectrogram of the LFP in A. between 4 to 12 Hz. **D.** Power spectrogram of the LFP in B. during stimulation. **E.** Correlation of LFP Power and Frequency for rest (<0.1 cm/sec) and run (>4 cm/sec). **F.** Same as shown in E for LFP recorded during optogenetic stimulation.

LFP oscillatory frequency in the hippocampus shifted significantly from resting to running states (see Figure 19A). Simultaneously, the power of the theta oscillations increased (see Figure 19C). The same holds true during stimulated running. The direct comparison revealed that there was no significant difference detectable between LFP frequency (see Figure 19B) and LFP power (see Figure 19D) either with or without stimulation during resting phases. Also during running, LFP frequency (see Figure 19B) and LFP power (see Figure 19D) showed no significant difference. The statistical

two way ANOVA analysis revealed, that while optogenetic stimulation did not increase LFP power, there was a small interaction between the running and the stimulation condition, so that in running animals stimulation actually slightly depresses LFP power (see Appendix table 1and Appendix table 2). This effect was not significant per se, only as interaction. In general, the optogenetic stimulation increases running behavior (but not speed), but has no effect on theta.

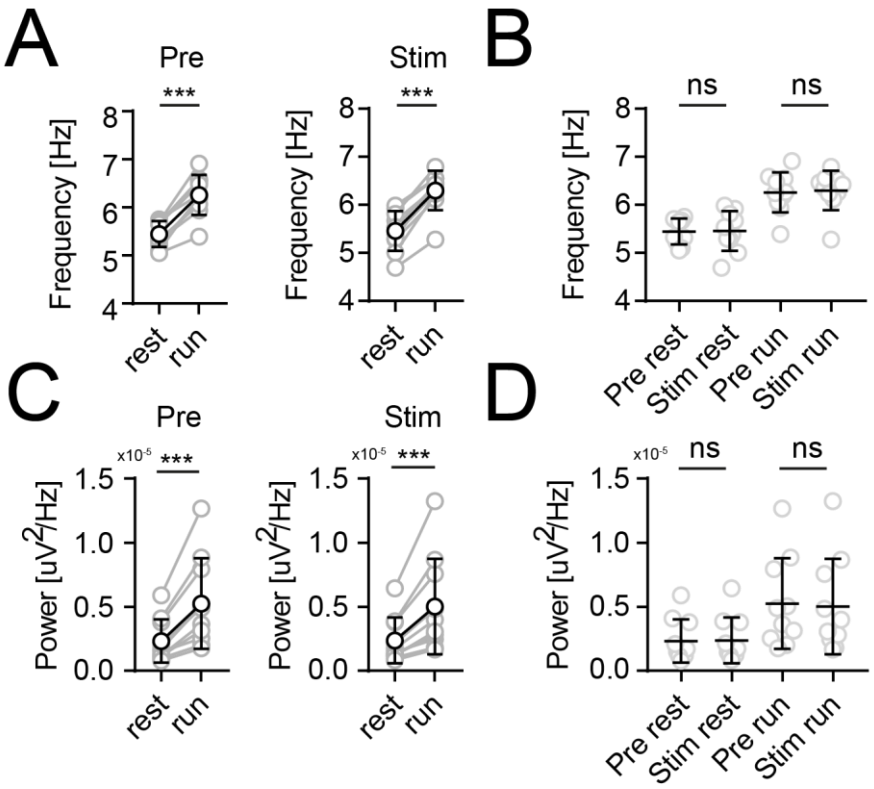

Figure 19 LFP frequency and LFP power analysis prior and during stimulation phases.
In **A.** the LFP frequency shift between resting and movement states is shown for n=10 mice with and without stimulation. Resting phases are defined as velocities >0.1 cm/sec and movement as >4 cm/sec. **B.** shows the direct comparison of Frequency with and without stimulation for resting and running phases. **C.** shows the increase of LFP power while moving, with and without stimulation. In **D.** LFP power is compared between phases with stimulation and without. (All statistical comparisons were performed with two way ANOVA and Sidak's multiple comparisons test (see **Appendix table 1** and **Appendix table 2**). Each gray line depicts one mouse with 6 averaged experiments. Mean values± SD.)

3.2 Pharmacological NE modulation of LC axon terminals in MSDB alters locomotor behavior

The LC sends noradrenergic projections to almost all regions of the brain, including premotor and motor areas (Aston-Jones and Waterhouse 2016; Chandler 2016). One aspect that always needs to be considered when using optogenetic or electrophysiological stimulation is antidromic impulse conduction (Tye et al. 2011;

Yizhar et al. 2011). Meaning, the stimulus propagates from the site of activation anterogradely and retrogradely along the axon, eventually reaching the soma. As a result, when retrogradely propagating action potentials accumulate in the LC, it is possible that as a consequence, other target sites of the LC get activated. To account for this possibility, noradrenergic modulatory drugs were applied in the following experiments at the site of optogenetic stimulation. Modulation of the optogenetically evoked behavior indicated, that the MSDB and no secondary antidromically activated regions were responsible for the behavioral effects observed.

3.2.1 Effect of pharmacological NE modulation on voluntary running

Active LC axon terminals in the MSDB release NE, which acts via different NE receptors on the local network (Haghdoost-Yazdi et al. 2009). By blocking these reactions with pharmacological NE receptor primary and secondary antagonists, the modulatory effect of NE release in the MSDB can be altered. To apply pharmacological agents while simultaneously applying optogenetic light stimulation, a hybrid fiber consisting of a light fiber and an infusion cannula was implanted, aimed at the MSDB.

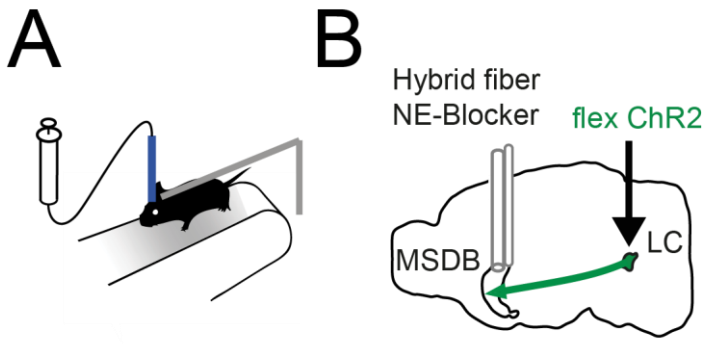

Figure 20 Head fixed mouse on a linear treadmill with a hybrid fiber implanted in MSDB.
A. Head fixed mouse on a linear treadmill with an implanted hybrid fiber, consisting of a light fiber coupled to a 473 nm laser and an infusion cannula. **B.** Floxed ChR2-EYFP injected into LC bilaterally in TH1-Cre mice. ChR2 gets transported via axonal projections towards the MSDB. The hybrid fiber is used to stimulate ChR2 in the axon terminals and also to apply pharmacology (2 µM prazosin, 10 µM clonidine, 10 µM propranolol).

The experiment was planned with six animals, all of which received a surgery with hybrid fiber placement in the MSDB and LFP recording electrodes in the HC (+ grounding electrodes in the cerebellum). In order to fix the mice on the linear treadmill, a metal bar was fixed to the skull. Two animals needed to be excluded due to the detachment of the metal bar and with it a displacement of the hybrid fiber. The hybrid fiber placement was confirmed post hoc in histological slices of the brain. As a result,

two more animals had to be excluded from the analysis, due to divergent placements of the hybrid fiber. The remaining two animals performed well on the treadmill, but all LFP recordings showed unexpectedly high noise levels, and hence were unusable. Since a meaningful statistical evaluation with two animals was not possible, a one-way ANOVA was used to individually test for significant changes in behavior over the course of the five-day experiment for each individual animal.

In order to target α1, α2 and ß receptors, and to block NE signaling in the MSDB, three corresponding NE receptor ligands - prazosin, clonidine and propranolol - were chosen (see Table 2). All three ligands were applied simultaneously via the hybrid fiber. Subsequently, modulatory effects on locomotor behavior were measured on the treadmill. During 5 experiments on two mice baseline running was observed upon drug administration on 5 consecutive days. Every experiment consisted of three times 3 minutes baseline running with sham ACSF infusion. Followed by the ligand application and a 2 minute incubation phase. Then, six times 3 min running with pharmacological modulation were recorded, followed by a 20 min washout phase. Afterwards, three times 3 minutes baseline running with sham ACSF infusion were recorded again (see example in Figure 21).

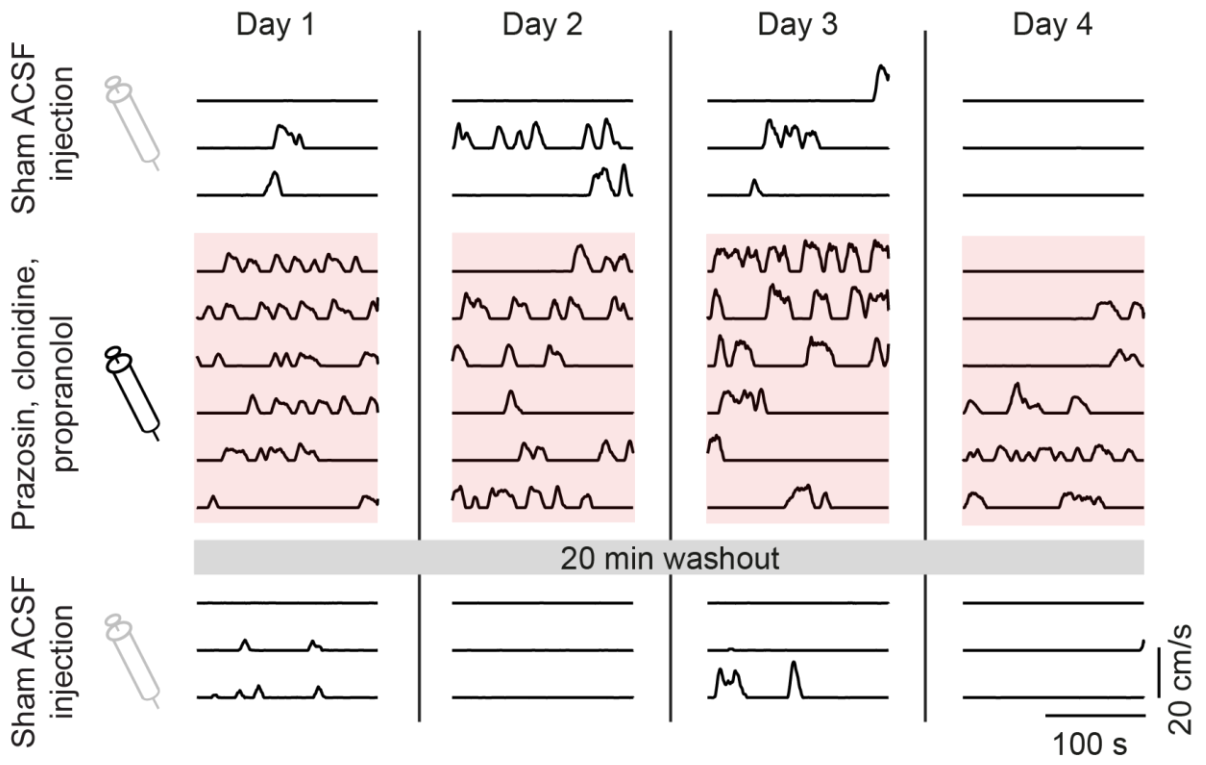

Figure 21 Example running traces during NE modulation.
Running traces from four consecutive experiments are shown. After three rounds of baseline running, NE-modulatory drugs were administered. Six rounds of voluntary running under drug

influence were recorded. After a 20 min washout phase three additional rounds were recorded.

Upon pharmacological NE modulation, locomotor behavior was significantly increased compared to baseline conditions. The duration of running periods (see Figure 22C) and the number of running initiations per minute (see Figure 22D) was significantly increased in both animals. After the 20 min washout period the mice returned to baseline running rates. The overall velocity increased as well, due to the increased running to rest ratio (see Figure 22B). Excluding the resting periods, revealed instead, that the running velocity did not change significantly upon pharmacological modulation (see Figure 22A). Mouse #2 showed a reduced running velocity after the 20 min washout phase.

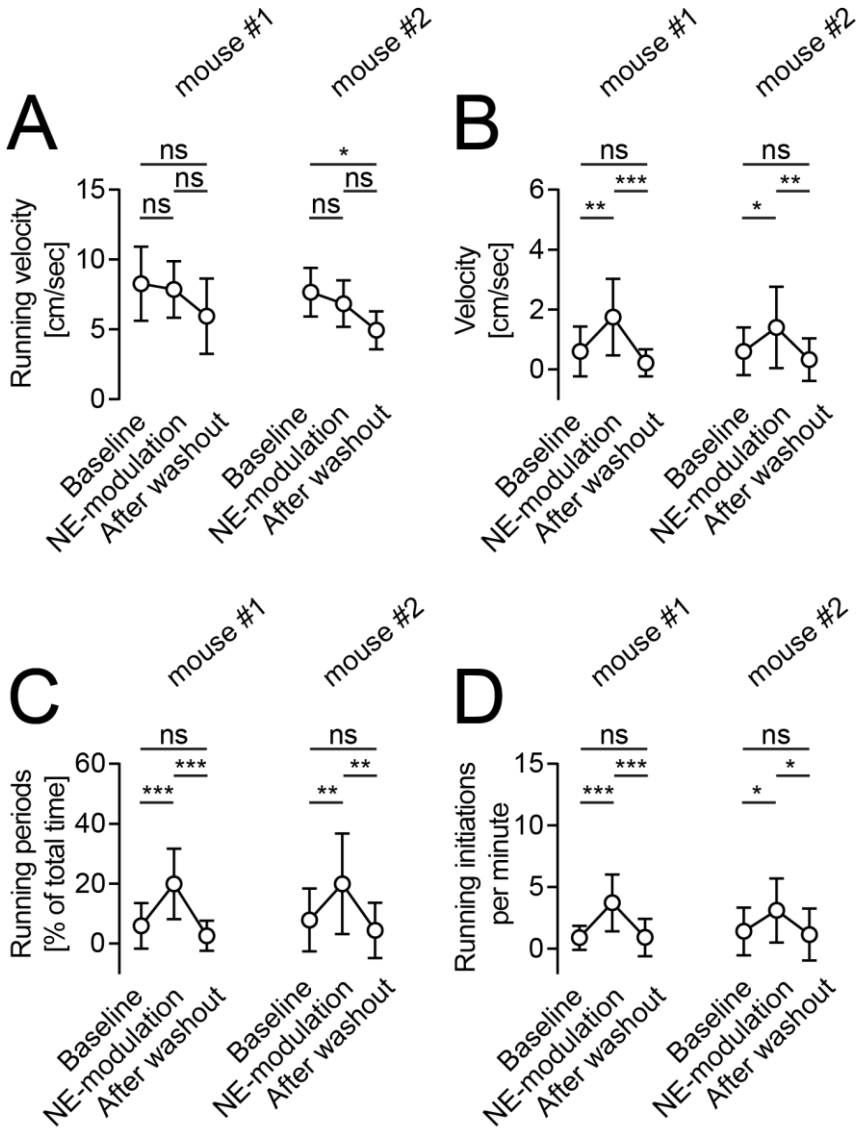

Figure 22 Analysis of unstimulated running behavior under NE modulation.
A. Comparison of running velocity [cm/sec], excluding all resting phases, for baseline

conditions vs. NE modulation (Prazosin, clonidine, propranolol) and after 20 min washout. **B.** Same comparison for the overall velocity during the different phases of the experiment. **C.** % of time the mice spent running for all three phases. **D.** Running initiations per minute for all three phases. (All statistical comparisons were performed throughout all three phases with One-way ANOVA and Tukey's multiple comparisons test (see **Appendix table 3**). Each circle depicts average of five days. Mean values± SD.)

3.2.2 Effect of pharmacological NE modulation on stimulated running

Modulating the NE system in the MSDB, either by optogenetic stimulation of LC-terminals or pharmacological manipulation of NE receptors leads to changes in locomotor behavior. The following experiment examined whether the effects on running behavior were caused by the activation of ARs in the MSDB. The experimental setup combines the optogenetic stimulation with a 473 nm laser at 3 Hz and the application of the NE modulatory drugs prazosin, clonidine and propranolol. A phase of baseline running was initiated alongside a sham injection of ACSF, followed by a phase of optogenetic stimulation. Then a post-stimulation phase followed. After 3 repetitions of sham ACSF, the combination of NE modulatory drugs was applied. Concentration, infusion rate and incubation time were the same as in previous experiments. A phase of pharmacologically modulated running was followed by a phase of combined optogenetic and pharmacological modulation and then a post-stimulation phase with pharmacological modulation still in effect. After 6 repetitions a 20 minute washout phase followed without any further drug application or optogenetic stimulation. The mice were kept on the treadmill during washout. Finally 3 repetitions of baseline running with ACSF sham injections, followed by optogenetic stimulation and then a post-stimulation phase was carried out. The experiment was performed on 5 consecutive days (see example in Figure 23). A two-way ANOVA was used to individually test for significant changes in behavior over the course of the five-day experiment for each individual animal.

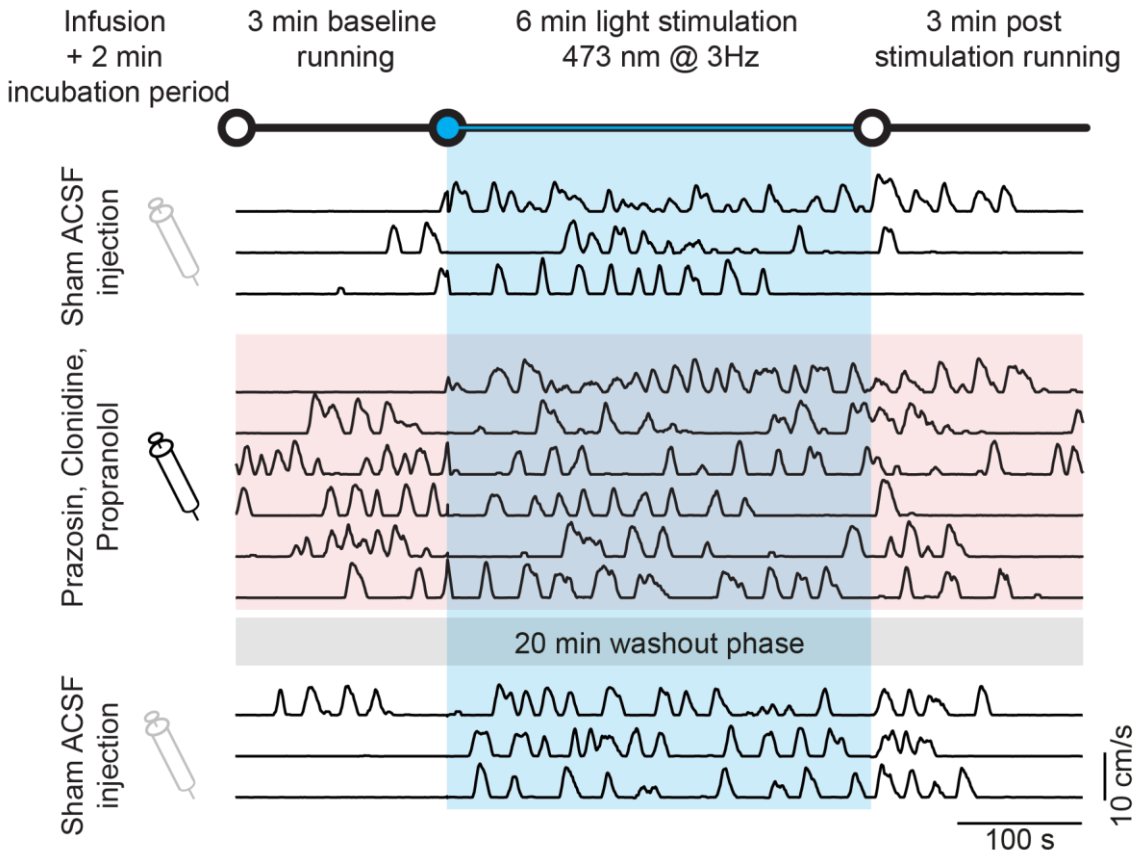

Figure 23 Example running trace with light stimulation and pharmacological NE modulation. A mouse was head fixed on a linear treadmill with an implanted hybrid fiber consisting of a light fiber and an infusion cannula. For three rounds, ACSF was administered as a sham control, then baseline running was recorded for 3 minutes followed by a 6 minute period of light stimulation and again 3 minutes without stimulation. Prior to round 4, NE agonists and antagonists were administered, followed by a 2 minute incubation period. Then baseline running and running with light stimulation was recorded as before. In total, 6 rounds of drug application were performed. Round 10 to 12 follow the initial scheme with ACSF sham infusion.

In line with my previous experiments, mice showed an increased number and duration of running periods when LC projections in MSDB were optogenetically activated during control with ACSF sham injection (see Figure 24C and D). Running speed was not affected (see Figure 24A). The subsequent infusion of pharmacological NE modulators lead to increased running behavior, also when light stimulation was not active. Turning on the laser stimulation did not further affect movement in terms of the duration of running periods (see Figure 24G) and initiations per minute (see Figure 24H). Also, running speed was not further altered from baseline running under drug influence (see Figure 24E). Both mice showed comparable responses to optogenetic as well as pharmacological modulation. In comparison, mouse #1 showed a less consistent increase in running parameters upon optogenetic stimulation than mouse #2, -

especially after the 20 min washout phase. Both mice are consistent in their locomotor increase in response to the pharmacological modulation.

The combination of optogenetic and pharmacological modulation resulted in increased locomotor behavior, comparable to both treatments individually. Optogenetic stimulation did not result in further increased running behavior during pharmacological treatment. In terms of the measured running parameters, simultaneous modulation did not exceed the behavioral limits measured before. Since the pharmacological modulation was a localized application, the blockade suggested that only the MSDB and no other regions were stimulated by optogenetic stimulation, e.g. by antidromic impulse conduction. After a 20 washout period the measured running behavior without stimulation was back to baseline levels and optogenetic stimulation resulted in detectable changes of locomotor behavior again.

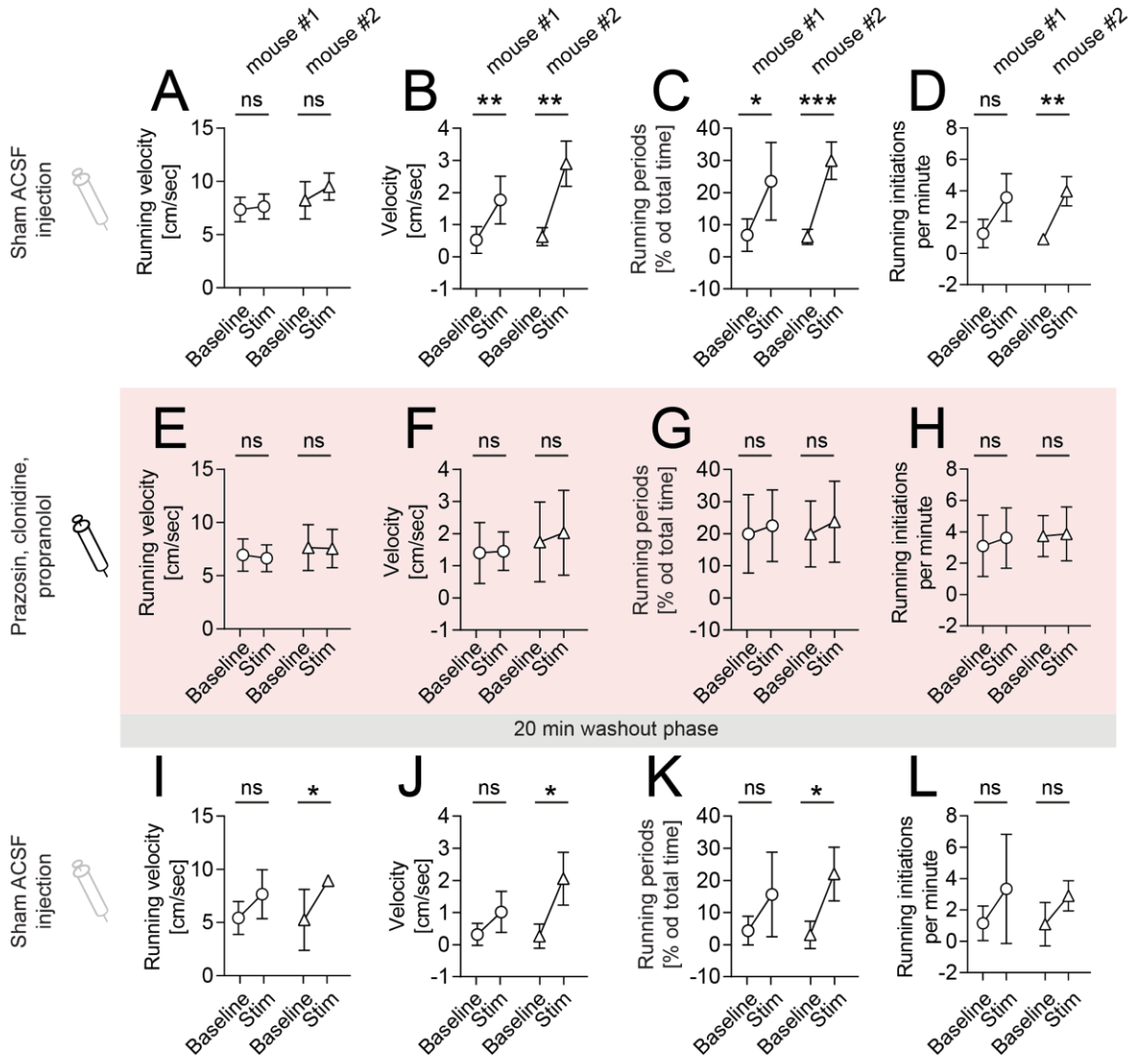

Figure 24 Analysis of running behavior during optogenetic NE fiber stimulation and pharmacological NE modulation for mouse #1 and mouse #2 side by side.
The results are shown for both mice side by side for each parameter. **A.** Comparison of running velocity [cm/sec], excluding all resting phases, for baseline conditions vs. NE modulation and 20 min after washout. **B.** Same comparison for the overall velocity during the different phases of the experiment. **C.** % of time the mice spend running for all three phases. **D.** Running initiations per minute for all three phases. **E.**, **F.**, **G.** and **H.** Same parameters measured during pharmacological NE modulation with prazosin, clonidine and propranolol. **I.**, **J.**, **K.** and **L.** Same parameters 20 minutes after drug administration. Statistics see **Appendix table 4**.

Due to the small number of animals the statistical power of the results is reduced. An in between group comparison was not possible. Instead all results for the two animals are shown side by side. The results are calculated by averaging the performance of all consecutive days of the experiment. In order to take the simultaneous effect of optogenetic and pharmacological modulation into account, a two way ANOVA was

used to determine significant impacts on the measured running behavior (see Appendix table 4).

3.3 MSDB network activity is altered by optogenetic and pharmacological NE modulation

3.3.1 Identification and distribution of MSDB network units

Optogenetic stimulation of afferent LC long-range axons in MSDB led to increased running behavior (see Figure 14). Pharmacological modulation of NE receptors on MSDB neurons also resulted in increased locomotion (see Figure 22). During pharmacological NE modulation, further excitation of the MSDB network was blocked, suggesting that the locomotion enhancing effects were mediated by the influence of NE in the MSDB and no other locomotion-associated region.

Using a MEA allowed me to further investigate how the MSDB network reacts to NE modulation. MEAs for extracellular single unit recordings were introduced by Thomas Jr. et al. (1972) and Gross et al. (1977). Current MEA chips with up to 4000 electrodes enable the simultaneous recording and stimulation of large populations of excitable cells for days without inflicting mechanical damage to the neuron's plasma membrane, as it is necessary with conventional single patch techniques. Extracellular field potential recordings reflect the spike activity of individual neurons or the superposition of fast APs or synaptic potentials.

For MEA experiments, 14 TH1-Cre mice were used with the same stereotactic injections like those used on the linear treadmill. Noradrenergic neurons in LC were transduced with an adeno-associated virus (AAV), resulting in ChR2-EYFP expression within the axon terminals of MSDB. Mounting a brain slice including the MSDB on the MEA chip, extracellular activity from all neurons in proximity to the 6x10 electrodes (see Figure 25A) was recorded. With a 100 µm spacing in between the electrodes and a 30 µm diameter the MEA covered an area of 800 µm by 1200 µm. For every experiment, the relative position of the MEA to the MSDB was documented and later aligned with the Paxinos mouse brain atlas (see Figure 25B; Franklin & Paxinos "The mouse brain in stereotaxic coordinates", Third Edition, Academic Press; 0.98 cm from Bregma).

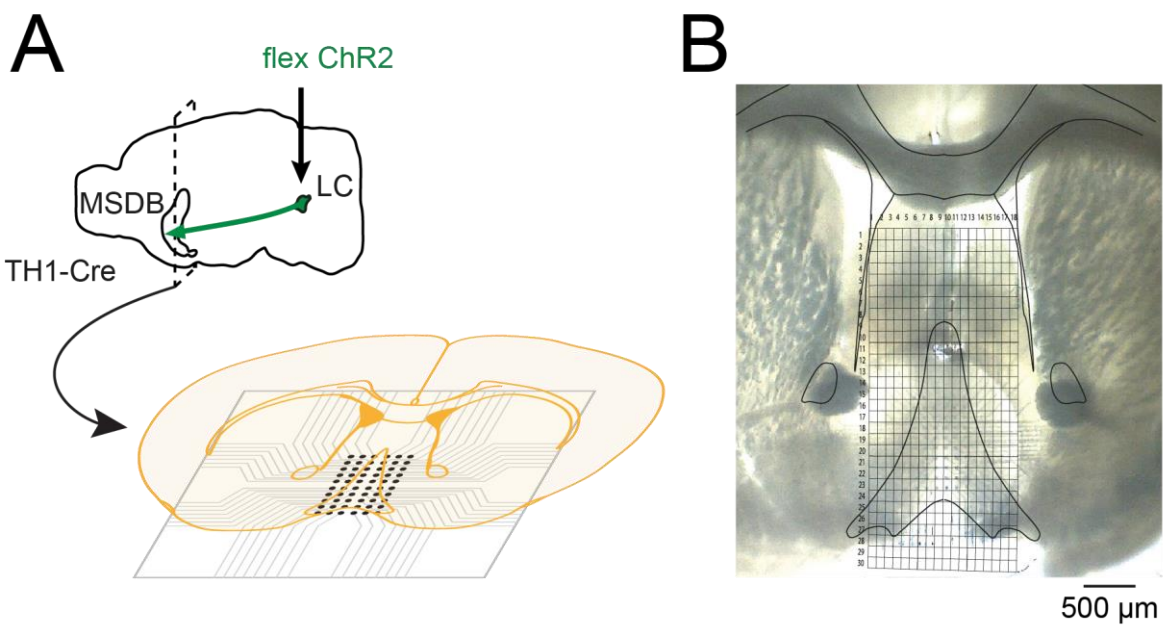

Figure 25 **MEA experimental setup and relative position of the microelectrode array to the MSDB.** **A.** Floxed ChR2 was bilaterally injected into the LC of TH1-Cre mice. Coronal slices of the MSDB were mounted on the MEA. **B.** Exemplary photo of a mouse brain slice, including the MSDB. Underlying the 6x10 MEA electrodes are visible and a MSDB scheme is superimposed on top.

14 experiments covered all of the dorsal medial septum and most of the more ventral diagonal band of Broca (see Figure 26A). Using an offline sorting algorithm, it was possible to extract 1001 separate units from the extracellular recordings (N = 14 mice with 71.36 ± 21.71 units in average): 741 units in the more dorsal part and 260 in the ventral part. Due to higher overlap towards the center of the MSDB, the number of units recorded in this area was higher compared to the lateral septum and the limbs of the diagonal band of broca (see Figure 26B).

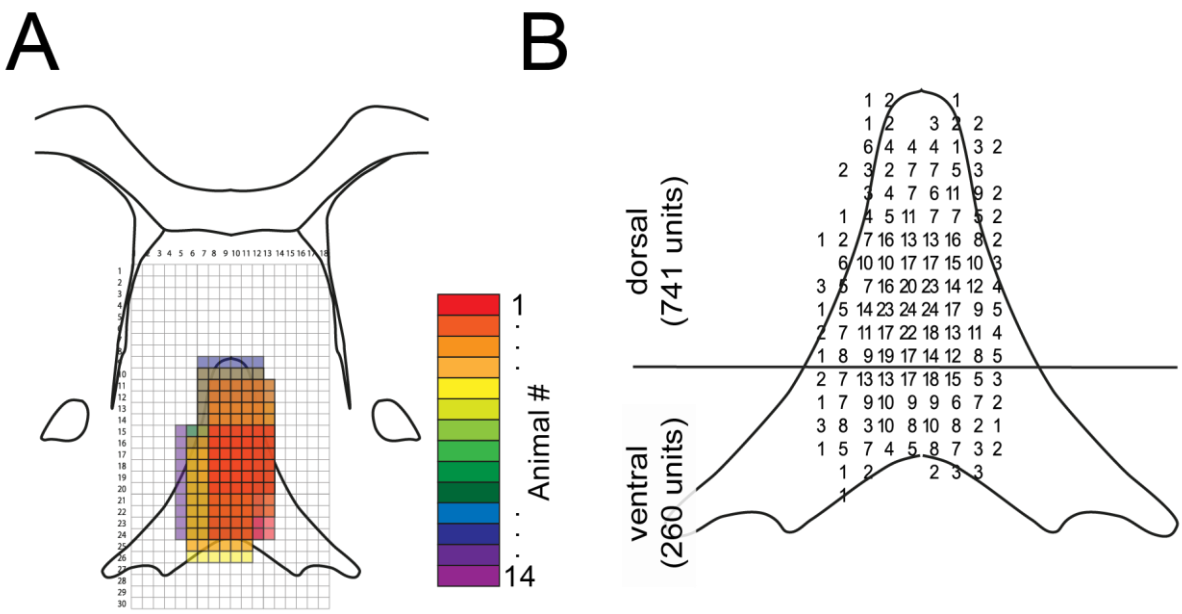

Figure 26 **Coverage of the MSDB with 14 MEA recordings. Distribution of sorted units.**
A. All MEA positions from 14 experiments, color coded and superimposed onto the MSDB 0.98 mm from Bregma. **B.** Sum of all units, recorded at various positions within the MSDB.

The discrimination of single units took into account several characteristic parameters. With a threshold filter, spikes were separated from the raw trace and grouped according to spike timing and the shape of the spike (see example in Figure 27). The spike amplitude reflects the distance to the firing neuron, whereas the width and the relation between peak and trough indicate whether it was a more proximal or distal part of the neuron the spike was recorded from (Buzsáki et al. 2012).

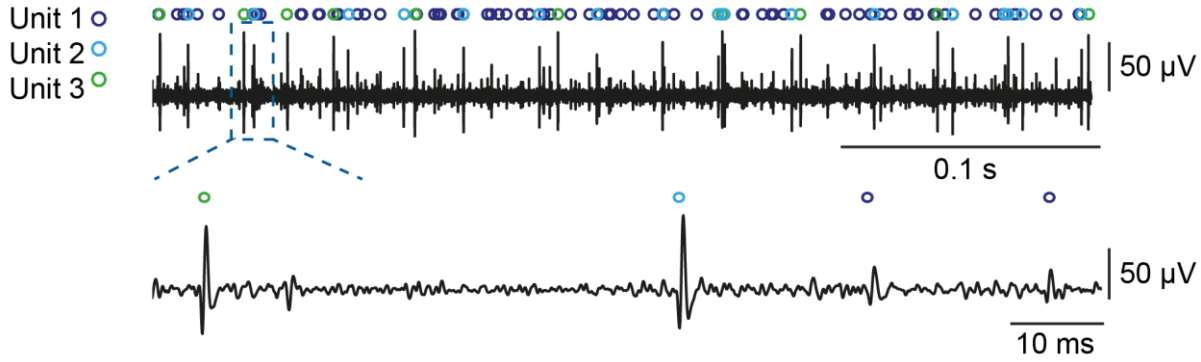

Figure 27 **Exemplary extracellular recording with sorted units.**
Exemplary raw trace from an extracellular MEA recording in the MSDB. Noise-level was ±10 µV. Spikes were separated with a 5x standard deviation threshold and sorted to three units.

Analyzing the position of the MEA electrodes with respect to their anatomical position in the MSDB formation allowed me to align all units from all experiments. For each position in the MSDB covered by a MEA electrode the average baseline firing frequency was calculated. Units recorded in the MSDB showed an average firing frequency of 11.09 ± 12.47 [Hz] in unstimulated conditions. The activity did not differ from dorsal to ventral (see Figure 28).

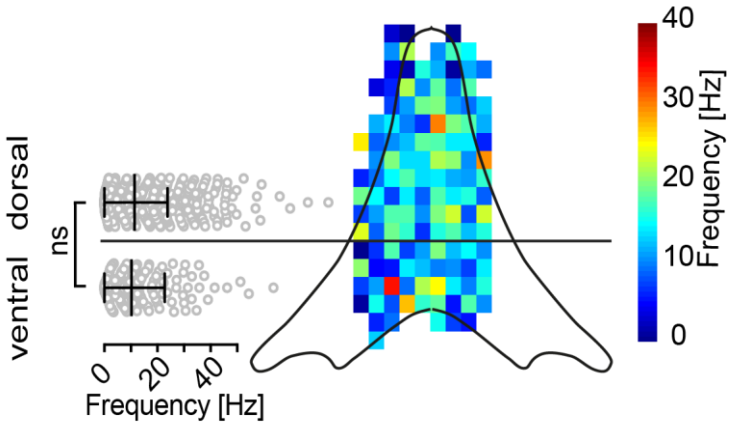

Figure 28 Baseline firing frequency recorded from 1001 units averaged per electrode.
2D distribution of 1001 units from 14 experiments within the MSDB formation. Color code represents mean firing frequency of units per location. Unit population splits into 741 units dorsal and 260 units ventral. Mean frequency with SD is shown for both populations and tested with nonparametric Mann Whitney test for significant differences.

3.3.2 Effect of optogenetic stimulation of LC fibers onto MSDB network activity

In order to activate ChR2 in the axon terminals of LC long range projections in the MSDB, a light fiber was placed in close proximity, shining 473 nm light with a frequency of 3 Hz onto the brain slice (see example in Figure 29A). In response to light activation, the MSDB network activity increased the average firing frequency of MSDB units (see example in Figure 29C).

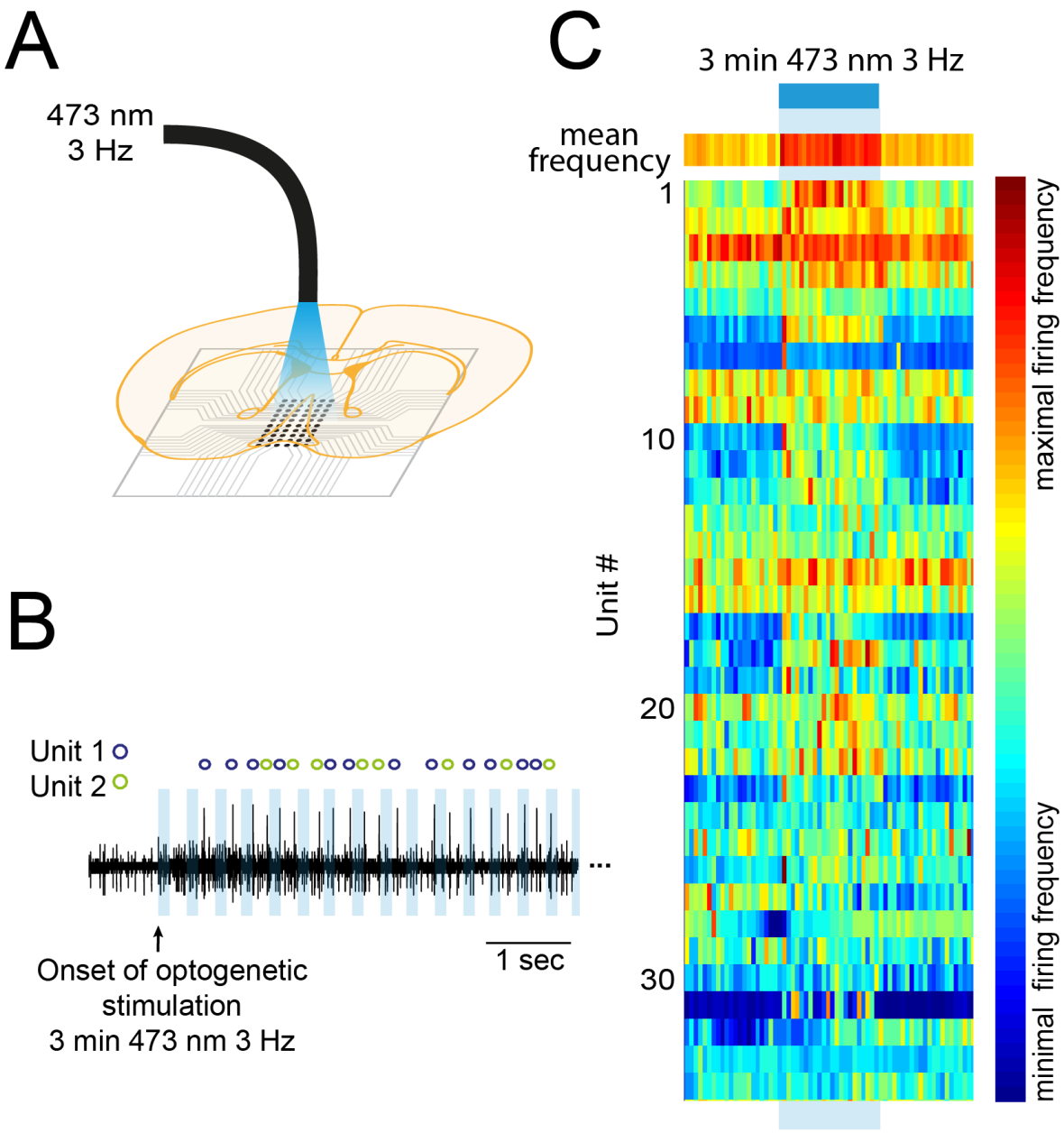

Figure 29 **MEA setup with light fiber, single unit and MSDB network response to light stimulation.** **A.** Coronal brain slice, including the MSDB, mounted on a MEA chip. Lightfiber aiming at the MSDB, emitting 473 nm light with 3 Hz frequency. **B.** Single unit responses to light stimulation. **C.** Exemplary MSDB network response to light stimulation with 34 units. The frequency is color coded from minimal to maximal firing frequency for each unit individually.

Averaging the firing rate of all measured units, the overall activity of the MSDB network increased upon light stimulation (see Figure 30A; n=14, $\mu_{Baseline}$=11.16 ± 6.21 [Hz], $\mu_{stimulation}$=11.82 ± 6.22 [Hz], paired t-test: p=0.0223, t=2.593). A closer look at single units' individual responses (n=14 experiments with 1001 units in total) showed that 41 units decreased their firing rate while 204 increased their activity. The remaining units did not change by more than 1 Hz (see Figure 30C). Between individual experiments,

the percentage of units increasing their activity varied between 0 and 50%, whereas the number of decreasing units ranged from 0% to 15% (see Figure 30C). Looking at the average across experiments, 16.5 % of units increased and 3.25 % decreased their activity (see Figure 30D; n=14, $\mu_{increase}$=16.50 ± 14.55 [%], $\mu_{decrease}$=3.25 ± 4.00 [%]).

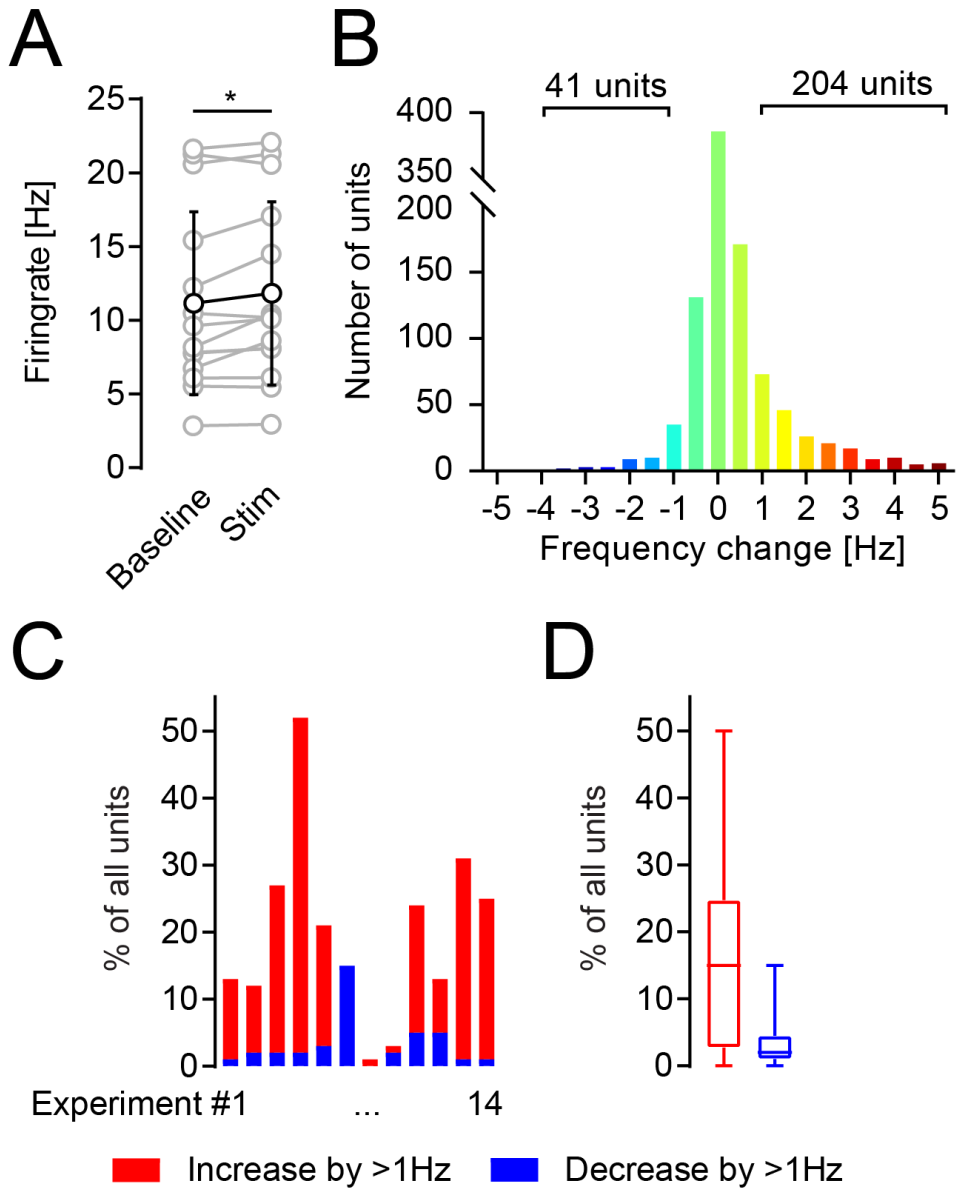

Figure 30 **Change in firing frequency due to optogenetic LC fiber stimulation.**
A. The overall firing rate in all experiments increased upon light stimulation (n=14 experiments). **B.** All units (n=1001 units) binned according to their change in firing frequency (1 Hz bins). **C.** Percentage of increasing (by >1 Hz) and decreasing (by >1 Hz) units in single experiments. **D.** Boxplot depicts mean with upper/lower bounds at the 95% confidence interval.

Anatomically, the units responding with increased activity upon stimulation were significantly more often located in the medial septum rather than the diagonal band of Broca (see Figure 31A, n_{dorsal}=741 units, $n_{ventral}$=260 units; Statistics see Appendix table 5). Separating frequency increasing units from decreasing units showed that this polarization applied to the unit population with positive response (see Figure 31B, n_{dorsal}=464 units μ_{dorsal}=1.36 ± 1.98 [Hz], $n_{ventral}$=148 units $\mu_{ventral}$=1.28 ± 3.83 [Hz]; Statistics see Appendix table 5), whereas decreasing units distributed equally between medial septum and diagonal band of Broca (see Figure 31C, n_{dorsal}=277 units μ_{dorsal}=-0.55 ± 1.46 [Hz], $n_{ventral}$=112 units $\mu_{ventral}$=-0.41 ± 0.55 [Hz]; Statistics see Appendix table 5).

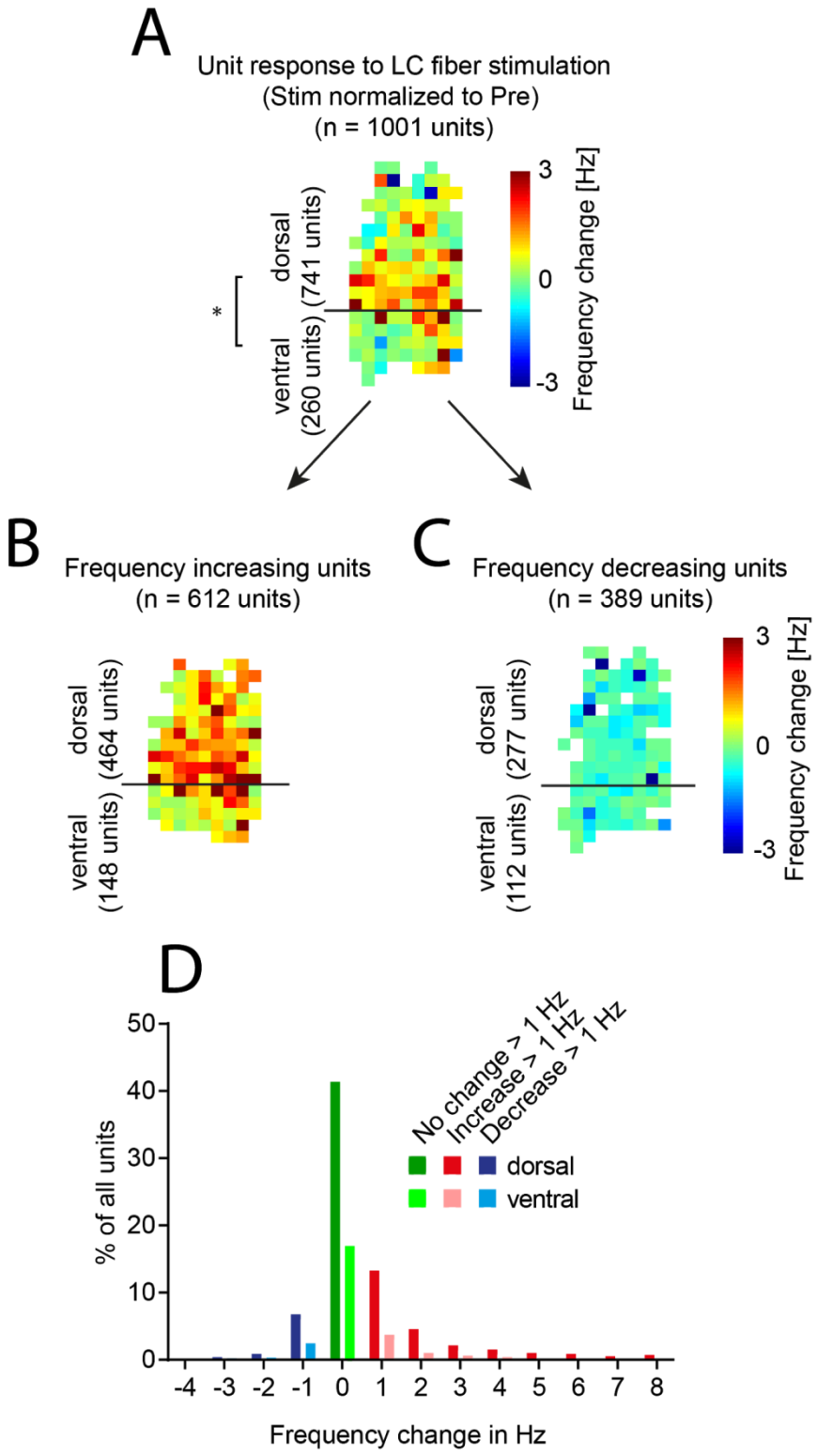

Figure 31 **Anatomical distribution of unit responses to LC fiber stimulation.**
A. Unit response to LC fiber stimulation. Frequency per electrode during stimulation normalized to baseline frequency on the same electrode. N=1001 units in total with 741 units dorsal and 260 units ventral. Statistics see **Appendix table 5 B.** Units with frequency increasing response (n=612 units), normalized to baseline activity. **C.** Units with frequency decreasing response (n=389 units), normalized to baseline activity. **D.** Histogram of frequency change in 1 Hz bins for dorsal and ventral MEA units.

3.3.3 Effects of pharmacological NE modulation on baseline MSDB network activity

To test the effects of NE modulatory drugs on the baseline activity of the MSDB network, prazosin, clonidine and propranolol (see Table 2) were added to the ACSF supply. After a 20 min incubation phase, the activity of single units was recorded. Single units showed diverse responses to the NE modulating drugs. Also, the average response of all units, reflecting the pharmacological effect on the network, varied from experiment to experiment. In general, the global activity of the network was reduced after drug application. A 20 min washout with untreated ACSF did not restore initial control activity levels (see example in Figure 32).

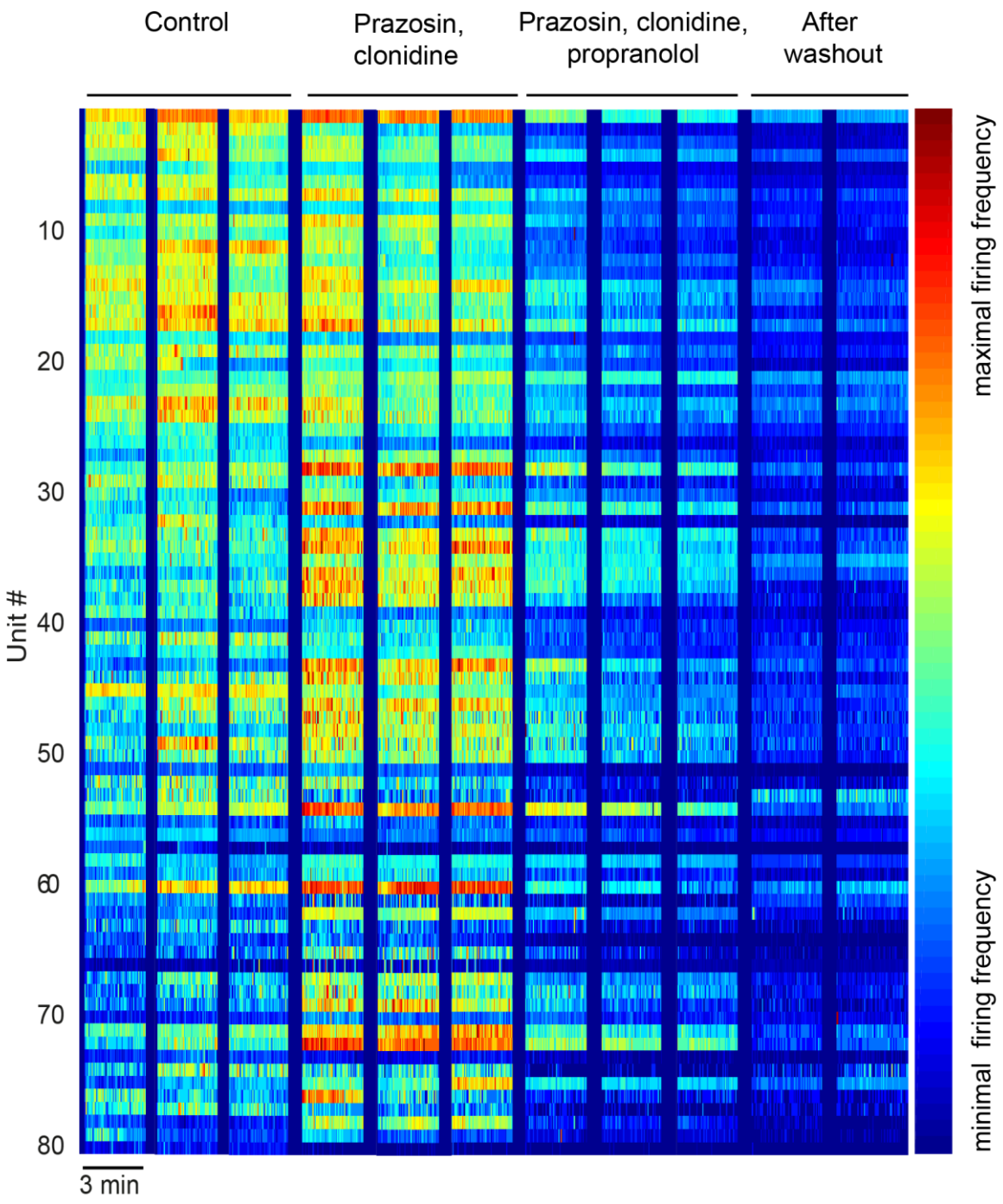

Figure 32 Example MSDB unit activity under control, NE α1+2-modulation, full NE modulation, and after washout conditions.
80 units from one sample experiment, with baseline activity (no light stimulation) under different pharmacological conditions: control (no drug applied), 2 µM prazosin + 10 µM clonidine (NE α1+2-modulation), 2 µM prazosin + 10 µM clonidine + 10 µM propranolol (NE α1+2 + ß-modulation), 20 min after washout (no drug applied). For each condition 3 times 3 consecutive minutes are shown. The frequency is color coded from minimal to maximal firing frequency for each unit individually.

Analysis of the anatomical distribution of units throughout the MSDB formation suggests a homogeneous network response to the NE modulation. Only under the

influence of all three ligands there was a slight but significant difference between the dorsal and the ventral mean rate of firing (Statistics see Appendix table 6). α_1 and α_2 receptor modulators prazosin and clonidine did not alter baseline network activity, whereas the additional application of the NE ß receptor modulating drug propranolol led to an overall decrease of network activity throughout the whole MSDB formation. This effect continued even after a 20 min washout phase (see Figure 33).

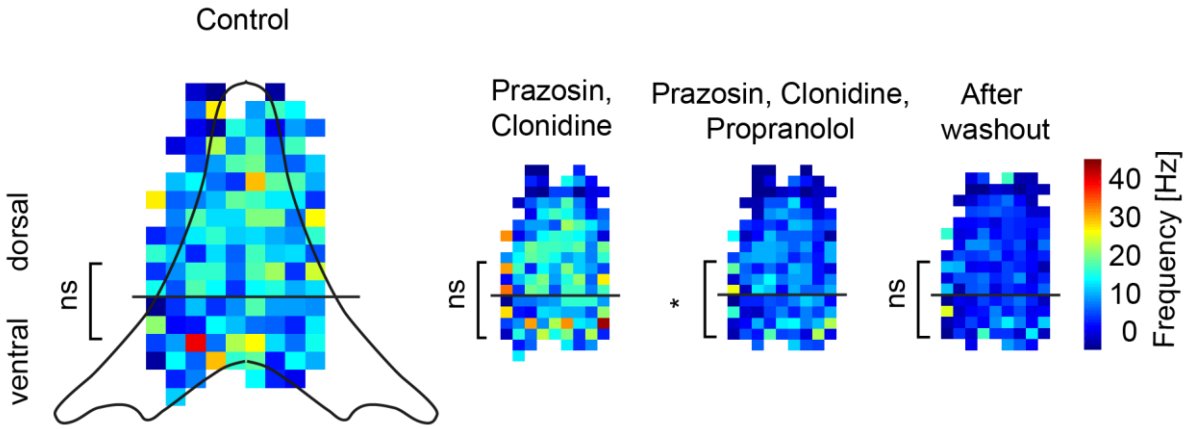

Figure 33 2D distribution of units, adapting their baseline activity to various levels of pharmacological NE-modulation.
Mean firing rate of units throughout the MSDB formation in control conditions, with pharmacological NE- α1+2-modulation, NE- α1+2 + ß-modulation and after 20 minutes washout (n=1001 units). Statistics see **Appendix table 6**.

Recordings from different brain slices showed varying responses to the NE modulating drug application. On average, the mean firing rate of all experiments did not change with the addition of prazosin and clonidine (see Figure 34B), although single experiments showed substantial changes between control conditions and NE α_{1+2} modulation. With propranolol added, the overall activity in nearly all experiments dropped, and significantly changed compared to control conditions (see Figure 34B; Statistics see Appendix table 7). This effect was not restored after a 20 minute washout phase (see Figure 34B).

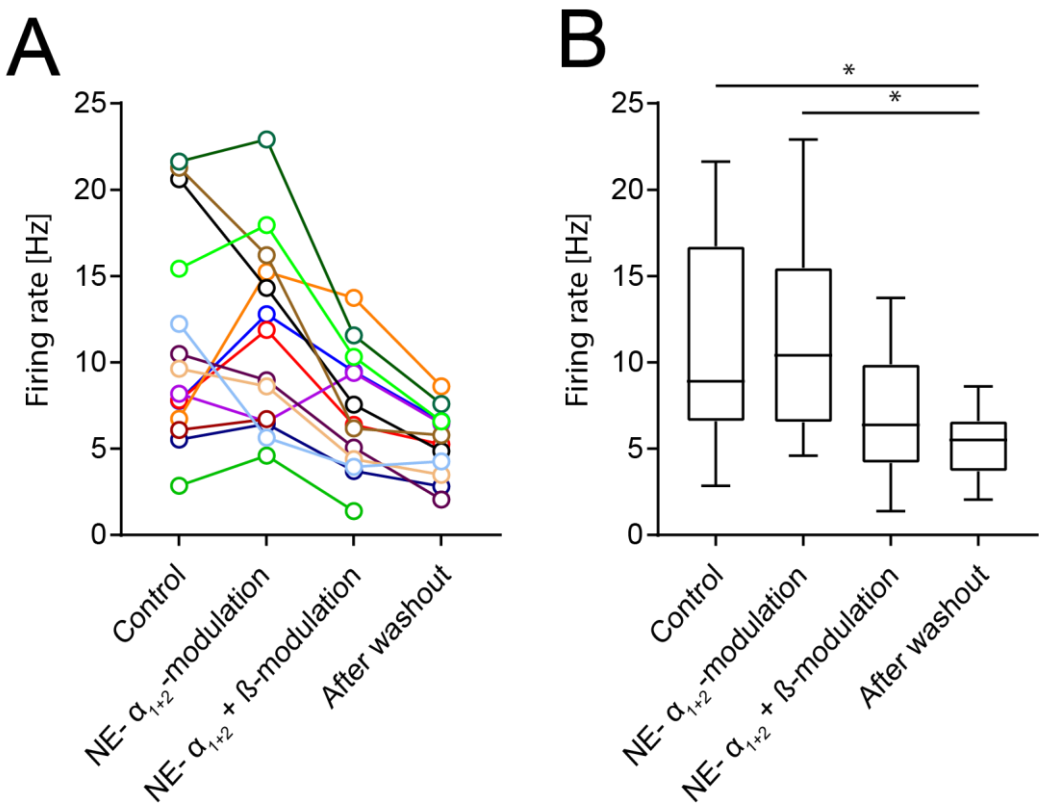

Figure 34 **MSDB network response to various phases of NE-modulation.**
A. global firing rate of n=14 MSDB network-recordings in control condition, with pharmacological NE- α1+2-modulation, NE- α1+2 + ß-modulation and after 20 minutes washout. **B.** Mean plus SD of firing rate change for all experiments. Statistics see **Appendix table 7**.

3.3.4 Effect of LC fiber stimulation during pharmacological NE modulation on MSDB network activity

ChR2 in the terminals of long-range LC axons allowed me to optogenetically modulate MSDB network activity. In 14 experiments, extracellular unit activity was recorded from coronal brain slices including the MSDB formation. In addition, a light fiber was placed in close proximity to the brain slice shining 473 nm light with 20 mW and 3 Hz stimulation frequency on the recorded area (see Figure 29A). The response of the unit network to optogenetic stimulation was recorded in different pharmacological NE modulated conditions (see example in Figure 35).

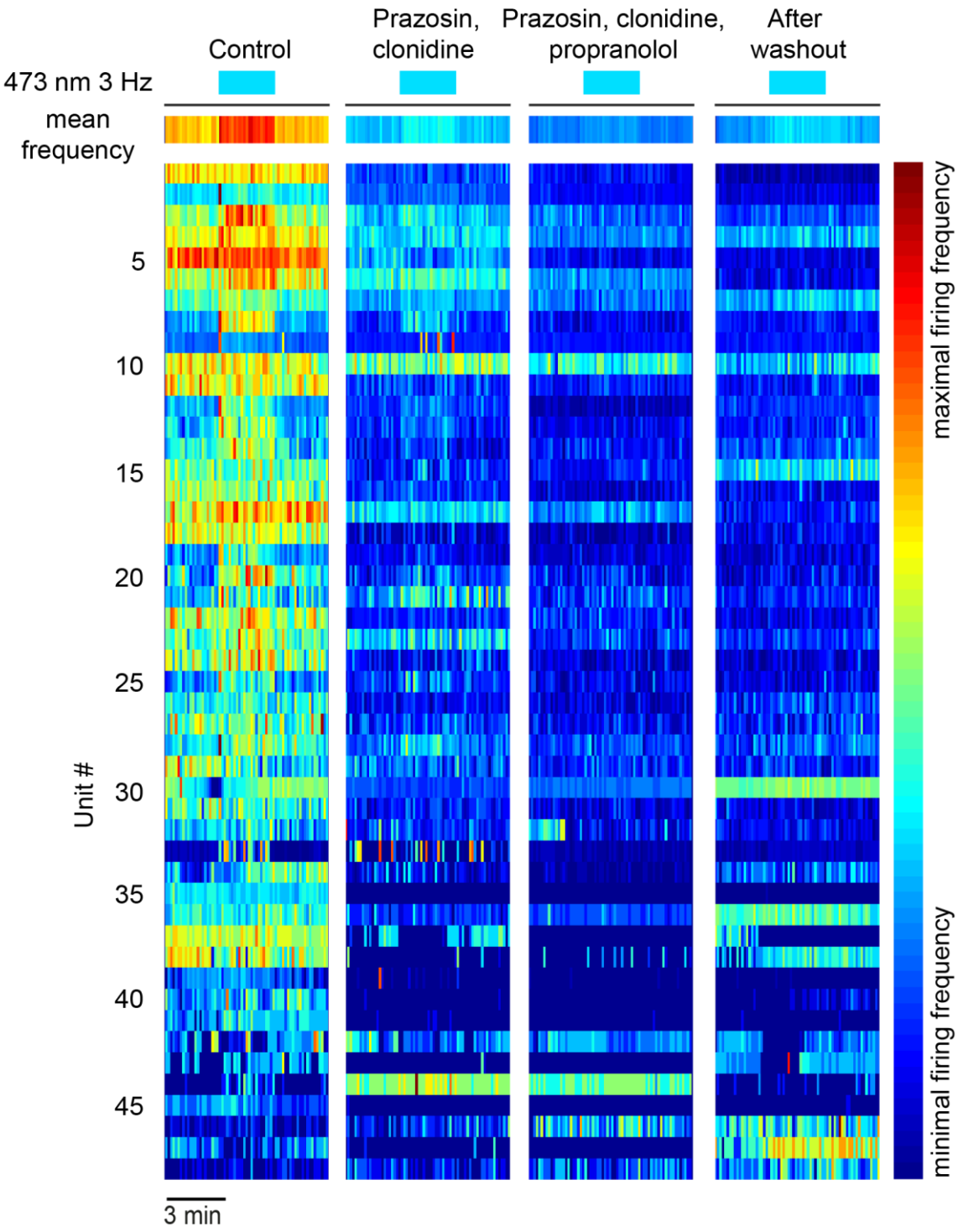

Figure 35 Exemplary unit recording with LC fiber stimulation during control, during NE α1+2 modulation, during NE α1+2 + ß modulation, and after 20 minutes washout.
Exemplary unit recording with 3 min 473nm 3 Hz light stimulation in control conditions (no drug applied), 2 µM prazosin + 10 µM clonidine (NE α1+2-modulation), 2 µM prazosin + 10 µM clonidine + 10 µM propranolol (NE α1+2 + ß modulation) and 20 min after washout (no drug applied). In the top row the mean frequency of all units is depicted. The frequency is color coded from minimal to maximal firing frequency for each unit individually.

After a set of control recordings with untreated ACSF, prazosin and clonidine were added to the ACSF supply (see Table 2). Under control conditions, the network activity increased in response to light stimulation (see Figure 36). Prazosin and clonidine treatment cancel this effect (see Figure 36). For the next set of recordings, in addition to prazosin and clonidine, propranolol was added to the ACSF supply (see Table 2). In these conditions the mean network activity was significantly reduced (see Figure 36; Statistics see Appendix table 8). Also, the activation of ChR2 did not increase network activity. After a 20 min washout phase with standard ASCF, the mean firing rate was still significantly reduced, compared to control conditions. The statistical analysis with a two way ANOVA reveals that there is a strong interaction between optogenetic stimulation and pharmacological modulation (see Appendix table 8A). This means that the effects of optogenetic stimulation were dependent on the pharmacological environment within the experiment.

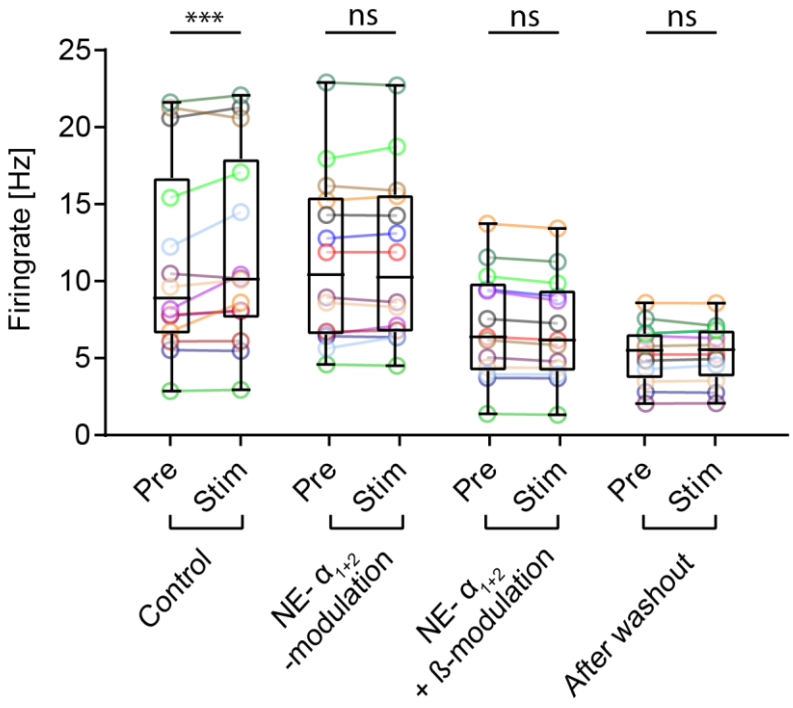

Figure 36 Frequency change in response to LC fiber stimulation in different NE-modulatory conditions.
Firing rate of n = 14 experiments in response to LC fiber stimulation in different NE modulated conditions. Boxplots show median firing rate with SD for all experiments. Statistics see **Appendix table 8**.

The two-dimensional structure of the MEA chips allowed me to anatomically locate units responding to the LC fiber stimulation. Under control conditions with untreated

ACSF, most of the firing frequency increasing units were located towards the center of the medial septum, rather than the limbs of the diagonal band of Broca. Under NE modulated conditions with prazosin, clonidine (and eventually propranolol), this heterogeneous distribution was not observed anymore. After washout, there was no difference between dorsal and ventral unit populations within the MSDB (see Figure 37, $n_{Control\text{-}dorsal}$ = 741, $\mu_{Control\text{-}dorsal}$ = 0.65 ± 2.03, $n_{Control\text{-}ventral}$ = 260, $\mu_{Control\text{-}ventral}$ = 0.55 ± 3.03, $p_{Control\ dorsal\ vs\ ventral}$ = 0.0296).

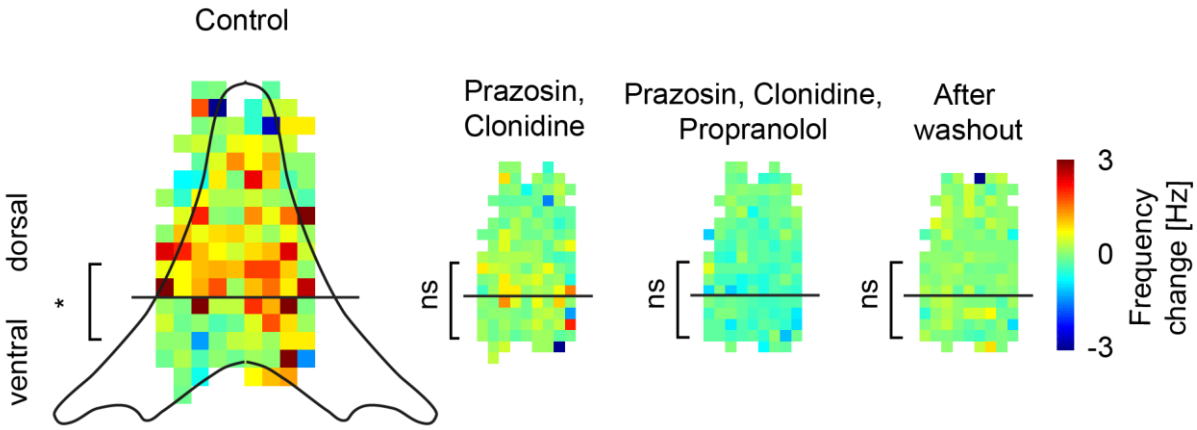

Figure 37 Anatomical distribution of unit responses to LC fiber stimulation under different NE modulated conditions normalized to baseline activity.
Color codes for firing frequency normalized to baseline activity [Hz]. Unit population (n = 1001) splits into 741 units dorsal and 260 units ventral. Differences between dorsal and ventral activity changes were tested with nonparametric Mann Whitney test.

3.3.5 Theta modulated units in MEA recordings

When recording extracellular activity of units in the MSDB, the identity of the recorded neurons remains largely unanswered. However, some characteristic features can be extracted. Next to firing frequencies and responses to optogenetic and pharmacological modulation, it was possible to sort the detected units according to their frequency modulation. The medial septum is crucial for the generation of LFP theta oscillations in the hippocampal formation (Buzsáki 2002). To assess theta modulation of individual units in the MSDB, the action potential (AP) timing was correlated to the phase of theta oscillation. By individually determining whether a MS unit was linked to the theta cycle, 225 out of a total of 1001 cells could be identified as preferentially active at distinct phases of theta (see example in Figure 38). Studies combining the histochemical identification of MSDB cells with patch clamp recordings have identified GABAergic cells as the predominantly theta-modulated cell population in the MSDB (Brazhnik and Fox 1999; Simon et al. 2006).

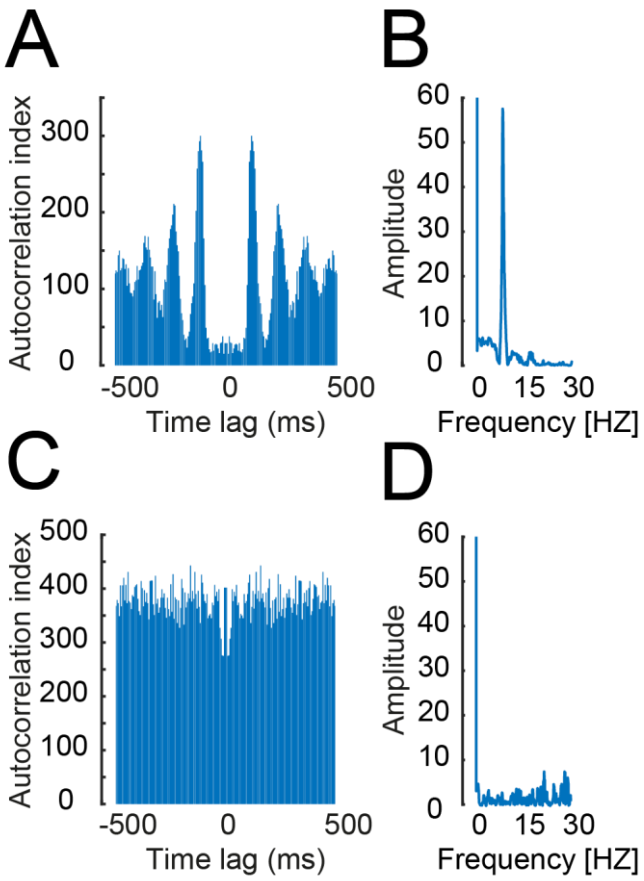

Figure 38 Example Units from MEA recordings with and without theta modulation.
A. Autocorrelation of an example theta modulated unit recorded in the MSDB formation. **B.** FFT of the autocorrelation displaying a peak at ~9 Hz. **C.** Autocorrelation of an example unit with no theta modulation, recorded in the MSDB formation. **D.** FFT of the autocorrelation displaying no peak between 4-12 Hz.

In 14 experiments, the mean proportion of theta units was 20.82 ± 8.78 % (mean ± SD; N = 14; see Figure 39A). 5 out of 14 experiments needed to be excluded from this analysis, because the MEA positioning did not cover the ventral diagonal band of broca. In the remaining 9 experiments, there were significantly more theta modulated units in the dorsal medial septum rather than the more ventral diagonal band of broca (see Figure 39C; N = 9; μ_{dorsal}=25.72 ± 8.97 [% of total units in dorsal], $\mu_{ventral}$=20.88 ± 9.482 [% of total units in ventral], paired t-test, p=0.0140, t=3,132). Within the theta range from 4 to 12 Hz, the units detected spread equally throughout the frequency range (see Figure 39B).

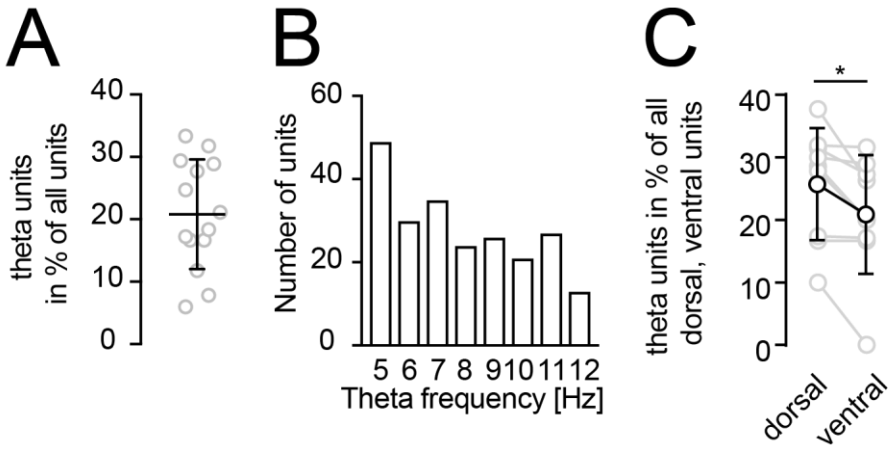

Figure 39 Analysis of theta modulated units in MEA recordings .
A. Proportion and mean+SD of theta units in n=14 experiments. **B.** Distribution of n=225 theta units across the theta frequency range. **C.** Proportion of theta units for dorsal and ventral units compared to total population across all experiments. Statistical analysis with paired t test.

The optogenetic activation of LC fibers in the MSDB led to an overall increase of activity during light stimulation (see Figure 30A). Units with theta modulated firing maintained their frequency tuning upon light stimulation but increased the amplitude, as seen in the FFT of the autocorrelation (see example in Figure 40).

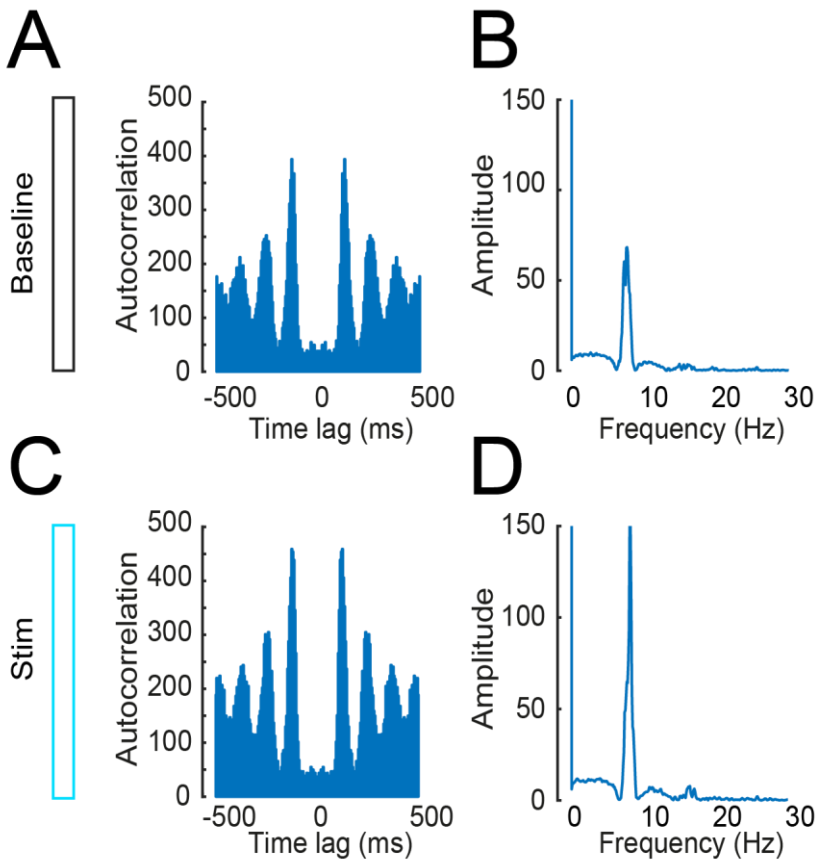

Figure 40 **Examples of unit theta-modulation with LC fiber stimulation in MSDB.**
A. Autocorrelation of an example theta modulated unit in baseline conditions without stimulation. **B.** FFT of the autocorrelation displaying a peak at ~9 Hz with an amplitude of ~70. **C.** Autocorrelation of the same unit during LC fiber stimulation in MSDB. **D.** FFT of the autocorrelation displaying a peak at ~9 Hz with an increased amplitude of ~150.

Although the optogenetic NE modulation of the MSDB network increased its general activity, the proportion of theta units per experiment remained stable (see Figure 41A). Also, the mean theta frequency of these units did not change (see Figure 41B). Only the amplitude of the autocorrelation FFT increased significantly (see Figure 41C; Statistics see Appendix table 9).

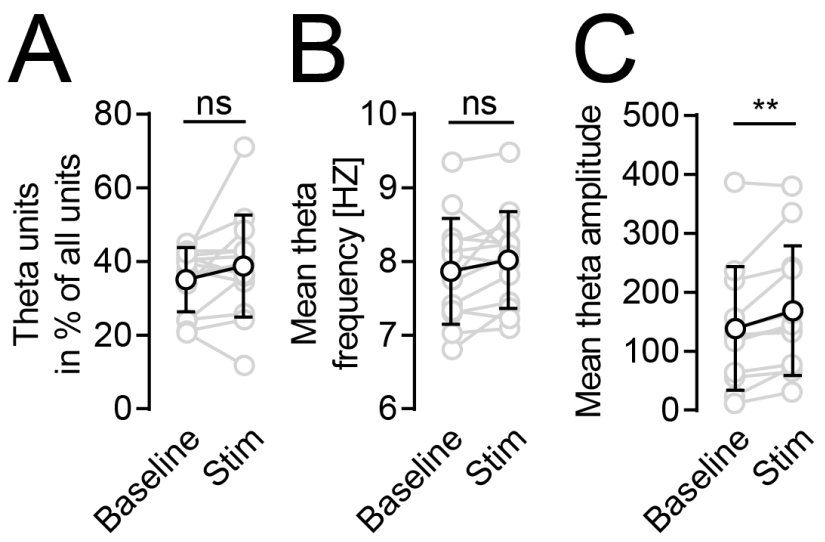

Figure 41 **Analysis of unit theta modulation upon LC-fiber stimulation in MSDB.**
A. Change of proportion of theta units with optogenetic NE modulation compared to baseline without stimulation. **B.** Mean theta frequency with and without stimulation. **C.** Mean theta amplitude with and without stimulation. Statistical analysis with Wilcoxon matched-pairs signed rank test (see **Appendix table 9**).

In order to investigate the modulatory influence of NE on the MSDB network activity, prazosin, clonidine and propranolol were added to the ACSF supply. In contrast to changes in the general network activity, units showing theta modulation did not change their internal properties. In comparison to control conditions, the proportion of theta modulated units and their frequency, as well as amplitude remained the same under different NE modulated conditions (see Figure 42A+B; Statistics see Appendix table 10).

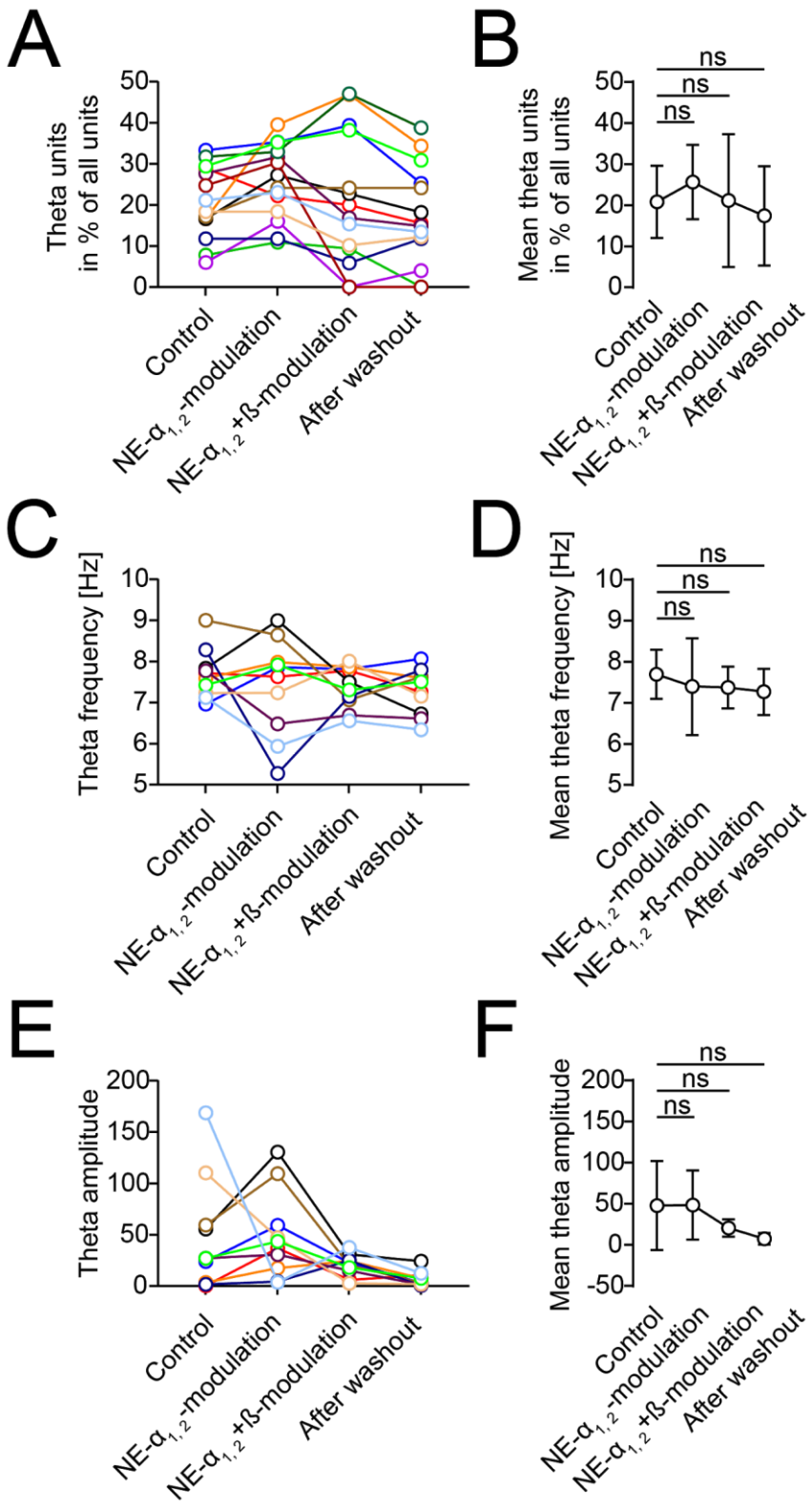

Figure 42 **Analysis of theta unit modulation in different NE-modulatory conditions.**
A. Proportion of theta units in single experiments (n=14) in different NE-modulatory conditions. **B.** Mean proportion of theta units in all experiments (Statistics see **Appendix table 10**). **C.** Frequency for theta modulated units in single experiments in different NE-modulatory conditions. **D.** Mean frequency of theta modulated units in all experiments (Statistics see **Appendix table 10**). **E.** Theta amplitude for theta modulated units in single

experiments in different NE-modulatory conditions. **F.** Mean amplitude of theta modulated units in all experiments (Statistics see **Appendix table 10**).

A closer look at the anatomical distribution of theta modulated units within the MSDB shows that the mean proportion of theta units in the dorsal medial septum was higher compared to the ventral diagonal band (see Figure 43B+D; Statistics see Appendix table 11). This distribution did not change with prazosin and clonidine modulating NE-α_{1+2}-receptor activity (see Figure 43D). With propranolol added to the ACSF supply, the variation between experiments increased, some showed a substantial loss of theta modulated units, some showed even an increase (see Figure 42A). On average, this led to a balancing of theta units between dorsal and ventral (see Figure 43B+D; Statistics see Appendix table 11). Even though the overall activity in the MSDB slices failed to recover after the 20 min washout period (see Figure 34B), the heterogeneous distribution of theta units between dorsal and ventral MSDB restored (see Figure 43D; Statistics see Appendix table 11). With a two way ANOVA the statistical analysis takes both factors, the anatomy (dorsal, ventral) and the pharmacological modulation into account (see Appendix table 11). It showed, that there is a significant difference between the proportion of theta modulated units in dorsal and ventral MSDB. The ANOVA also shows, that over the course of the experiment the pharmacological modulation was not a significant source for variation. Yet, the Sidak's multiple comparisons test of the different pharmacological treatments confirms, that the ratio between dorsal and ventral theta units changes (see Appendix table 11).

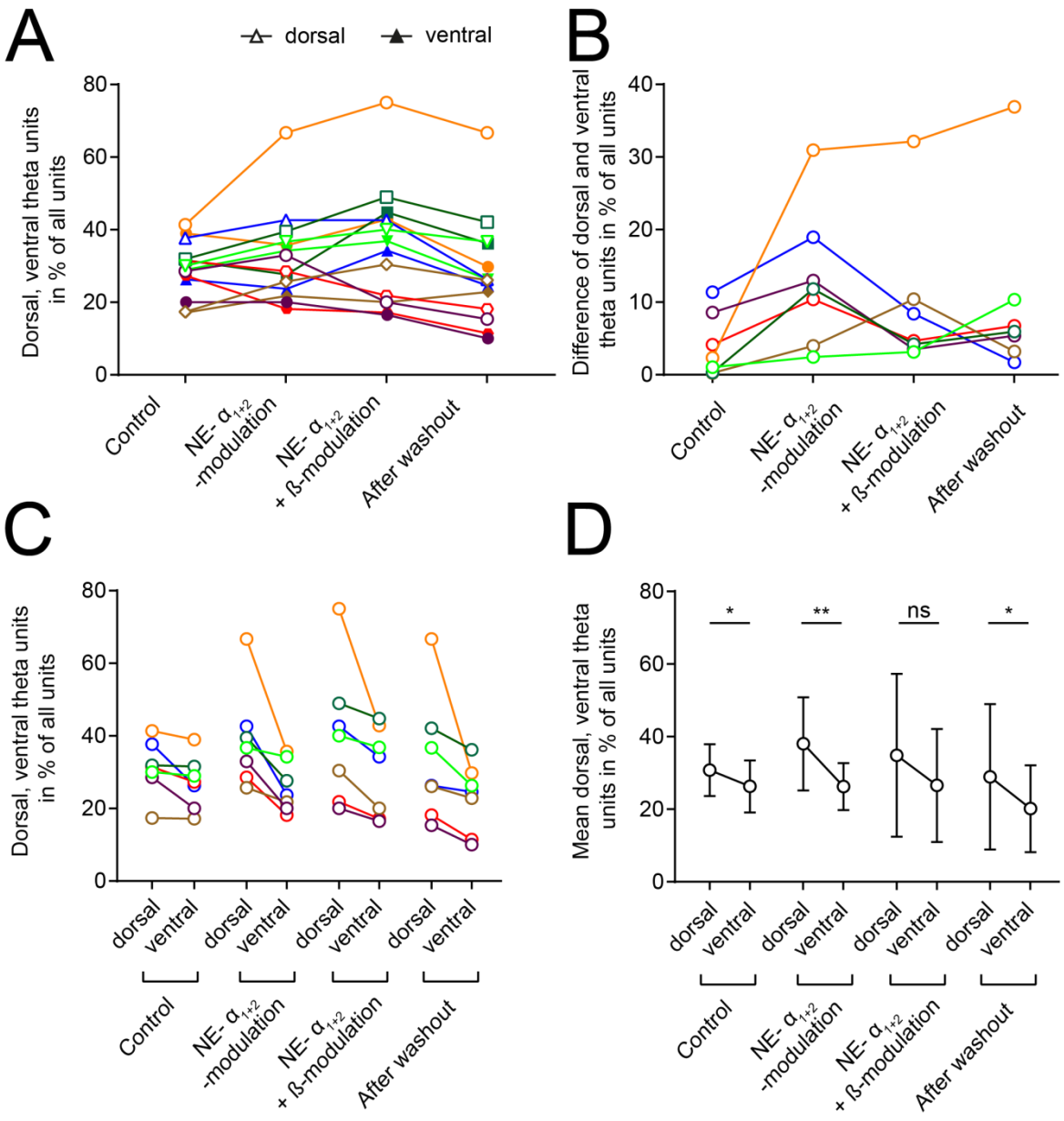

Figure 43 Proportion of dorsal and ventral theta modulated units in different NE modulated conditions.
A. Proportion of theta modulated units in % for all experiments (n=7) under control and pharmacological NE modulation conditions. Dorsal theta units are marked with open symbols and ventral theta units with solid symbols. **B.** Difference of dorsal and ventral theta modulated units in % of all units for all conditions. **C.** Direct comparison of dorsal vs. ventral theta modulated units in % for all experiments (n=7) in all conditions. **D.** Mean dorsal and ventral theta units in % of all units in different control and pharmacological modulation conditions. Statistical test were performed with a two-way ANOVA and Sidak's multiple comparisons test (see **Appendix table 11**).

The MEA experiments with optogenetic LC fiber stimulation and drug application show that the mean frequency increase of the MSDB network depends on intact NE input (see Figure 36). The number of theta modulated units did not change with LC fiber stimulation, regardless of the pharmacological conditions (see

Figure **44**A). Also, their frequency and amplitude did not change upon light stimulation (see

Figure 44C and E). The two way ANOVA analysis showed that indeed the optogenetic stimulation did not change the attributes of theta modulated units (see Appendix table 12). Instead, the pharmacological modulation resulted in significant differences in the number of theta modulated units and their amplitude, but not their frequencies (see Appendix table 12).

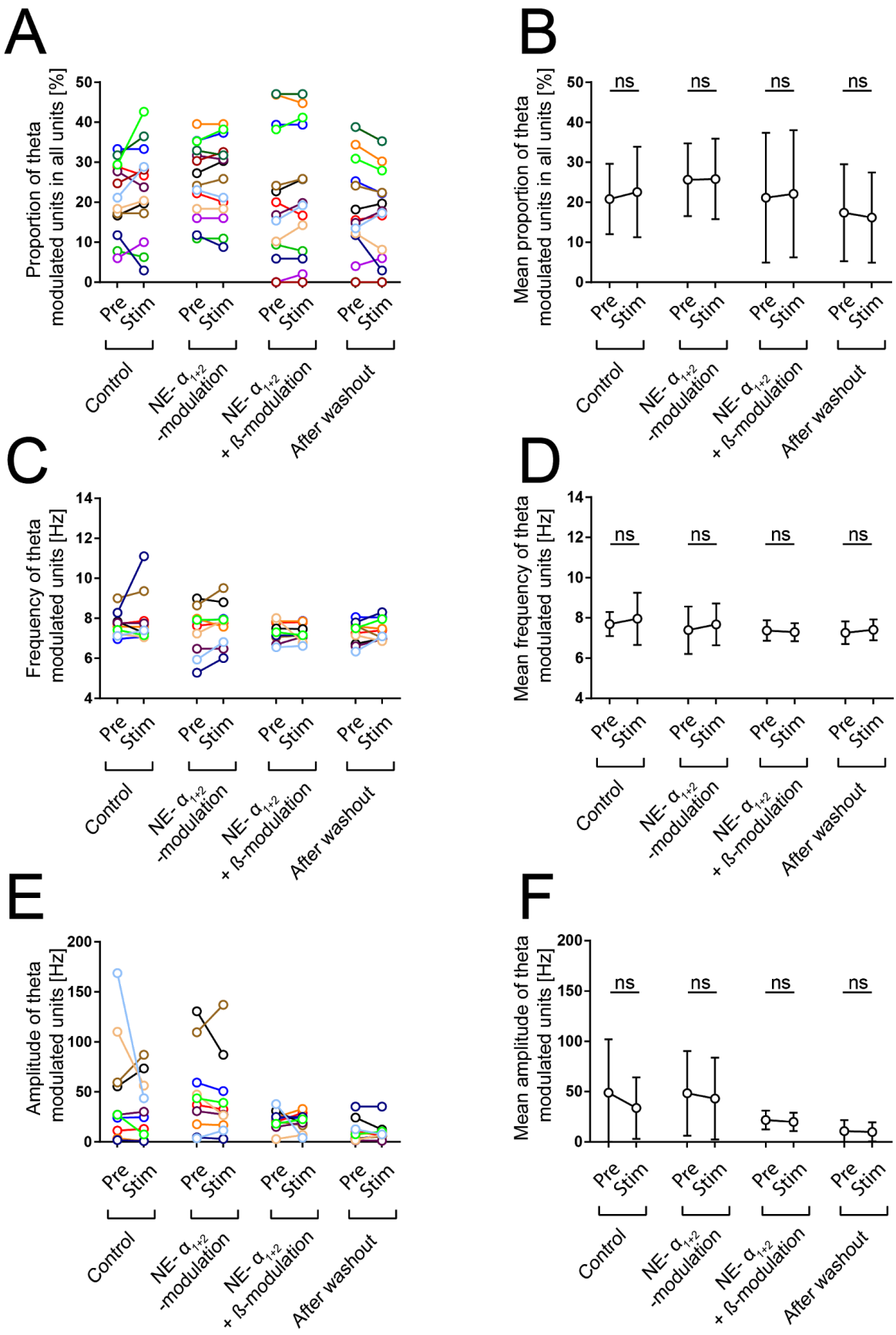
A
Proportion of theta modulated units in all units [%]
B
Mean proportion of theta modulated units in all units [%]
C
Frequency of theta modulated units [Hz]
D
Mean frequency of theta modulated units [Hz]
E
Amplitude of theta modulated units [Hz]
F
Mean amplitude of theta modulated units [Hz]
ns
Pre
Stim
Control
NE- α1+2 -modulation
NE- α1+2 + ß-modulation
After washout

Figure 44 Theta modulated units with LC fiber stimulation under different NE modulated conditions.
A. Theta unit proportion in n=14 experiments before and during LC fiber stimulation under different pharmacological NE modulated conditions. **B.** Mean proportion of theta units during optogenetic modulation in different pharmacological conditions. Statistical test: Two way ANOVA (see **Appendix table 12A**). **C.** Frequency of theta modulated units in baseline conditions vs. optogenetic stimulation. **D.** Mean frequency in different pharmacological conditions. Statistical test: Two way ANOVA (see **Appendix table 12B**). **E.** Theta amplitude during baseline and optogenetic stimulation with pharmacological modulation. **F.** Mean amplitude of theta modulated units before and during optogenetic stimulation in different pharmacological conditions. Statistical test: Two way ANOVA (see **Appendix table 12C**).

The investigation of network dynamics with the MEA has shown that the activity of units in the MSDB was modulated by NE release. Most of them increase their firing rate in response to the optogenetic stimulation of LC axon terminals. The pharmacological modulation confirms that these effects are mediated by ARs. How the drugs work individually cannot be said due to the simultaneous application. In addition, a general rundown of the brain-section viability must be taken into account when interpreting the effects. The analysis of the unit firing revealed theta modulated units in the MSDB. These were not affected by LC fiber stimulation, though.

3.4 Response of glutamatergic cells in MSDB to optogenetic LC fiber activation and pharmacological NE modulation

My in vivo experiments have shown, that the optogenetic stimulation of ChR2 in LC axonal projections in the MSDB region lead to changes in locomotor behavior. The MEA experiments further confirmed that the MSDB network is modulated by noradrenergic innervation. Fuhrmann et al. (2015) have identified the functional link between VGluT2 + cells in the MSDB and A / O interneurons in the hippocampus as the basis for speed modulation. To find out if VGluT2 + cells are modulated by the noradrenergic system, patch clamp experiments in MSDB slice preparations were performed. The experimental setup resembles the MEA experiments conducted before. For patch clamp experiments, 8 VGluT2-Cre transgenic mice were used. In order to label glutamatergic cells in the MSDB, a virus carrying the floxed coding information for tdTomato was stereotactically injected into the MSDB (see Figure 45A). The patched cells showed characteristic response patterns of VGluT2+ cells to −200 pA and +500 pA current injections (see Figure 45B). In addition, unfloxed ChR2-EYFP was injected bilaterally into the LC (see Figure 45A). As a result, mice showed green labeled NE fibers in the MSDB descending from the LC and red labeled glutamatergic cells in the MSDB (see Figure 50). For optogenetic stimulation, a light fiber was placed

in close proximity to the recording site. Also the wash in of the NE ligands prazosin, clonidine and propranolol was prepared like before with the same concentration.

The optogenetic stimulation pattern was 3 Hz for 3min with 20 mW, analogous to previous experiments. Cells that responded to light stimulation showed an immediate and closely coupled depolarization response to the light stimulus, followed by a slow decay back to resting potential (see example in Figure 45C). With faster stimulation, this effect summed up to a lasting depolarization plateau with triggered AP (see example in Figure 45D). After light stimulation, the membrane potential went back to resting levels.

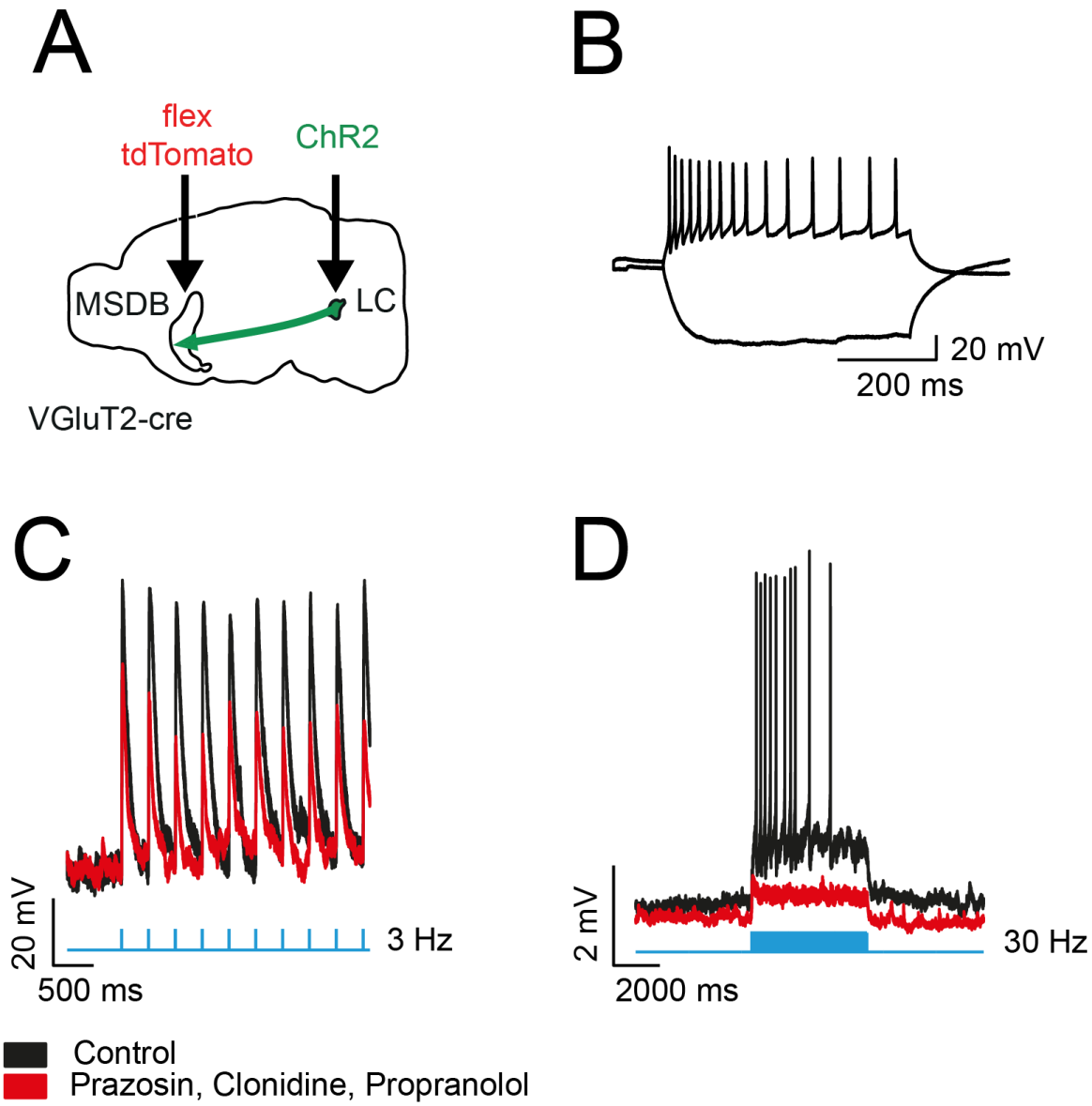

Figure 45 **Example units from patch clamp experiments in MSDB.**
A. Injection scheme for patch clamp experiments. With unfloxed ChR2 injected in the LC bilaterally, transfecting all afferents from the LC. In addition floxed tdTomato was expressed in VGluT2+ MSDB cells. **B.** Characteristic response pattern of VGluT2+ MSDB cell to −200 pA and +500 pA current injections. **C.** Example patch clamp recording from a VGluT2+ identified unit in MSDB showing depolarization responses upon 3 Hz light stimulation of LC fibers. Recording under control conditions is shown in black. Pharmacological NE modulated conditions with prazosin, clonidine and propranolol are shown in red. **D.** Same unit as in A with 30 Hz stimulation.

Analogous to the *in vivo* experiments and the MEA recordings, ChR2 in LC axon terminals was optogenetically activated with a light fiber emitting 473 nm light onto the MSDB region of the brain slice. In total, 28 red labeled putative glutamatergic cells were recorded, from which 10 showed an electrophysiological response to the LC fiber stimulation. The majority of those cells (n=8) was located in the dorsal MS region rather than the ventral DB region (see Figure 46A; Statistics in Appendix table 13). The

mean depolarization of all cells upon light stimulation under control conditions was 9.38 ± 8.80 mV. Under the influence of prazosin, clonidine and propranolol, this effect changed to 7.82 ± 4.90 mV in average (see Figure 46C). This change turns out to be insignificant in the test, although the statistical starting point is probably underpowered (see Appendix table 14).

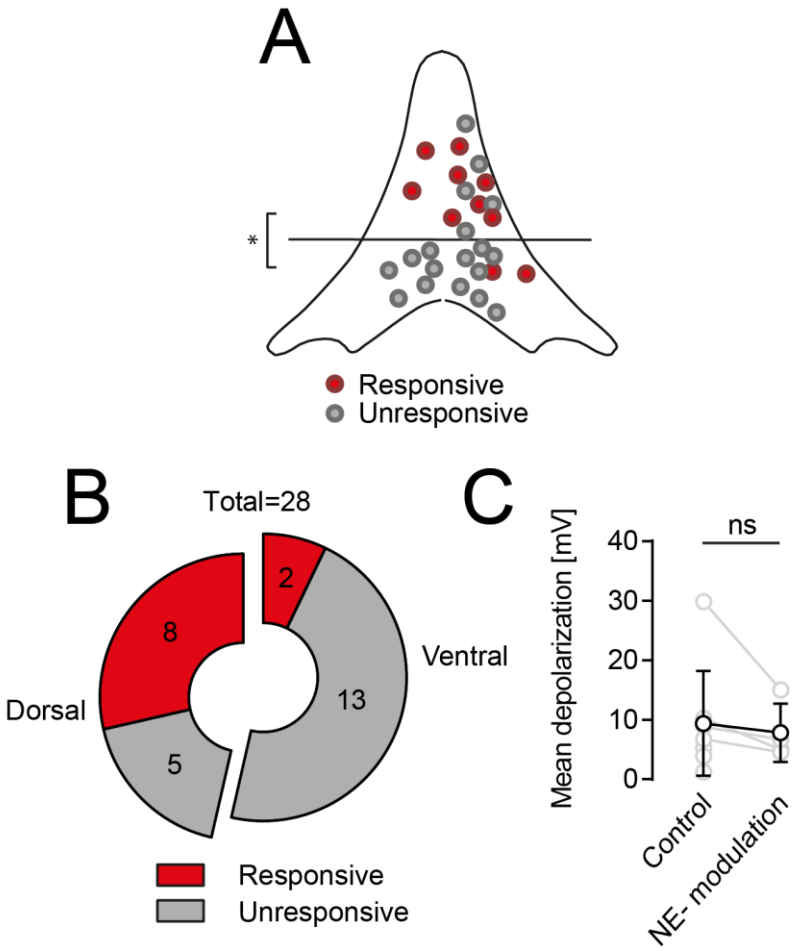

Figure 46 **Analysis of patch clamp recordings of VGluT2 identified units in MSDB.**
A. Spatial distribution of n=28 red labeled recorded cells. Cells responding to the optogenetic LC fiber stimulation are marked in red. Unresponsive cells are marked in grey. Statistical test: Contingency, Fisher's exact test (see **Appendix table 13**). **B.** Proportions of responsive and unresponsive glutamatergic cell in the dorsal and ventral MSDB **C.** Mean depolarization response upon LC fiber stimulation of n=10 cells under control conditions and n=4 cells under pharmacological NE modulated conditions. Statistical test: Wilcoxon matched-pairs signed rank t-test (see **Appendix table 14**).

Glutamatergic cells patched in MSDB slice preparations showed clear responses to the optogenetic stimulation of long range LC projections. The proportion of responsive cells was significantly higher in the dorsal MS then the ventral DB. Upon phasic light stimulation they show clear sharp depolarization events with short decay times. With high-frequency stimulation, this depolarization adds up to a plateau in which even

action potentials are triggered. The pharmacological modulation with NE ligands showed only mild non-significant effects.

3.5 Histology: Stereotactic LC injection and hybrid fiber placement

3.5.1 Expression in LC

Floxed ChR2, green labeled with EYFP, was selectively expressed in NE cells in the LC in both hemispheres (see Figure 47). After completion of each experiment, each animal's brain was removed and stored in PFA. To validate ChR2-EYFP expression, all brains were sliced at 50 µm thickness using a Leica VT-1200S vibratome (Leica Microsystems, Wetzlar, Germany). The green fluorescence of the EYFP tag was enhanced with an anti-GFP immunostaining (abcam ab5449, goat polyclonal), resulting in brightly green labeled NE cells and projecting fibers in the region of the LC.

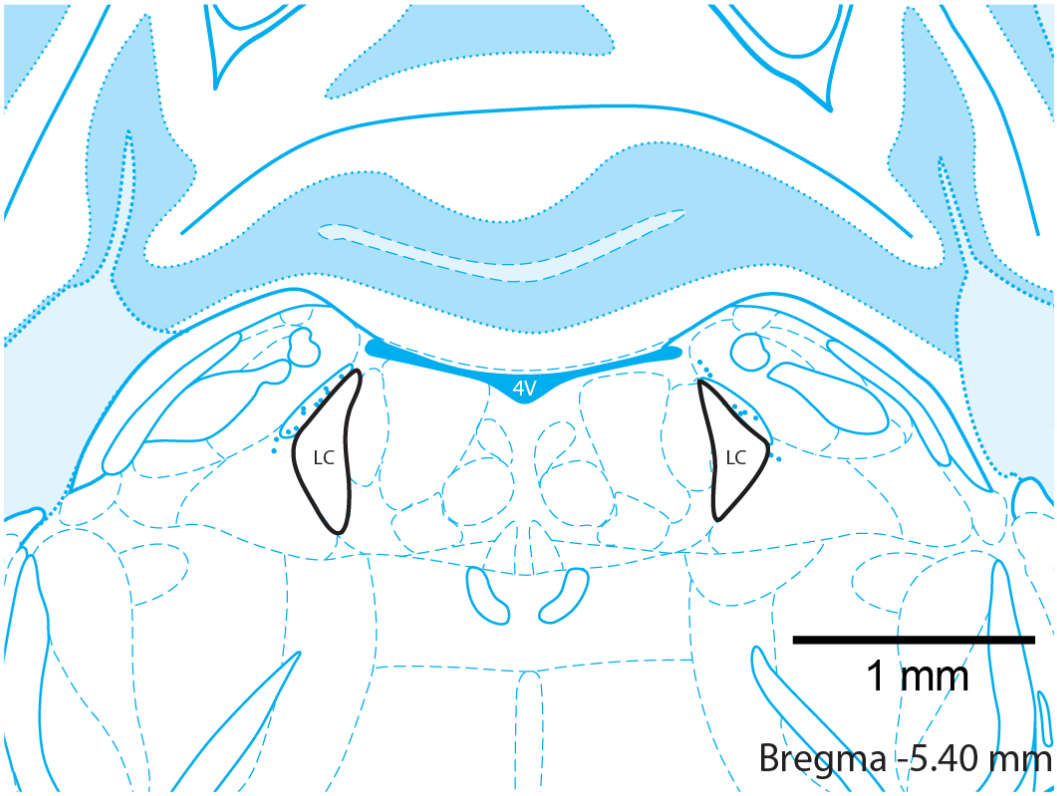

Figure 47 Location of the LC in the brainstem, bilaterally. See Franklin & Paxinos "The mouse brain in stereotactic coordinates".
Schematic atlas drawing of the anatomical position of LC, 5.4 mm caudal of Bregma, in the brainstem.

Histological sections show locally confined expression of ChR2-EYFP in the LC area. Green labeled fibers indicate that projecting neurons carry ChR2 along the fibers towards the targeted presynapse (see example in Figure 48A). A more detailed view at higher magnification also reveals green labeled somata of ChR2-EYFP expressing NE cells (see example in Figure 48B).

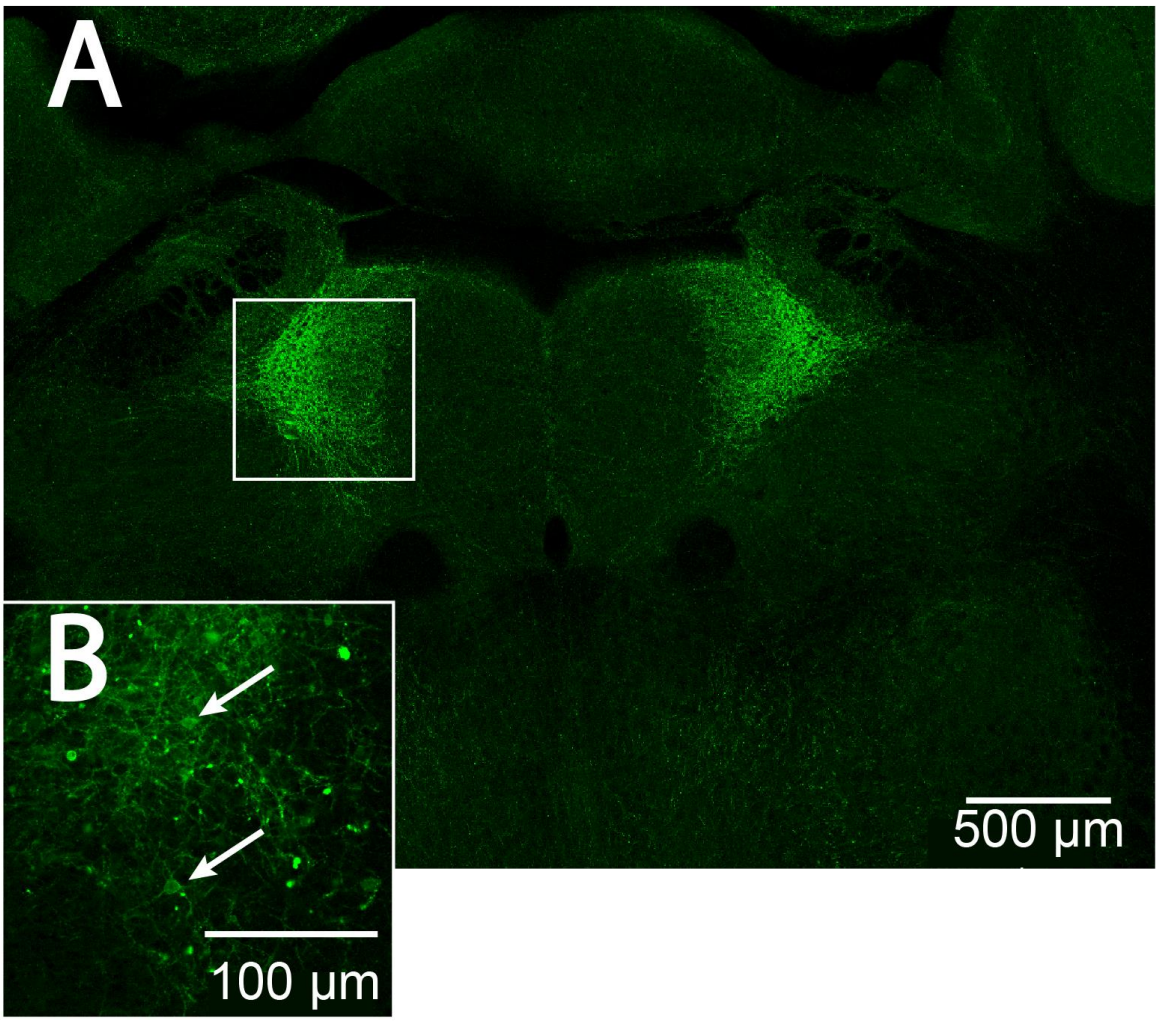

Figure 48 ChR2-EYFP expression in LC, bilaterally.
In **A.** both LC nuclei with widespread green fluorescent projecting fibers can be seen. **B.** shows a detail including labeled NE cell bodies.

3.5.2 LC axon fibers in MSDB and hybrid fiber placement

Injecting floxed ChR2 with an EYFP fluorescence tag in both LC nuclei resulted in green labeling of the noradrenergic system's extensively descending projections. Green fibers in the MSDB area confirmed that also the basal forebrain is targeted by the LC (see example in Figure 49B). For each mouse tested in *in vivo* experiments, the existence of such green projecting fibers was confirmed in histological slices of 50 µm

thickness. Additionally, the positioning of the hybrid fiber used for light and drug delivery was confirmed and compared to the Paxinos mouse atlas for each animal (see example in Figure 49A).

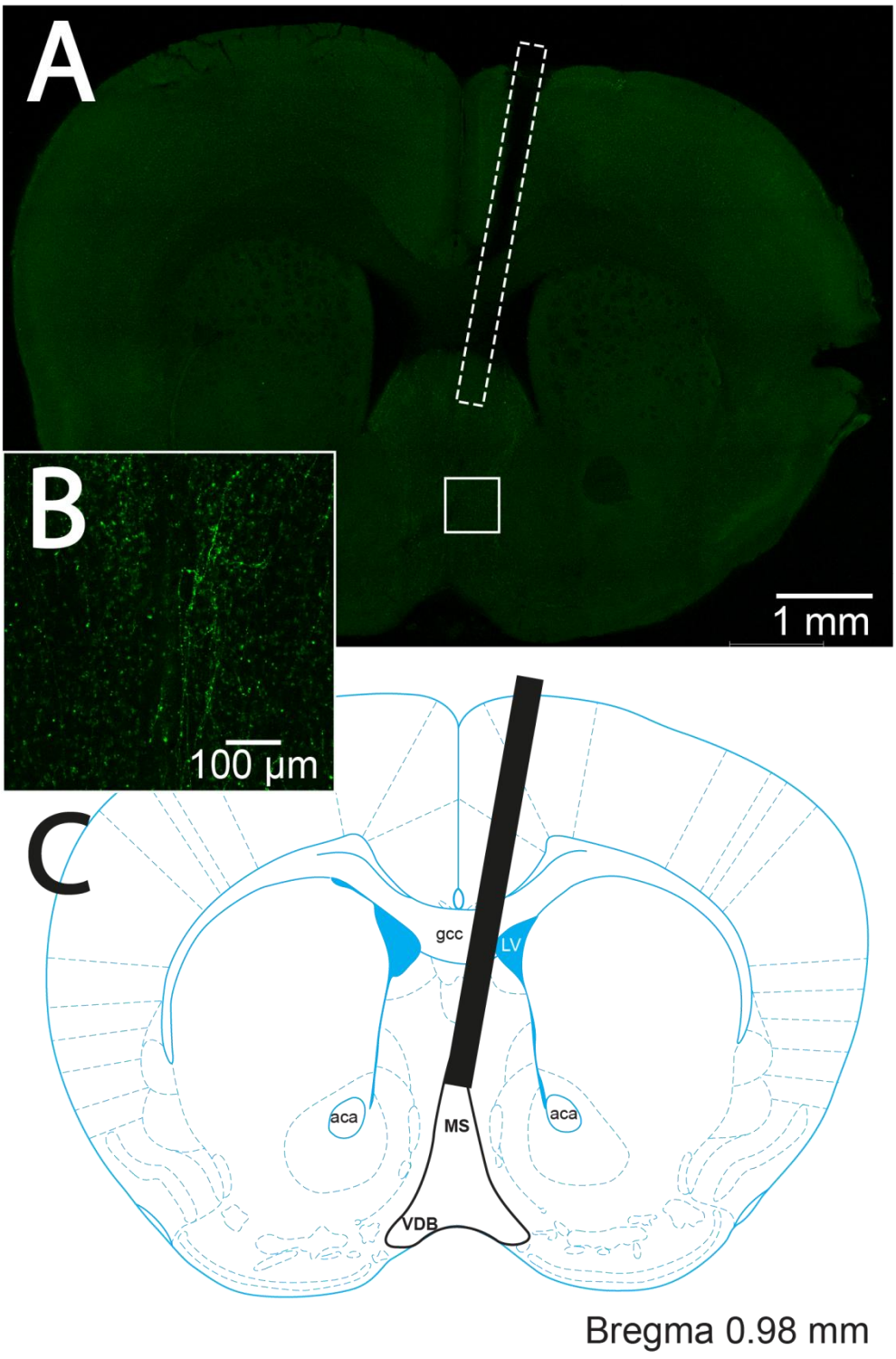

Figure 49 Hybrid fiber positioning in a coronal brain section including MSDB.
A. shows a coronal brain section including the MS and VDB area. **B.** Detail, with green

fluorescent axonal projections from LC in the MSDB area. **C.** The position of the hybrid fiber is indicated in white and compared to the Paxinos mouse brain atlas.

3.5.3 Red labeled cells and green fibers from LC in patch clamp experiments

For single cell recordings, VGluT2-Cre mice were injected with floxed tdTomato in the MSDB. In addition, unfloxed ChR2 labeled with green fluorescent EYFP was stereotactically injected into LC bilaterally. For all patch clamp experiments, red labeled cells were patched and green fluorescent descending LC fibers were confirmed (see Figure 50A).

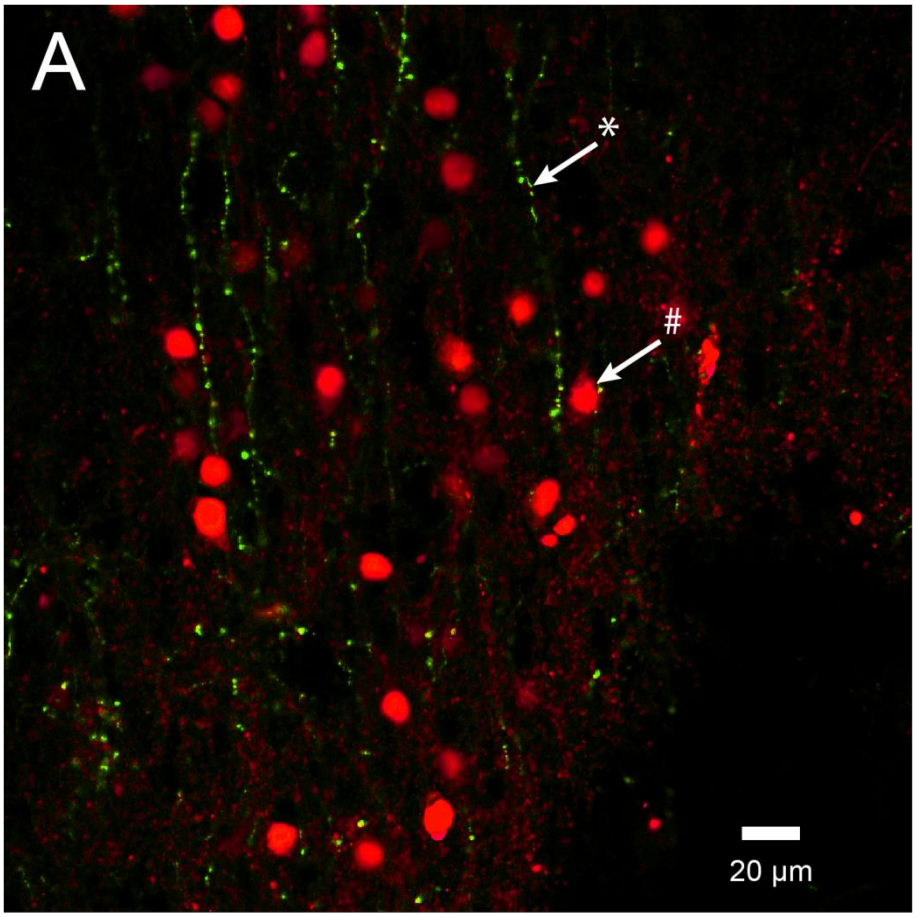

Figure 50 MSDB sagittal VGluT2-Cre brain slice with red labeled glutamatergic cells and green labeled descending fibers from LC.
VGluT2-Cre mice were injected with floxed tdTomato to label glutamatergic cells in the MSDB (arrow #). In addition, unfloxed ChR2 tagged with green fluorescent EYFP was injected in LC bilaterally in order to label descending NE fibers in the MSDB (arrow *).

4 Discussion

It is not fully understood how different levels of arousal modulate the integration of environmental information and locomotor behavior (Devilbiss et al. 2006). Many previous studies addressed the role of the noradrenergic system in regulating neuronal activity in virtually all brain regions (Berridge and Waterhouse 2003; Carter et al. 2010; Stone et al. 2003; Chandler 2016). The LC in particular has largely been studied for its influence on sleep to wake transition (Berridge et al. 2012; Rho et al. 2018). The present study investigated the physiological processes that are involved regulating locomotor behavior. It was shown that NE enhances motor neuron responsiveness to alerting stimuli (Nam and Kerman 2016; White et al. 1996; White and Neuman 1980). The central structure for declarative memory consolidation, including navigational purposes, is the hippocampus (Morris et al. 1982). Fuhrmann et al. (2015) showed, that in addition to environmental attributes such as location and heading direction, running speed is also integrated in the CA1 region of the hippocampus. A structure that integrates sensory information and forwards them to the hippocampus is the MSDB, located in the basal forebrain (Wallenstein and Hasselmo 1997). The present study confirmed existing models on the noradrenergic innervation of the MSDB and adds significant insights on both MSDB network regulation and single cell modulation. By stimulating glutamatergic cells in the medial septum Fuhrmann et al. were able to demonstrate a modulation of locomotor behavior. Direct modulatory, bidirectional connections between the hippocampus and the LC have been described before (Takeuchi et al. 2016; Smith and Greene 2012). In contrast, this thesis investigates the modulatory influence of the LC on locomotor behavior via the path of MSDB and HC. It extends previous approaches by investigating the influence of noradrenergic modulation on MSDB network activity on three experimental levels: Running behavior on the linear treadmill, MSDB population activity on the MEA, and single cell patch clamp recordings.

The main findings of this study are:

(1) The optogenetic stimulation of LC-MSDB projections in vivo lead to increased running behavior, in terms of running initiations and the total time spent running, but not running speed. Pharmacological modulation confirmed that the changes in behavior were dependent on ARs in the MSDB. At the same time hippocampal LFP was not changed.
(2) In vitro stimulations of LC-MSDB projections increases the firing rate of single units recorded on the MEA. Reactive units are located mostly in the dorsal MS.

Pharmacological modulation confirms that changes in MSDB network activity are mediated by ARs. Theta modulated units are located in the dorsal MS and are modulated by NE pharmacology.

(3) Patch clamp experiments of VGluT2+ cells in MSDB slice preparations show responses to optogenetic activation of LC afferents. Reactive cells are mostly located in the dorsal MS. Pharmacological modulation barely affects VGluT2+ cells.

4.1 Baseline running

Mice have relatively high activity levels per day. When given access to running wheels, mice run for a total distance of ~4 to 20 km per day and a total activity time of ~3 to 7 hours a day (Manzanares et al. 2018). Remarkably, this behavior is also observed in feral wild mice when running wheels are placed in nature (Meijer and Robbers 2014). Motor pathways in vertebrates are largely consistent across classes and share similar neuroanatomical structures. Local control of muscle movements is regulated by pools of motor neurons in the spinal cord that are part of a dispersed locomotor central pattern generator network (Goulding 2009). Descending reticulospinal, rubrospinal and vestibulospinal pathways control the locomotor network in the spinal cord (Berridge and Waterhouse 2003). The reticulospinal pathway, including the LC, is the primary pathway for initiating locomotion (VanderHorst and Ulfhake 2006; Mogenson et al. 1980). Motor actions are also initiated by the motor cortex, via descending projections to the motor neurons in the spinal cord. The cerebellum serves as a feedback and control center, which integrates sensory and internal feedback (Goulding 2009). In this way it optimizes motor pattern and coordinates motor behaviors.

To understand the influence of the LC and the noradrenergic system on behavior, this study has focused on locomotor behavior measured on a linear treadmill. The treadmill reduces behavioral flexibility but allows a precise readout of the different running modalities like, velocity, initiations and duration. However further studies with freely moving animals will be needed to investigate the influence of the NE system on behavior in a broader context. The mice used in this study were carefully handled and well trained to the experimental setup. Head fixed and centered on a freely circulating belt, the mice were able to show voluntary running movement following their natural habit. The movement on the belt can be reduced to a chronological sequence of resting and running phases. Typically, this movement occurs in short bursts of running, lasting between 5-20 s. This pattern resembles the behavior of a mouse in a novel

environment, exploring or food seeking (Loos et al. 2014; Navarro-Castilla et al. 2018). The amount of running periods reflects the level of arousal the mouse is experiencing, with comparatively less running behavior in phases of calm exploration, compared to many running phases during stress or excitement (Zimprich et al. 2014).

4.2 Optogenetic LC fiber stimulation in MSDB increases locomotor behavior

In order to simulate increased LC activity, noradrenergic fibers in the MSDB were stimulated optogenetically using blue laser activation of ChR2. Stimulating NE fibers in the MSDB activates one aspect of an elaborate system that in its entirety is suited to deal with positive stimuli (food, social interaction) as well as threats (predator). Stimulating all NE fibers in the MSDB is comparable to a state of high arousal, how it can be observed in situations of increased arousal, e.g. social interactions, alertness, food seeking. In response, the mouse shows physiological signs of arousal, such as increased skin conductance, higher grooming rates, changes in pupil diameter and more movement (DiNuzzo et al. 2019; Joshi et al. 2016; Naegeli et al. 2018). In this study, I was able to show functionally and in histological preparations, that the MSDB receives long-range NE input from LC by injecting ChR2-EYFP bilaterally in LC. This study confirms the anatomical connection between the basal forebrain and the LC via the dorsal noradrenergic bundle with long-range green fluorescent fibers, visible in the histological MSDB preparations, as it was first described by Pickel et al. (1974). The stimulation of the descending LC fibers results in an increase in running behavior, in terms of running initiations and the total time spent running (see Figure 12 C and D), but not running speed (see Figure 12 A). Fuhrmann et al. (2015) describe the role of the MSDB and its connection to the HC on locomotor initiation as well as running speed. They found that glutamatergic neurons projecting to HC alveus/oriens interneurons not only communicate running speed but also predict movement onsets. Doing so, the running speed of the mice increased with the stimulation frequency (Fuhrmann et al. 2015). The running behavior in these experiments was not self-determined and, especially with higher stimulation rates, exceeded the running speed the mice were showing during voluntary running. The observations made in the present study also suggest a direct involvement of the MSDB in the initiation and control of locomotor behavior, but in contrast to the direct optogenetic stimulation of glutamatergic neurons, the global activation of NE afferents in the MSDB does not

seem to address the same speed controlling mechanisms that were described by Fuhrman et al., or at least not to the same extent. In contrast, it has been shown that all cell types in the MSDB receive noradrenergic input, with GABAergic cells being the major target (Kitchigina et al. 2003). This functional link provides the basis for a working model that combines the results of this study with the current knowledge about the functioning of the MSDB and its role in the modulation of locomotor behavior (see Figure 51).

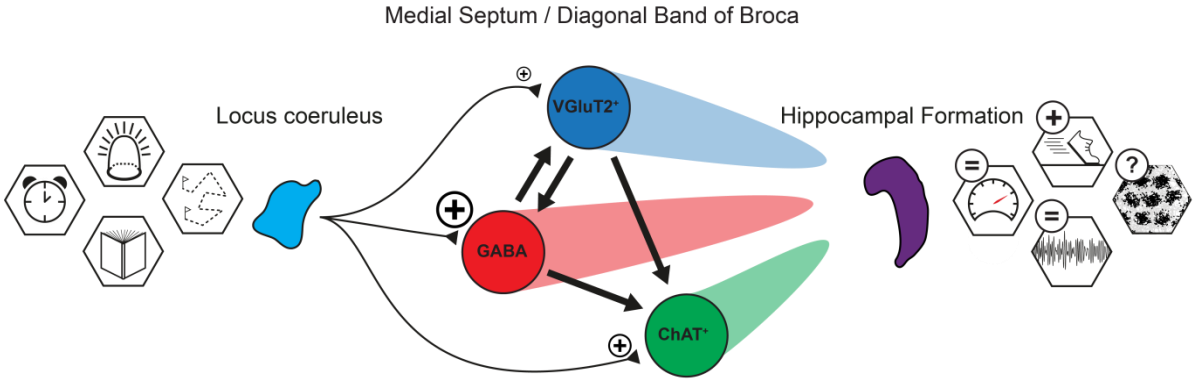

Figure 51 Scheme of the modulatory influence of the LC on the MSDB network and the downstream effects on behavior controlled by the hippocampus.
The Locus coeruleus is the central nucleus of the noradrenergic system, controlling sleep to wake transition, excitation state, navigational behavior and cognitive functions. All cell types in the MSDB receive direct input, with GABAergic cells being the main target. In response to noradrenergic stimulation, the MEA experiments show a focus of excitement in the dorsal region of the MSDB, the region with the highest proportion of GABAergic cells. Patch clamp experiments show that only a fraction of VGluT2 + cells respond to noradrenergic stimulation. Pharmacological modulation suggests that the response of glutamatergic cells is characterized by the input of GABAergic and cholinergic cells. This way, LC might influence the vigor of locomotion, but not directly the speed.

Building up on the findings of Fuhrmann et al. (2015), this thesis extends the role of the MSDB as an integrational hub for running related information to a dedicated site of action for the NE-system to modulate locomotor involved behavior in general. In contrast to the direct stimulation of glutamatergic neurons in MSDB like it was done from Fuhrmann et al. the optogenetic stimulation of LC afferent fibers in MSDB did not result in an immediate onset of running. The mice kept their natural pattern of movement, consisting of alternating short phases of rest and running. The running speed never exceeded the natural behavior the mice showed during baseline running. The direct stimulation of glutamatergic neurons compared to the indirect modulation via stimulated NE afferents resulted in an alternative activation of the MSDB network.

Locus coeruleus neurons fire tonically from 1–3 Hz during awake states, decrease firing during NREM sleep, and are virtually silent during REM sleep (Aston-Jones and

Bloom 1981; Berridge et al. 2012). During the presentation of salient stimuli cells of the LC show phasic short bursts (500ms) of 8-10 Hz (Sara 1998). Discharge activity varies substantially among LC neurons. Yet, cells ensembles with similar efferent forebrain projections show correlated activity (Totah et al. 2018). Studies suggest that several functional properties of LC neurons vary according to their terminal field projection (Chandler et al. 2014). LC cells also change their firing rate in response to the presented stimuli. Discrete and moderately aversive stimuli result in a heterogeneous and patterned activation of LC neurons. However, the same populations were robustly co-activated in response to more intense aversive experiences (Uematsu et al. 2017).

Results such as these suggest that the MSDB is also innervated with varying frequency. Future experiments could further investigate the precise release rates of NE within the MSDB. New tools, like a genetically encoded fluorescent NE sensor, enables tracking of the intensity and timing of NE release in LC terminal fields on a millisecond time scale in behaving animals (Feng et al. 2019). In this way, it is possible to identify stimulation frequencies that are based on the natural input of LC.

4.3 Yellow-laser control

The control experiment with a long wavelength laser confirms that the effects on running behavior due to the optogenetic stimulation of LC fibers in the MSDB is caused by the specific activation of ChR2 with blue light. All other aspects of the light stimulation, such as the light fiber placement, the energy emission or light emission in general does not change the spontaneous running behavior the mouse is showing on the treadmill (see Figure 17). For future experiments, an additional control group expressing only EYFP could rule out potential stimulatory effects blue light might have on the mouse's visual system. Comparable control experiments in similar studies have shown that stimulation with 473 nm light does not lead to behavioral changes (Carter et al. 2010).

4.4 Optogenetic LC fiber stimulation does not alter hippocampal LFP

When moving through an environment, EEG measurements of the hippocampus show rhythmic activity in the theta range (Buzsáki 2002). This sign of arousal is considered key for processing sensory information and integration with memory within the hippocampus (Sugisaki et al. 2011; Vertes and Kocsis 1997). One relay station for passing sensory information towards the hippocampus is the septal formation,

including the medial septum and the diagonal band of Broca (Tsanov 2015). It is connecting the hippocampus with other limbic and cortical regions, involved in memory processing (Rolls 2015). With a large percentage of MSDB neurons showing rhythmic activity in the theta range, the MSDB is known as the central pacemaker for the hippocampus (Robinson et al. 2016; Hangya et al. 2009). Consequently, hippocampal theta is disturbed when fimbria fornix, the connection between MSDB and HC, is destroyed (Hagan et al. 1988).

LFP recordings during running in stimulated versus control conditions reveal further differences between direct stimulation of MS glutamatergic neurons as it was performed by Fuhrmann et al. (2015) and the indirect modulation of the MSDB network by LC fibers. When driving glutamatergic cells in the MS and also their afferents in the HC formation, the oscillations within CA1 adapted to the frequency of the light stimulation. This effect held true for different frequencies accompanied by the respective speeds of the evoked running behavior. In this study, the stimulation of LC efferents in MSDB, also resulted in altered running behavior but simultaneously recorded LFP in CA1 showed no significant changes, in terms of frequency and power, compared to unstimulated conditions. This holds true for resting and running phases (see Figure 19B + D).

The results of this study underline the role of the MSDB as an integrating hub for incoming sensory information (McBurney-Lin et al. 2019). The LC modulates the activity of the MSDB network and its output to downstream structures. As a result of the artificial activation of LC afferents in the MSDB, the mice spent more time running. However, the integrating function of the MSDB ensures that this behavior remains in the natural limits. With the increased running, the theta oscillations in the hippocampus increased as well, also within the natural limits.

4.5 Pharmacological NE modulation in MSDB affects locomotor behavior

The optogenetic stimulation of LC axons in MSDB resulted in increased locomotor behavior (see Figure 15). In order to confirm the involvement of AR in these effects, pharmacological ligands for all three AR were administered locally into the MSDB. The modulatory effects on baseline and stimulated running behavior were recorded on the linear treadmill. Upon administration of these ligands, locomotor behavior increased, independently of the optogenetic stimulation (see Figure 22). In fact, no further

changes in running behavior could be observed by optogenetic stimulation (see Figure 24).

This experiment initially started with six animals, but difficulties during surgery and post-hoc controls left only two animals to analyze. The results of two animals do not allow a comparative statistical analysis, let alone a conclusive statement on the investigated processes. Nevertheless, the results can be considered as an indication that must be confirmed in future experiments with more animals.

4.5.1 Antidromic impulse conduction towards LC as a consequence of local axon stimulation in MSDB

The idea of activating ChR2 in axon terminals is to depolarize the presynaptic membrane, and ultimately to release neurotransmitter vesicles. Even if the exact process has yet to be confirmed in future experiments, the results of this study suggest a modulating effect through optogenetic stimulation. As with all artificial stimulations, antidromic impulse conduction originating in the stimulated fiber terminals towards the LC needs to be considered (McCall et al. 2017). The LC is connected to a variety of movement related areas, including the motor cortex (Aston-Jones and Waterhouse 2016; Chandler 2016). The activation of ChR2 in LC axon terminals in the MSDB region might lead to an antidromic activation of LC and therefore secondary recruitment of downstream motor related areas (Tye et al. 2011; Yizhar et al. 2011). To show that the behavioral changes induced by optogenetic stimulation are mediated by activities in the MSDB, a pharmacological intervention at the site of activation was chosen. When prazosin, clonidine and propranolol were administered there was an immediate effect on the behavior observed (see Figure 22). These results indicate that α1, α2, and / or ß ARs are key elements in the regulation of motion behavior in the MSDB. At the same time, complete blockade of optogenetic stimulation confirms that within the MSDB, a1, a2, and ß receptors are the major targets for noradrenergic projections from the LC (see Figure 24). For the experiment it can also be ruled out that the observed increase in running is caused by antidromic impulse conduction. This way, the local application of modulating drugs confirms that the behavioral effects observed are due to ARs in MSDB, and the release of NE from LC-MSDB projections.

4.5.2 Pharmacological properties of adrenergic receptors

Besides the natural transmitter noradrenaline and its derivative epinephrine, ARs can be activated by a broad variety of artificial compounds (Broese et al. 2012). They vary in their selectivity for different ARs and subtypes, and show varying effectivity rates (T.

C. Westfall 2009). In this study, the α1 antagonist prazosin, the α2 agonist clonidine and the ß receptor antagonist propranolol were used. The activation of α1 ARs is associated with a generalized increase in motor activity (Villégier et al. 2003), accompanied by a reduced fine motor control (Aono et al. 2015). In amphetamine and cocaine experiments, the blockade of α1 ARs antagonized the locomotor stimulation. Prazosin is the prototypic antagonist for α1 ARs, with an equal affinity for all three α1 subtypes. It was patented in 1965 and came into medical use in 1974. Prazosin is often used for the treatment of post-traumatic stress disorder (Sara 2009).

Since α1 and α2 work in an antagonistic manner, α2 antagonists like yohimbine facilitate NE function by blocking autoreceptor function resulting in increased locomotor behavior (Villégier et al. 2003; Jiménez-Rivera et al. 2006). To simultaneously block NE from activating the postsynapse while also blocking new NE release from the presynapse, we chose an α2 agonist like clonidine. Clonidine came into medical use in 1966 and is used to relax arteries and treat high blood pressure, attention deficit, hyperactivity or drug withdrawal (Stähle 2000).

In 1964, James Black synthesized the first ß blocker for clinical use – propranolol. ß blockers find the greatest use in the treatment of high blood pressure and the prevention of heart attacks (T. C. Westfall 2009). It blocks the action of noradrenaline and epinephrine on cells of the heart muscles, airways, arteries and kidneys. For this study, it was chosen because of its selectivity for all three ß subtypes. The activation of ß ARs at LC presynapses increases excitatory input onto Purkinje cells in the cerebellum and improves motor function (Di Mauro et al. 2013; Lippiello et al. 2015). In turn, propranolol blocks locomotor behavior induced by amphetamine (Snoddy and Tessel 1985).

4.5.3 Effects of pharmacological modulation on running behavior

The simultaneous application of all three drugs makes it hard to interpret which drug causes which effect and to what extent. Yet, we reasoned that by blocking all ARs in the MSDB area pharmacologically, the movement-modulating effects of optogenetic stimulation-induced NE release should be blocked. Surprisingly, the combined application of all three NE modulatory drugs led to a change in baseline running behavior in the absence of any optogenetic stimulation. Upon combined administration of prazosin, propranolol, and clonidine, baseline running was increased (see Figure 22), similar to stimulated running under no drug conditions, in terms of both running duration and running initiations (see Figure 15). This change in behavior was

independent of any mechanical artifacts caused by the injection of a sample volume, as suggested by sham injection experiments (see Figure 21). Kitchigina et al. (2005) reported increased theta activity upon the systemic administration of clonidine in the lateral ventricles. Clonidine is known for acting in a dose-dependent manner on α2 receptors in the MSDB (Arnsten 2000). The presence of high density of a2-ARs has been well documented in the hippocampus and the septal complex (Rosin 2000; Milner et al. 1998), suggesting their important role in the regulation of septo-hippocampal activity. Clonidine modulates theta oscillations in the septo-hippocampal system depending on the concentration. Low doses of clonidine (0.5 µg in 5 µl; 4 µM) lead to reduced theta activity, whereas high concentrations (5 µg in 5 µl; 40 µM) potentiate hippocampal oscillations (Kitchigina et al. 2005). The concentration of clonidine used in the present study was comparably lower (10 µM), but administered directly into the tissue, in contrast to the systemic administration performed by Kitchigina et al. (2005). So in comparison to the administration into the lateral ventricles, the concentration of clonidine in this study could have been high enough to trigger comparable results as described for high dosages by Kitchigina et al. (2005). Although the authors could not report any effects on movement as the animals were immobilized, higher oscillatory activity in the hippocampus might be accompanied by increased movement rates (Geisler et al. 2007; Bender et al. 2015), as they were observed in the present study.

Kitchigina et al. (2005) suggest that the different effects induced by different concentrations of clonidine might derive from differences in the sensitivities of pre- and postsynaptic α2 ARs to clonidine. Presynaptic α2 receptors have a 10 times higher sensitivity and become activated in behavioral situations like quiet wakefulness and relaxed interaction with the environment (Maura et al. 1985). They already respond to low LC activity and therefore low NE release rates (Carter et al. 2010). By becoming activated first, they further decrease NE release presynaptically. Postsynaptically, α2 ARs decrease adenylate cyclase activity and therefore decrease intracellular cAMP release (Schmidt and Weinshenker 2014). In an activity state like this, the brain is best suited for flexible allocation of energy throughout different functional neuronal systems, for example fine motor control. Also learning and long-term plasticity is promoted (Coull 1994). With more intense behavioral situations, and thus increased NE release rates, postsynaptic α2 ARs change their signaling mechanisms and change from decreasing effects to excitatory mechanisms. High clonidine doses may affect postsynaptic AR in the same way as pure NA. It induces significant increases in the

frequency and regularity of the theta rhythm in the septo-hippocampal system and supports the selective filtering of signals (Kitchigina et al. 2003).

Prazosin, acting on α1 receptors, and the ß blocker propranolol proved to be effective drugs for suppressing both NE transmission and evoked locomotor behavior in response to amphetamine or cocaine administration (Snoddy and Tessel 1985; Schmidt and Weinshenker 2014). In the present study, prazosin and propranolol were administered together with clonidine. Under baseline conditions, without any optogenetic stimulation, high clonidine doses led to activating effects on postsynaptic α2 receptors (see Figure 17). Nevertheless, during stimulation conditions, with NE release from LC terminals, prazosin and propranolol blocked all α1 and ß receptors and prevented further stimulation of the downstream septo-hippocampal network and therefore increased running behavior (see Figure 19). Thus, the results indicate that regardless of the dose-dependent excitatory effects of clonidine, the blockade of a1 and β receptors causes isolation of the MSDB from NE modulating effects.

For future experiments, the effects of pharmacological modulation on the different AR types should be investigated separately with consecutive administration of the respective modulatory drug. In this way, it would be easier to estimate to what degree the individual ARs are involved in the modulation of running behavior. Also, the administered concentration could be staggered, giving insights into the dose-response relationship of the drugs used.

The limited readout of the treadmill setup does not allow to deduce the results of this study to free and complex movement behavior. Comparative studies of global modulation vs. localized intervention in specific core areas have shown that interventions in the entire noradrenergic system affect several behaviorally relevant centers (Warden et al. 2012). Some of these cell populations have antagonistic functions. Their modulation results in more modest behavioral effects, while more-targeted inhibition of specific cell populations produces more robust behavioral consequences (Uematsu et al. 2015). Also, the direct stimulation of ARs in the MSDB can lead to different results if at the same time the connection to the HC is modulated. To understand the role of the NA system in the modulation of locomotion, the results of the present study must be placed in the context of further experiments in other associated brain regions (Chandler et al. 2014).

4.6 Histology confirms LC – medial septal area projections

In this study, genetically modified mice expressing the protein Cre-recombinase are used. By making this expression dependent on the tyrosine hydroxylase 1 promoter, the Cre-protein expression is confined to neurons in which catecholamine biosynthesis takes place (Savitt et al. 2005). Together with locally confined stereotactic injections into the LC, noradrenergic neurons could be exclusively labeled. In the histological preparation, the transfected area is labeled with the green fluorescent protein EYFP that is coupled to the light activatable ion channel ChR2 (see Figure 48). The labeled area is congruent with former anatomical studies by España and Berridge (2006) defining the boundaries of the LC nucleus by immunohistochemical visualization of dopamine ß hydroxylase (DBH), the NE synthesizing enzyme.

In the same study, direct monosynaptic projections between the medial septal area and the LC nucleus were shown using fluoro-gold retrograde tracing. In the present study, such monosynaptic projections are visible as green fluorescent EYFP labeled fibers in medial septal histological slices (see Figure 49B). The green fibers are spread throughout the whole septal structure, providing no indication for locally confined targeting of MS subpopulations. Previous tracing studies suggest that LC projections to the basal forebrain are distributed uniformly within the LC, indicating that all structures of the basal forebrain, including the MSA are modulated uniformly (España and Berridge 2006). As a result, the LC is capable of modulating anatomically distinct yet functionally related structures of the basal forebrain simultaneously in a concerted manner. On the one hand, the distribution of LC fibers visible in the histological preparations of this study support these findings, on the other hand the response to optogenetic activation of LC fibers in MSDB shows a clear dorso-ventral gradient in the MEA experiments.

The efferent projections of LC organize along three major pathways: the dorsal noradrenergic bundle, the cerebellar pathway, and the descending pathway down the spinal cord. España and Berridge (2006) show that the LC is a heterogeneous structure with functionally distinct subpopulations. Noradrenergic fibers in the MSA originate from neurons rather dorsal within the LC nucleus traversing along the anterior NE bundle, while cerebellum- and spinal cord-projecting LC neurons are located more ventrally. In this study, Cre-dependent EYFP expression labels all noradrenergic neurons in the LC area. However, the methods used in this study do not allow to distinguish where exactly the MSA-projecting neurons are located within the LC nucleus. Also, the experimental setup gives no information on the nature (ChAT+, PV+

or VGluT2+) of the LC targeted cells within the MSA. The patch clamp experiments in this study suggest that VGluT + cells in the MSDB are not the primary target when it comes to modulating running behavior (see 4.8). Although optogenetic stimulation leads to the depolarization of glutamatergic cells, this is probably due to the excitation of GABAergic and Chat + cells in the MSDB network (Fuhrmann et al. 2015; Yang et al. 2017).

Transsynaptic viral tracers (Lo and Anderson 2011) can label only those neurons in MSDB receiving direct monosynaptic input from LC. In future experiments, co-labeling of LC axons and noradrenergic receptors in MSDB could further investigate specific noradrenergic projections to different cells in the MSDB. Because these different MSDB cell types have individual projection areas and are embedded in different functional networks (Yang et al. 2017), experiments like these could help to gain deeper insights into the way the LC modulates behavior via the MSDB.

4.7 In vitro MEA recordings of MSDB network activity with and without optogenetic LC fiber stimulation

The 1.2 mm by 0.68 mm rectangular microelectrode array (MEA) I used allowed me to capture the electrophysiological activity of the MSDB network across a 2D plane. Extracellular recordings, as obtained from a MEA, do not allow unambiguous identification of a cell's neurochemical identity or its precise location (Buzsáki et al. 2012). Yet, the characteristics of individual spiking events allow separation from background noise and assignment to individual units (Weir et al. 2014; Becchetti et al. 2012). A frequency analysis of the recorded unit activity showed that 20.82 ± 8.78% of the measured MSDB units exhibit theta modulated firing (see Figure 39A). Studies combining the histochemical identification of MSDB cells with patch clamp recordings have identified GABAergic cells as the predominantly theta-modulated cell population in the MSDB (Brazhnik and Fox 1999; Simon et al. 2006). Cholinergic cells in the MSDB display long lasting afterhyperpolarization and slow firing rates, which limits their capacity for rhythmic bursting. Such characteristics suggest that the burst-firing neurons recorded in MSDB cannot be cholinergic. A widely accepted concept is that theta modulating units in MSDB comprise GABAergic cells, which pace the theta activity, while cholinergic ones, contribute to the theta amplitude (Brazhnik and Fox 1999; Apartis et al. 1998).

The geometry of the MEA covers all of the medial septum and the central parts of the diagonal band, excluding the lateral limbs. During the experiment on the MEA, it was not possible to accurately distinguish anatomically between MS and DBB. Since 70% of cells in the DBB are Chat+, the diagonal band can be visualized using acetylcholinesterase (AChE) and choline acetyltransferase (ChAT) sensitive immunostainings in histological preparations. In histological preparations of future experiments, it would be possible to differentiate between MS and DBB with the counting of Chat+ cells. Stereotactic probabilistic maps, such as those made by Zaborszky et al. (2008) for the basal forebrain, could aid in the orientation and post-hoc assignment of MEA electrodes. This technique uses a small sample of serially and histologically stained, post-mortem brain samples mapped on to a reference brain with magnetic resonance imaging (MRI) images, creating a probabilistic map, showing the likelihood for a certain structure found to be within a reference space in brain imaging. Another direct approach uses MEA electrodes coated with silver. After the measurements, the silver is then deposited with short current surges and remains as a marker in the examined tissue (Streeter et al. 2017).

During unstimulated baseline conditions, the unit activity recorded in the more dorsal part of the MSA preparation did not differ from units from the more ventral diagonal band (see Figure 28). However, the dorsal parts of the MSDB and the more ventral DB showed different responses to optogenetic and NE modulation. Optogenetic activation of LC afferent fibers resulted in a change of activity in a fraction of the recorded units. On average 16.5 % of units increased and 3.25 % decreased their activity (see Figure 30D). The remaining units (80,25 %) appeared not to change their activity in response to photo-stimulation (see Figure 30D). The distribution of the responding units across the MSDB structure reveals that the frequency increasing units are located more dorsally towards the medial septum, whereas the frequency decreasing units spread equally throughout the MSDB area (see Figure 31A). In an in vitro study, Alreja and Liu (1996) showed that especially septo-hippocampal projecting GABAergic neurons receive excitatory LC input. Immunolabeling studies also showed that glutamatergic neurons are located towards the more ventral part of the MSDB structure, indicating, that the responding units in this study are more likely to be cholinergic or GABAergic (Colom et al. 2005). Regarding the extent of NE input to VGluT MSDB neurons, the results of this study indicate, that VGluT neurons might be modulated by LC activity, as part of their roles within the MSDB network. However, including the observations made in the in vivo experiments, LC does not seem to address the speed controlling mechanisms described in Fuhrmann et al. (2015).

4.7.1 Pharmacological modulation of MSDB network activity

Upon application of the α1 noradrenergic agonist prazosin and the α2 receptor modulating clonidine, the mean firing rate of 14 MSDB preparations showed divergent results. In eight experiments, the overall firing rate increased, sometimes considerably. In six experiments the firing rate dropped below baseline (see Figure 34B). This inconsistent result could be the result of variations in baseline conditions, either in the experimental setup or the MSDB preparation used, leading to varying responsiveness of the neuronal network. The network activity in the slice preparation depends largely on the continuous supply of oxygen and stable temperatures (Ivanov and Zilberter 2011; Haas et al. 1979). A constant negative pressure within the recording chamber used helped to optimize the saturation of the preparation, by perfusing oxygenated ACSF through the slice and the perforated MEA. Differences in the thickness of the measured brain slices, due to flattening processes during the incubation, might influence the perfusion rate and result in variations of neuronal activity.

Contrary to what was expected, the activity of the brain slices in the MEA experiments decreases after washing out the noradrenergic ligands (see Figure 34A + B). This constant decrease in the mean firing rate is consistent in almost all experiments. With repeated optogenetic stimulation experiments in four consecutive phases, the measurements on the individual brain slices extended over up to three hours. As the duration progresses, the quality of the brain slices decreases, the faster the older the animal is at the time point of tissue removal (Humpel 2015). It seems likely that this limitation is due, in part, to a developmental shift from anaerobic- to aerobic-based tissue metabolism, due to decreasing ATP availability in the cells (Dailey 2002). Moreover, the brain tissues suffer from stress under the hypoxic and hypoglycemic conditions that may occur during the tissue isolation procedures (Ivanov and Zilberter 2011). The results of this study, in particular the blocking effect of the noradrenergic antagonists, might be overestimated and should be interpreted in the light of this effect. Future experiments should include a control experiment, investigating the long-term viability of slice preparations on the MEA. The results could be used to correct the measured network activity for a general rundown of neuronal activity.

Also, within the MSDB structure, the proportion of glutamatergic, cholinergic and GABAergic neurons changes from caudal to rostral (Kiss et al. 1997). With 500 µm thick slices the composition of the neuronal network could vary, depending on the exact anatomical slice of the MSDB structure that was recorded from. Differences in

the response between individual slices might indicate that the MSDB receives anatomically distinct modulatory NE input depending on specific neuronal subpopulations.

Another possible explanation for the divergent responses observed during pharmacological modulation lies in the dual mode of action of clonidine, the α2 AR modulating drug, also used in the in vivo experiments. The presence of a high density of α2 ARs has been well documented in the hippocampus and the septal complex (Milner et al. 1998), suggesting their important role in the regulation of septo-hippocampal activity. As discussed for the in vivo experiments, clonidine has a dual mode of action. The dose-dependent effect of clonidine is in good agreement with earlier studies, which have shown, that presynaptic α2 receptors have a 10 times higher affinity to endogenous NE or its correspondent agonists, e.g. clonidine, compared to postsynaptic α2 receptors. Pre- and postsynaptic α2 ARs differ in their stereochemical structure and are assigned to separate subtypes (Rosin 2000). Low concentrations of clonidine bind to the presynaptic α2 receptors and block the release of NE vesicles. In addition, clonidine - at a low dose - may also reduce the terminal release of other excitatory transmitters, in particular glutamate and acetylcholine, which would further inhibit neuronal excitation (Boehm 1999). High concentrations, on the other side, lead to an alternative activation of postsynaptic α2 AR and altered intracellular mechanisms, resulting in an increased network activity. In the study describing the concentration depending action of clonidine 4 µM is used as a low concentration and 40 µM is used for high concentration experiments (Kitchigina et al. 2003). In the present study 10 µM was used, settling in between those two concentrations. This could either lead to effects resembling the results for low concentrations or show excitatory effects comparable to the results described for high concentrations like it was described by Kitchigina et al. (2003). Consequently, Kitchigina et al. (2003) also describe mixed effects for an intermediate dose of clonidine injected into the MSDB. Clonidine in high concentrations increased the number of theta modulated units in MSDB. In the present study, the number of units was increased as well, although not in significant numbers relative to the whole recorded unit population. Also, the power of the unit theta modulation is increased due to high clonidine concentrations, comparable to Kitchiginas findings. The broad spectrum of reactivity in response to the activation of noradrenergic fibers in the MSDB and to the pharmacological modulation of AR provides possible explanations, how the noradrenergic system is involved in the regulation of behavior, reaching from sleep and low arousal to situations of stress and high alert. The activation of either

presynaptic or postsynaptic α2 ARs depends on different levels of arousal in the brain. In calm and safe situations the processing of sensory information is reduced. Locus coeruleus is releasing small amounts of NA. Therefore only high affinity presynaptic α2 ARs get activated, reducing the release of NA at the axon terminals and consequently the activity in structures like the MSDB and the Hippocampus. Sudden situations of high alert induce an immediate activation of the LC and the release of large amounts of NE. High NE concentrations activate postsynaptic α2 ARs, resulting in a depolarization of the postsynapse and prevailing over the presynaptic inhibitor effects. In a concerted fashion MSDB and Hippocampus enhance their theta rhythm enabling the system for higher information processing rates.

To block NE modulation completely, propranolol was added to the infusion chamber, and, as a result, the activity in all slice preparations decreased substantially. Under normal conditions, ß receptors get activated upon high LC activity in situations of increased stress (fight or flight). Both α2 and β ARs are G-protein coupled receptors, each affecting adenylyl cyclase in opposite directions, namely by decreasing (α2 ARs) or increasing (β ARs) the intracellular concentrations of cAMP. Since α2 and ß receptors share the same downstream signaling cascade, high LC activity and therefore ß ARs activation contradict α2 mediated signaling. The effects set in motion by activating postsynaptic ß receptors overrules a1 and α2 activity and therefore the blockade of all ß receptors by its antagonist propranolol shut down all excitatory effects by possible high clonidine concentrations. Due to the already long experimental sequence, the time period for drug washout was limited to 20 min. In comparable studies, the duration of NE modulating effects lasted for 22 to 36 min (Kitchigina et al. 2003). The use of beta-blockers as a heart medication is always associated with side effects on the CNS due to their strong lipophilic character and the associated high permeability of the blood-brain barrier (McAinsh and Cruickshank 1990). Especially propranolol is very lipophilic, which can make the complete washout difficult (Fumagalli et al. 2019). In future experiments with shorter run-times, the problem of general activity rundown would be minimized and longer wash-out periods could be realized. Ideally, the individual pharmacological ligands are first administered individually and in staggered concentrations to determine the individual pharmacokinetics.

4.8 Modulation of VGluT2+ neuron activity in MSDB by optogenetic LC fiber activation

By performing intracellular current clamp experiments on MSDB slice preparations, the modulatory effects of optogenetic LC afferent activation was investigated on a third level. In addition to the response of a functional organism, investigated in the in vivo experiments and the complete network response pictured by the MEA experiments, patch clamp experiments give insights to the physiology of single neurons affected by NE release. Regarding the findings of Fuhrmann et al. (2015) on the speed modulating nature of MSDB VGluT neurons, the patch clamp experiments aimed to investigate the degree of direct modulation of glutamatergic neurons by NE LC afferents. Glutamatergic neurons were labeled in red with a VGluT2-Cre transgenic mouse that was injected with an adeno associated virus carrying floxed genes for tdTomato expression. Analogous to the in vivo and MEA experiments, LC afferent fibers were labeled in green with ChR2 coupled to the green fluorescent protein EYFP. As a result, the slice preparations used for patch clamp experiments showed green descending LC fibers within the MSDB structure in addition to red labeled glutamatergic neurons. Due to the low concentration of the virus used, the labeling of glutamatergic neurons was sparse, making it easier to target single cells for patch clamp experiments. On the other side, it wasn't possible to confirm findings about the overall anatomical distribution of glutamatergic neurons in the MSDB structure as they were made by Kiss et al. (1997). However, the histological slice preparations confirmed the anatomical proximity of green labeled LC afferents to the red labeled glutamatergic neurons. Upon optogenetic stimulation of the ChR2 in the LC fibers, the number of glutamatergic neurons showing excitatory responses (see Figure 46B) are in line with the rather small amount of NE reactive VGluT2 neurons within the MSDB presented by previous studies (Alreja and Liu 1996). With GABAergic neurons being the major target for LC afferents, only a small number of neurons patched was modulated by the optogenetic induced NE release. Also, the cells patched tended to spike spontaneously under the light stimulus (see Figure 45D). This means, that in addition to providing an increased baseline depolarization and therefore increasing the general excitability, the NE released was sufficient to depolarize the cells enough for immediate spontaneous activity. Even if glutamatergic neurons in the MSDB were not the main target for LC projections, they were still being modulated and contributed with excitatory synaptic transmission to the excitation of GABAergic and cholinergic neurons within the MSDB network. A combination of NE modulatory drugs (prazosin, clonidine and propranolol)

reduced the depolarizing effects, but due to the small number of successfully treated cells (N = 4) no significant effect could be determined. In those cases where the patched cells were treated with prazosin, clonidine and propranolol the effect of optogenetic NE release was still visible in the cells' membrane potential. However, the depolarization was reduced and with higher stimulation rates (30 Hz) no spontaneous AP could be observed anymore. These observations indicate, that glutamatergic cells in the MSDB possess noradrenergic a1, α2 or ß receptors, and that those receptors are affected by noradrenergic modulatory drugs. On the other hand, the incomplete block indicates that $VGluT2^{+}$ neurons receive some other NE modulated input, presumably from the surrounding network. In future patch clamp experiments, various concentrations should be applied to illuminate the pharmacodynamics of the receptor proteins in detail. Another factor that needs to be considered are neuropeptides like vasopressin, somatostatin and neuropeptide Y who are co-released with NE and are able to affect the postsynaptic membrane potential in various ways (reviewed in Aston-Jones et al. (2004) (Aston-Jones et al. 2004)). Studies in the dorsal hippocampus confirm that LC axonal projections also corelease dopamine, activating the dopamine D1/D5 receptor (Kempadoo et al. 2016). Doing so, they promote selective attention and spatial learning.

5 Conclusion

To investigate the role of the LC and the entire noradrenergic system on the modulation of behavior, one needs to distinguish between global manipulations and region specific circuits and mechanisms. As an example for effects of global manipulations of the noradrenergic system, unspecific LC stimulations led to mixed results in fear conditioning experiments in terms of excitation/inhibition and performance (Uematsu et al. 2017). The underlying mechanisms for this are not entirely clear, but research on the heterogeneity and composition of the LC reveals functionally distinct cell populations with overlapping but confined projecting fields (Uematsu et al. 2017). Similarly, the targeted regions interconnect in feedback mechanisms, integrating the noradrenergic input into adaptive behavior. Studies targeting specific cell populations resulted in more robust behavioral consequences (Warden et al. 2012). As a consequence, the present study isolated one specific noradrenergic projection and very restricted readout parameters to address the question if and how LC modulates running behavior. The running behavior observed on the linear track limits behavioral quantification to the measurable aspects of

locomotion. On the one hand, this approach allowed me to clearly observe an increase in running behavior due to LC fiber stimulation in MSDB. On the other hand, it gives no answer to which behavioral context this mechanism comes into play. However, this study shows directly that the stimulation of molecularly defined Th^+ fibers in the MSDB alters behavior. Previous studies have demonstrated that noradrenergic tonic cell firing in the LC increases following stressful stimuli (McCall et al. 2015; Aston-Jones et al. 1999). This study demonstrates that selective activation of Th^+ LC terminals from these neurons modulates MSDB neuronal activity in vivo and in vitro.

Furthermore, the pharmacological modulation of ARs in MSDB, specifically the concentration specific dual mode of action of clonidine revealed, that the noradrenergic influence of LC is an adaptive system, not only in the interplay of brain regions, but also on the scale of a single system like the MSDB. Findings like this might be relevant for the understanding of single AR function in distinct brain regions and their modulation with specific drugs. Clonidine and prazosin are used in treating anxiety disorders like PTSD which are highly resistant to psychotherapeutic intervention (Berardis et al. 2015). Basal levels of noradrenaline are abnormally high in the cerebrospinal fluid of these patients, indicating dysfunction in the central noradrenergic system (Strawn and Geracioti 2008).

One central goal of this study was to address whether LC afferents affect the $VGluT2^+$ neuron-mediated speed modulation via septo-hippocampal projections (Fuhrmann et al. 2015). Although locomotor behavior was indeed increased by LC fiber stimulation in MSDB, speed was not affected. Also, in contrast to the direct stimulation of glutamatergic neurons, as it was performed by Fuhrmann et al. (2015), hippocampal theta oscillations never exceeded the boundaries visible during unstimulated running. The MEA experiments allowed narrowing down excitatory influence mainly to the dorsal parts of the MS rather than the DB. Together with immunolabeling studies, showing glutamatergic neurons being located more towards the ventral part of the MSDB (Colom et al. 2005), these findings indicate a rather indirect influence of the NE system on septal glutamatergic neurons. However, direct patch experiments confirmed NE input on $VGluT2^+$ neurons, suggesting them to be an active part of the NE-modulated network within the MSDB.

Further work will be necessary to further corroborate the results of this study, especially the pharmacological modulation of ARs in vivo and in vitro. Additional experiments with single drug treatment can thus expand the understanding of ARs in the MSDB. Using specific genetically modified mouse lines and immunostaining

methods, it is also possible to investigate which cell types in the MSDB get targeted from noradrenergic projections. They will help to understand the cell-type and projection-specific relationship between LC-NE modulation of MSDB activity and its ability to drive locomotor behavior through downstream circuits and motor systems.

6 Appendix

6.1 Additional figures and tables

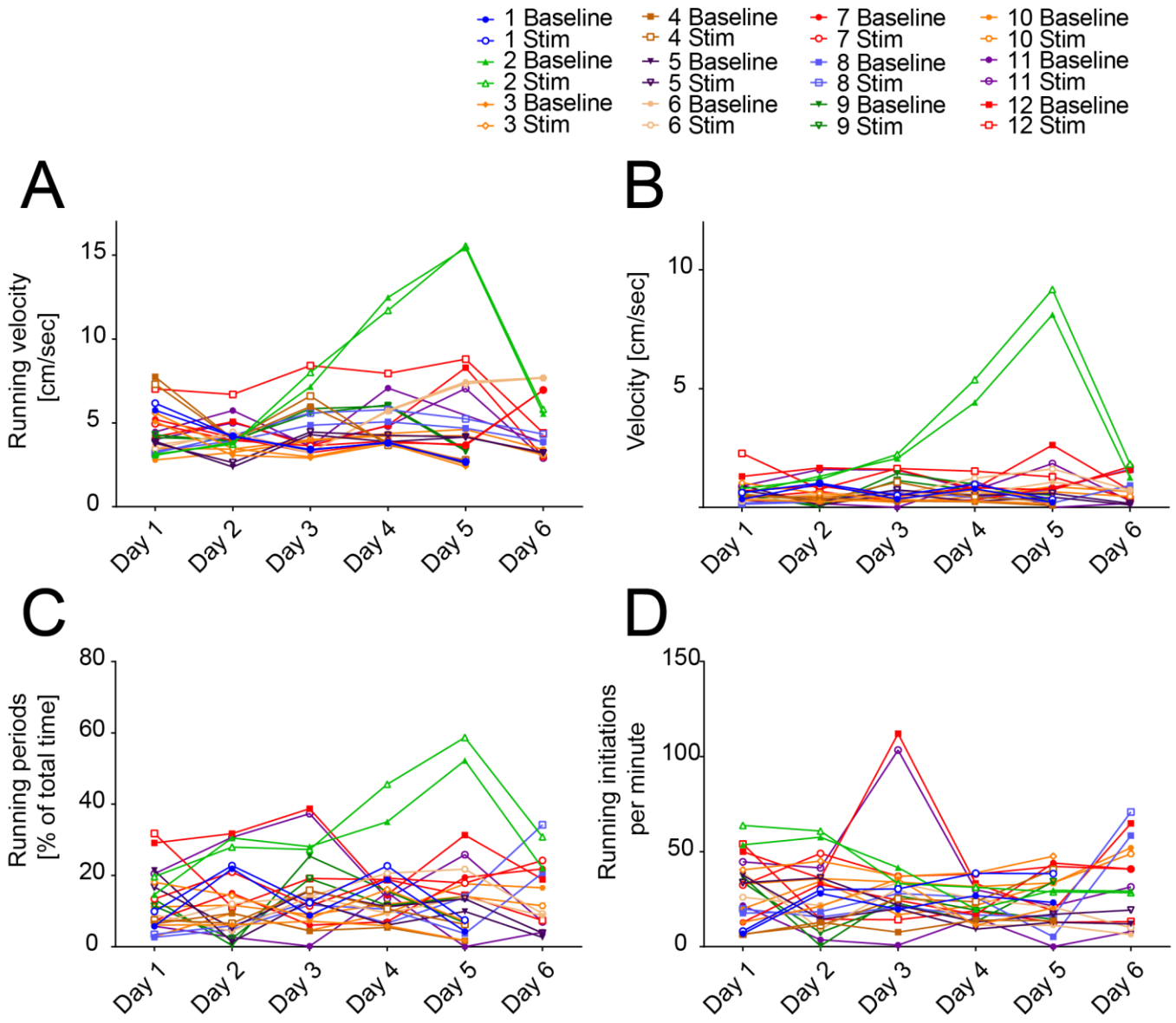

Appendix figure 1 **Individual effects of optogenetic LC fiber stimulation in MSDB on running behavior**
A. Mean running velocity for all 12 mice individually for each day. Full symbols show unstimulated baseline running. Open symbols show running under optogenetic stimulation. **B.** Same as A. for the velocity including all resting phases. **C.** Same as A. for the % of running periods of the total time. **D.** Same as A. for the running initiations per minute.

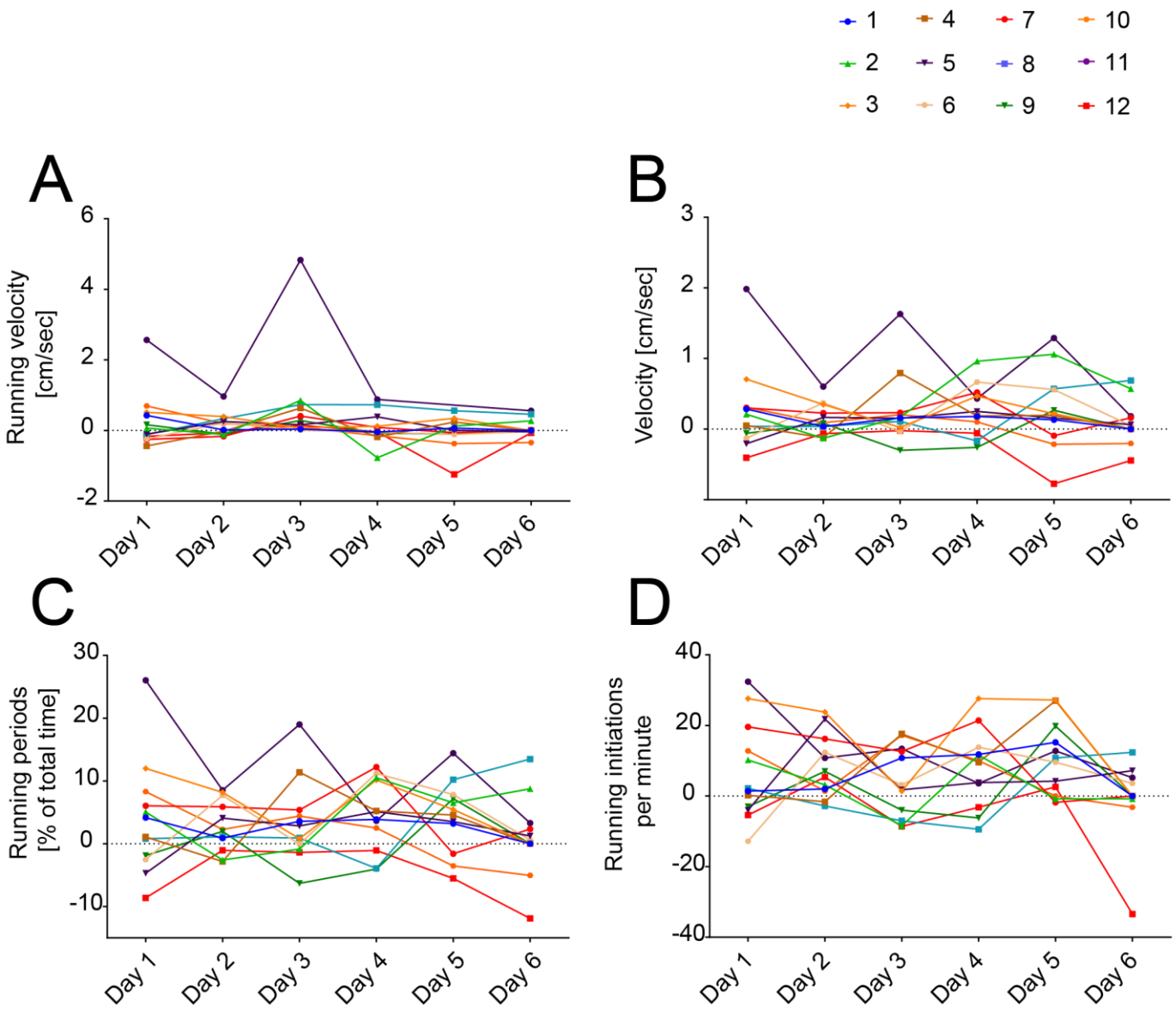

Appendix figure 2 **Individual difference of stimulated vs. baseline running behavior**

A. Difference of running velocity upon optogenetic stimulation for all 12 mice individually for each day. **B.** Same as A. for the velocity including all resting phases. **C.** Same as A. for the % of running periods of the total time. **D.** Same as A. for the running initiations per minute.

Appendix table 1 **LFP frequency analysis prior and during stimulation phases**

LFP Frequency with the two conditions run vs. rest and pre vs. during stimulation was analyzed with a two way ANOVA and Sidak's multi comparison test

LFP Frequency
Two-way ANOVA;
Matching: Both factors

Source of Variation	% of total variation	P value	P value summary	Significant?
Movement phase	56,65	<0,0001	****	Yes
Optogenetic stimulation	0,05835	0,5305	ns	No
Interaction: Movement phase x Optogenetic stimulation	0,01826	0,7155	ns	No
Interaction: Movement phase x Subjects	3,579			
Interaction: Optogenetic stimulation x Subjects	1,234			
Subjects	37,3			

Sidak's multiple comparisons test

	Mean [Hz]			Mean [Hz]	Mean Diff,	95,00% CI of diff,	Significant?	Summary	Adjusted P Value
Rest:Pre	5,445	vs.	Rest:Stim	5,457	-0,01172	-0,1991 to 0,1756	No	ns	>0,9999
Rest:Pre	5,445	vs.	Run:Pre	6,258	-0,8136	-1,001 to -0,6263	Yes	****	<0,0001
Rest:Pre	5,445	vs.	Run:Stim	6,3	-0,8551	-1,042 to -0,6677	Yes	****	<0,0001
Rest:Stim	5,457	vs.	Run:Pre	6,258	-0,8019	-0,9892 to -0,6146	Yes	****	<0,0001
Rest:Stim	5,457	vs.	Run:Stim	6,3	-0,8434	-1,031 to -0,656	Yes	****	<0,0001
Run:Pre	6,258	vs.	Run:Stim	6,3	-0,04146	-0,2288 to 0,1459	No	ns	0,9796

Appendix table 2 **LFP power analysis prior and during stimulation phases**

LFP power with the two conditions run vs. rest and pre vs. during stimulation was analyzed with a two way ANOVA and Sidak's multi comparison

LFP Power

Two-way ANOVA; Matching: Both factors

Source of Variation	% of total variation	P value	P value summary	Significant?
Movement Phase	20,89	0,0013	**	Yes
Optogenetic Stimulation	0,02195	0,348	ns	No
Interaction: Movement Phase x Optogenetic Stimulation	0,05707	0,0399	*	Yes
Interaction: Movement Phase x Subjects	8,926			
Interaction: Optogenetic Stimulation x Subjects	0,2015			
Subjects	69,82			

Sidak's multiple comparisons test

	Mean [Hz]			Mean [Hz]	Mean Diff,	95,00% CI of diff,	Significant?	Summary	Adjusted P Value
Rest:Pre	2,32E-06	vs.	Rest:Stim	2,38E-06	-5,52E-08	-3,225e-007 to 2,121e-007	No	ns	0,9148
Rest:Pre	2,32E-06	vs.	Run:Pre	5,25E-06	-2,93E-06	-3,192e-006 to -2,658e-006	Yes	****	<0,0001
Rest:Pre	2,32E-06	vs.	Run:Stim	5,01E-06	-2,69E-06	-2,957e-006 to -2,422e-006	Yes	****	<0,0001
Rest:Stim	2,38E-06	vs.	Run:Pre	5,25E-06	-2,87E-06	-3,137e-006 to -2,603e-006	Yes	****	<0,0001
Rest:Stim	2,38E-06	vs.	Run:Stim	5,01E-06	-2,63E-06	-2,902e-006 to -2,367e-006	Yes	****	<0,0001
Run:Pre	5,25E-06	vs.	Run:Stim	5,01E-06	2,35E-07	-3,187e-008 to 5,027e-007	No	ns	0,0874

Appendix table 3 **One way ANOVA analysis of running behavior upon pharmacological modulation**

A. Running velocity, **B.** overall velocity, **C.** running periods and **D.** running initiations were analyzed for significant (Sig.) changes with and without pharmacological modulation for two mice (mouse #1 and #2) individually. All running parameters were tested during baseline conditions with sham ACSF injections, pharmacological modulation and after a 20 min washout period.

A

Running velocity [cm/sec]			Mouse #1		Mouse #2	
			Sig.	P value	Sig.	P value
Sham ACSF injection	vs.	Prazosin, clonidine, propranolol	ns	0,86	ns	0,3403
Sham ACSF injection	vs.	After washout sham ACSF injection	ns	0,1466	*	0,0189
Prazosin, clonidine, propranolol	vs.	After washout sham ACSF injection	ns	0,2066	ns	0,0926

B

Velocity [cm/sec]			Mouse #1		Mouse #2	
			Sig.	P value	Sig.	P value
Sham ACSF injection	vs.	Prazosin, clonidine, propranolol	**	0,0015	*	0,0195
Sham ACSF injection	vs.	After washout sham ACSF injection	ns	0,6108	ns	0,7186
Prazosin, clonidine, propranolol	vs.	After washout sham ACSF injection	***	0,0003	**	0,0057

C

Running periods [% of total time]			Mouse #1		Mouse #2	
			Sig.	P value	Sig.	P value
Sham ACSF injection	vs.	Prazosin, clonidine, propranolol	****	<0,0001	**	0,0039
Sham ACSF injection	vs.	After washout sham ACSF injection	ns	0,6363	ns	0,7246
Prazosin, clonidine, propranolol	vs.	After washout sham ACSF injection	****	<0,0001	**	0,0013

D

Running initiations per minute			Mouse #1		Mouse #2	
			Sig.	P value	Sig.	P value
Sham ACSF injection	vs.	Prazosin, clonidine, propranolol	****	<0,0001	*	0,0179
Sham ACSF injection	vs.	After washout sham ACSF injection	ns	0,9996	ns	0,9405
Prazosin, clonidine, propranolol	vs.	After washout sham ACSF injection	***	0,0002	*	0,02

Appendix table 4 **Two way ANOVA analysis of running behavior upon optogenetic and pharmacological modulation**

Running velocity, overall velocity, running periods and running initiations were analyzed for significant (Sig.) changes with and without optogenetic stimulation for two mice (mouse #1 **A. – D.** and #2 **E. – H.**) individually. All running parameters were tested during baseline conditions with sham ACSF injections, pharmacological modulation and after a 20 min washout period.

A

Mouse #1 Running velocity [cm/sec]

Sidak's multiple comparisons test	Mean Baseline	Mean Stim	Significant?	Summary	Adjusted P Value
Sham ACSF injection	7,356	7,642	No	ns	0,9858
NE modulation	6,952	6,653	No	ns	0,9816
After washout	5,431	7,665	No	ns	0,1083
Source of Variation	**% of total variation**	**P value**	**P value summary**	**Significant?**	**F (DFn, DFd)**
Interaction	11,69	0,1572	ns	No	F (2, 26) = 1,988
Optogenetic modulation	5,468	0,1843	ns	No	F (1, 26) = 1,861
Pharmacological modulation	6,436	0,3495	ns	No	F (2, 26) = 1,095

B

Mouse #1 Overall velocity [cm/sec]

Sidak's multiple comparisons test	Mean Baseline	Mean Stim	Significant?	Summary	Adjusted P Value
Sham ACSF injection	0,5208	1,767	Yes	**	0,008
NE modulation	1,397	1,453	No	ns	0,9984
After washout	0,32	1,02	No	ns	0,2763
Source of Variation	**% of total variation**	**P value**	**P value summary**	**Significant?**	**F (DFn, DFd)**
Interaction	9,49	0,1162	ns	No	F (2, 28) = 2,326
Optogenetic modulation	17,85	0,0062	**	Yes	F (1, 28) = 8,751
Pharmacological modulation	15,56	0,0343	*	Yes	F (2, 28) = 3,813

C

Mouse #1 Running periods [% of total time]

Sidak's multiple comparisons test	Mean Baseline	Mean Stim	Significant?	Summary	Adjusted P Value
Sham ACSF injection	6,745	23,52	Yes	*	0,0269
NE modulation	19,92	22,47	No	ns	0,9651
After washout	4,373	15,65	No	ns	0,2615
Source of Variation	**% of total variation**	**P value**	**P value summary**	**Significant?**	**F (DFn, DFd)**
Interaction	5,937	0,2757	ns	No	F (2, 28) = 1,349
Optogenetic modulation	18,01	0,0079	**	Yes	F (1, 28) = 8,186
Pharmacological modulation	14,45	0,0523	ns	No	F (2, 28) = 3,285

D

Mouse #1 Running Initiations per minute

Sidak's multiple comparisons test	Mean Baseline	Mean Stim	Significant?	Summary	Adjusted P Value
Sham ACSF injection	1,267	3,567	No	ns	0,1442
NE modulation	3,1	3,606	No	ns	0,9596
After washout	1,147	3,347	No	ns	0,2347
Source of Variation	**% of total variation**	**P value**	**P value summary**	**Significant?**	**F (DFn, DFd)**
Interaction	3,981	0,4807	ns	No	F (2, 28) = 0,752
Optogenetic modulation	16,35	0,0192	*	Yes	F (1, 28) = 6,176
Pharmacological modulation	5,556	0,3635	ns	No	F (2, 28) = 1,049

E

Mouse #2 Running velocity [cm/sec]

Sidak's multiple comparisons test	Mean Baseline	Mean Stim	Significant?	Summary	Adjusted P Value
Sham ACSF injection	8,245	9,528	No	ns	0,6055
NE modulation	7,661	7,57	No	ns	0,9997
After washout	5,289	8,956	Yes	*	0,0396

Source of Variation	% of total variation	P value	P value summary	Significant?	F (DFn, DFd)
Interaction	13,81	0,1079	ns	No	F (2, 21) = 2,481
Optogenetic modulation	15,04	0,0302	*	Yes	F (1, 21) = 5,402
Pharmacological modulation	12,67	0,1276	ns	No	F (2, 21) = 2,274

F

Mouse #2 Overall velocity [cm/sec]

Sidak's multiple comparisons test	Mean Baseline	Mean Stim	Significant?	Summary	Adjusted P Value
Sham ACSF injection	0,6271	2,896	Yes	**	0,0019
NE modulation	1,742	2,027	No	ns	0,946
After washout	0,2643	2,053	Yes	*	0,0306

Source of Variation	% of total variation	P value	P value summary	Significant?	F (DFn, DFd)
Interaction	12,32	0,0683	ns	No	F (2, 22) = 3,04
Optogenetic modulation	36,15	0,0003	***	Yes	F (1, 22) = 17,84
Pharmacological modulation	6,945	0,2034	ns	No	F (2, 22) = 1,714

G

Mouse #2 Running periods [% of total time]

Sidak's multiple comparisons test	Mean Baseline	Mean Stim	Significant?	Summary	Adjusted P Value
Sham ACSF injection	6,205	29,92	Yes	***	0,0004
NE modulation	19,88	23,73	No	ns	0,8473
After washout	3,082	22,04	Yes	*	0,0105

Source of Variation	% of total variation	P value	P value summary	Significant?	F (DFn, DFd)
Interaction	12,29	0,0414	*	Yes	F (2, 22) = 3,693
Optogenetic modulation	41,22	<0,0001	****	Yes	F (1, 22) = 24,77
Pharmacological modulation	9,884	0,0721	ns	No	F (2, 22) = 2,97

H

Mouse #2 Running Initiations per minute

Sidak's multiple comparisons test	Mean Baseline	Mean Stim	Significant?	Summary	Adjusted P Value
Sham ACSF injection	0,9067	3,967	Yes	**	0,0014
NE modulation	3,723	3,867	No	ns	0,9966
After washout	1,083	2,908	No	ns	0,1154

Source of Variation	% of total variation	P value	P value summary	Significant?	F (DFn, DFd)
Interaction	12,96	0,0466	*	Yes	F (2, 22) = 3,537
Optogenetic modulation	25,48	0,0012	**	Yes	F (1, 22) = 13,91
Pharmacological modulation	21,27	0,0095	**	Yes	F (2, 22) = 5,804

Appendix table 5 **Chi-square analysis of the unit response, distributed to the dorsal MS and the ventral DB**

A. Number of dorsal and ventral units sorted according to their frequency increasing or decreasing response to the optogenetic stimulation. **B.** Contingency table, testing MSDB units in a cross-sectional study of the link between anatomical position within the MSDB and the frequency increasing or decreasing response to optogenetic stimulation.

A

Number of units	dorsal	ventral	Total
increase by >1Hz	167	37	204
decrease by >1Hz	27	14	41
Total	194	51	245
No change > 1 Hz	545	211	756

B

Percentage of grand total	dorsal	ventral
increase by >1Hz	68,16%	15,10%
decrease by >1Hz	11,02%	5,71%

Test	Chi-square and Fisher's exact test
P value	0,0332
One- or two-sided	Two-sided
Statistically significant?	Yes

Appendix table 6 **Dorsal vs. ventral MSDB network response to various phases of NE-modulation**

Mean unit activity, divided in dorsal and ventral MSDB. Mann Whitney test was used to compare the dorsal and ventral mean activity in different pharmacological conditions.

	Baseline		Prazosin, clonidine		Prazosin, clonidine, propranolol		After washout	
	dorsal	ventral	dorsal	ventral	dorsal	ventral	dorsal	ventral
Number of values	741	260	741	260	706	206	642	206
Mean	11,37	10,23	11,85	12,03	7,512	8,18	5,346	6,238
Std. Deviation	12,43	12,53	12,33	12,47	8,375	8,174	5,936	6,885
Std. Error of Mean	0,4568	0,777	0,4531	0,7734	0,3152	0,5695	0,2343	0,4797

Mann Whitney test

P value	0,3397	0,3551	0,0311	0,0628
Exact or approximate P value?	Approximate	Approximate	Approximate	Approximate
P value summary	ns	ns	*	ns
Significantly different (P < 0.05)?	No	No	Yes	No
One- or two-tailed P value?	Two-tailed	Two-tailed	Two-tailed	Two-tailed
Sum of ranks in column A,B	375071 , 126430	367532 , 133970	315119 , 101209	266838 , 93139
Mann-Whitney U	92500	92621	65548	60435

Appendix table 7 **MSDB network response to various phases of NE-modulation**

Mean activity of all MSDB units measured with the MEA. A one way ANOVA and Holm-Sidak's multiple comparisons test was used to compare the activity with different pharmacological treatment.

	Mean [Hz]			Mean [Hz]	Mean Diff. [Hz]	Significant?	Summary	Adjusted P Value
Baseline	11,16	vs.	NE-α1+2-modulation	11,34	-0,181	No	ns	0,9192
Baseline	11,16	vs.	NE-α1+2+ß-modulation	7,161	4,000	No	ns	0,0968
Baseline	11,16	vs.	After washout	5,36	5,801	Yes	*	0,0143
NE-α1+2-modulation	11,34	vs.	NE-α1+2+ß-modulation	7,161	4,182	No	ns	0,0968
NE-α1+2-modulation	11,34	vs.	After washout	5,36	5,982	Yes	*	0,013
NE-α1+2+ß-modulation	7,161	vs.	After washout	5,36	1,801	No	ns	0,5686

Appendix table 8 **Two way ANOVA multi comparison analysis of network activity changes in response to optogenetic stimulation during different pharmacological modulations**

A. Sidak's multiple comparisons test of the MSDB network activity pre vs. during optogenetic stimulation with different pharmacological treatment.
B. Tukey's multiple comparisons test of network activity during different pharmacological modulations with and without optogenetic stimulation.

A

Pre vs. Stim	Median 1	Median 2	Significant?	Summary	Adjusted P Value
Control	10,06	10,30	Yes	****	<0,0001
NE a1+2 modulation	12,33	12,51	No	ns	0,8662
NE a1+2 + ß modulation	6,97	6,72	No	ns	0,2337
After washout	5,51	5,55	No	ns	0,9999

Source of Variation	% of total variation	P value	Significant?	Summary	F (DFn, DFd)
Optogenetic stimulation	0,02257	0,1473	No	ns	F (1, 11) = 2,431
Pharmacological modulation	35,74	<0,0001	Yes	****	F (3, 33) = 14,61
Interaction: Optogenetic stim. x Pharmacological mod.	0,1313	0,0002	Yes	***	F (3, 33) = 9,055
Interaction: Optogenetic stim. x Subjects	0,1021				
Interaction: Pharmacological mod. x Subjects	26,91				
Subjects	36,93				

B

Pre	Median 1	Median 2	Significant?	Summary	Adjusted P Value
Control vs. NE a1+2 modulation	10,06	12,33	No	ns	0,9997
Control vs. NE a1+2 + ß modulation	10,06	6,97	Yes	****	<0,0001
Control vs. After washout	10,06	5,51	Yes	****	<0,0001
NE a1+2 modulation vs. NE a1+2 + ß modulation	12,33	6,97	Yes	****	<0,0001
NE a1+2 modulation vs. After washout	12,33	5,51	Yes	****	<0,0001
NE a1+2 + ß modulation vs. After washout	6,97	5,51	Yes	****	<0,0001

Stim	Median 1	Median 2	Significant?	Summary	Adjusted P Value
Control vs. NE a1+2 modulation	10,30	12,51	Yes	***	0,0008
Control vs. NE a1+2 + ß modulation	10,30	6,72	Yes	****	<0,0001
Control vs. After washout	10,30	5,55	Yes	****	<0,0001
NE a1+2 modulation vs. NE a1+2 + ß modulation	12,51	6,72	Yes	****	<0,0001
NE a1+2 modulation vs. After washout	12,51	5,55	Yes	****	<0,0001
NE a1+2 + ß modulation vs. After washout	6,72	5,55	Yes	****	<0,0001

Appendix table 9 **Statistical analysis of theta modulation upon LC-fiber stimulation in MSDB**

A. Wilcoxon matched-pairs signed rank test of the proportion of theta modulated units upon LC fiber stimulation compared to baseline conditions.
B. Wilcoxon matched-pairs signed rank test of the mean theta frequency with and without stimulation.
C. Wilcoxon matched-pairs signed rank test of the mean theta amplitude with and without stimulation.

A

Proportion of theta modulated units upon LC fiber stimulation

	Minimum	Maximum	Mean	Std. Deviation		Adjusted P value	Summary	Significant?
Pre	20,59	44,94	35,1	8,773	Wilcoxon matched-pairs signed rank test	0,2734	ns	No
Stim	11,76	71,15	38,8	13,86				

B

Mean theta frequency with and without stimulation

	Minimum	Maximum	Mean	Std. Deviation		Adjusted P value	Summary	Significant?
Pre	6,803	9,349	7,87	0,7173	Wilcoxon matched-pairs signed rank test	0,1272	ns	No
Stim	7,09	9,483	8,02	0,6589				

C

Mean theta amplitude with and without stimulation

	Minimum	Maximum	Mean	Std. Deviation		Adjusted P value	Summary	Significant?
Pre	11,46	386,8	139	104,8	Wilcoxon matched-pairs signed rank test	0,0015	**	Yes
Stim	30,38	380,5	169	110,2				

Appendix table 10 **Analysis of theta unit modulation in different NE-modulatory conditions**

A. Summary of One way ANOVA analysis of mean percentage of theta units, mean frequency and mean amplitude of theta modulated units.
B. - D. All data were analyzed with repeated measurements and multi comparison against control conditions.

A

Repeated measures ANOVA summary	Mean theta units in % of all units	Mean theta frequency	Mean theta amplitude
F	3,39	0,7121	3,648
P value	0,0616	0,5034	0,0563
P value summary	ns	ns	ns
Statistically significant (P < 0.05)?	No	No	No
Geisser-Greenhouse's epsilon	0,5402	0,6637	0,5692
R square	0,2069	0,07332	0,2885

B

Mean theta units in % of all units

Dunnett's multiple comparisons test	Mean 1	Mean 2	Significant?	Summary	Adjusted P Value
Control vs. NE-a1,2-modulation	20,82	25,64	No	ns	0,0511
Control vs. NE-a1,2+ß-modulation	20,82	21,15	No	ns	0,9994
Control vs. After washout	20,82	17,39	No	ns	0,4957

C

Mean theta frequency

Dunnett's multiple comparisons test	Mean 1	Mean 2	Significant?	Summary	Adjusted P Value
Control vs. NE-a1,2-modulation	7,694	7,394	No	ns	0,7903
Control vs. NE-a1,2+ß-modulation	7,694	7,373	No	ns	0,55
Control vs. After washout	7,694	7,266	No	ns	0,2287

D

Mean theta amplitude

Dunnett's multiple comparisons test	Mean 1	Mean 2	Significant?	Summary	Adjusted P Value
Control vs. NE-a1,2-modulation	47,76	48,36	No	ns	>0,9999
Control vs. NE-a1,2+ß-modulation	47,76	20,31	No	ns	0,2867
Control vs. After washout	47,76	7,295	No	ns	0,0947

Appendix table 11 **Two way ANOVA analysis of dorsal and ventral theta modulated units in different NE modulated conditions**

Two-way ANOVA and Sidak's multiple comparisons test of theta modulated units in % for all experiments (n=7) under control and pharmacological NE modulation conditions.

Two-way RM ANOVA Matching: Across row

Source of Variation	% of total variation	P value	P value summary	Significant?	F (DFn, DFd)
Interaction	0,8363	0,0489	*	Yes	F (3, 42) = 5,7
Anatomical distribution	8,617	0,0477	*	Yes	F (1, 14) = 4,9
Pharmacological modulation	4,051	0,0696	ns	No	F (3, 42) = 2,5
Subjects (matching)	64,13	<0,0001	****	Yes	F (14, 42) = 8,6

Sidak's multiple comparisons test

percent dorsal - percent ventral	Mean % dorsal	Mean % ventral	Mean Diff,	95,00% CI of diff,	Significant?	Summary	Adjusted P Value
Control	30,77	26,28	4,484	-13,71 to 22,67	Yes	*	0,0456
NE-a1,2-modulation	38,02	26,22	11,8	-6,389 to 29,99	Yes	**	0,0085
NE-a1,2+ß-modulation	34,85	26,53	8,318	-9,872 to 26,51	No	ns	0,6738
After washout	28,93	20,14	8,786	-9,404 to 26,98	Yes	*	0,0423

Appendix table 12 **Two way ANOVA analysis of theta modulated units with LC fiber stimulation under different NE modulated conditions**

A. Two way ANOVA analysis of percent of theta units of all units before and during optogenetic stimulation during different pharmacological conditions. Repeated measurements and Sidak's multiple comparisons test of all 14 experiments. **B.** See A with frequency of theta modulated units. **C.** See A with amplitude of theta modulated units.

A

Proportion of theta modulated units, before vs. during optogenetic stimulation

Source of Variation	% of total variation	P value	P value summary	Significant?
Optogenetic modulation	0,03149	0,4973	ns	No
Pharmacological modulation	6,823	0,0099	**	Yes
Interaction: Optog. mod. x Pharma. mod.	0,2034	0,0823	ns	No

Sidak's multiple comparisons test

Baseline - Stim	Mean Diff,	95,00% CI of diff,	Significant?	Summary	Adjusted P Value
Control	-1,761	-3,889 to 0,3681	No	ns	0,14
NE-a1,2-modulation	-0,1929	-2,322 to 1,936	No	ns	0,9988
NE-a1,2+ß-modulation	-0,9721	-3,101 to 1,157	No	ns	0,6669
After washout	1,204	-0,9252 to 3,332	No	ns	0,4728

B

Frequency of theta modulated units, before vs. during optogenetic stimulation

Source of Variation	% of total variation	P value	P value summary	Significant?
Optogenetic modulation	0,8758	0,2202	ns	No
Pharmacological modulation	5,984	0,4392	ns	No
Interaction: Optog. mod. x Pharma. mod.	0,7836	0,4331	ns	No

Sidak's multiple comparisons test

Baseline - Stim	Mean Diff,	95,00% CI of diff,	Significant?	Summary	Adjusted P Value
Control	-0,2667	-0,7287 to 0,1953	No	ns	0,4404
NE-a1,2-modulation	-0,2843	-0,7463 to 0,1777	No	ns	0,3789
NE-a1,2+ß-modulation	0,08092	-0,3811 to 0,5429	No	ns	0,9839
After washout	-0,1461	-0,6081 to 0,3159	No	ns	0,8757

C

Amplitude of theta modulated units, before vs. during optogenetic stimulation

Source of Variation	% of total variation	P value	P value summary	Significant?
Optogenetic modulation	0,7676	0,2323	ns	No
Pharmacological modulation	19,57	0,0238	*	Yes
Interaction: Optog. mod. x Pharma. mod.	0,7438	0,526	ns	No

Sidak's multiple comparisons test

Baseline - Stim	Mean Diff,	95,00% CI of diff,	Significant?	Summary	Adjusted P Value
Control	15,15	-4,866 to 35,17	No	ns	0,1973
NE-a1,2-modulation	5,229	-14,79 to 25,25	No	ns	0,9333
NE-a1,2+ß-modulation	1,862	-18,15 to 21,88	No	ns	0,9986
After washout	0,7833	-19,23 to 20,8	No	ns	>0,9999

Appendix table 13 **Statistical analysis of patch clamp recordings of VGluT2 identified units in MSDB**
To test the distribution of responsive glutamatergic cells between dorsal and ventral MSDB, Fisher's exact test was used.

Test	Fisher's exact test
P value	0,0163
P value summary	*
One- or two-sided	Two-sided
Statistically significant (P < 0.05)?	Yes

Data analyzed	unresponsive	responsive	Total
dorsal	5	8	13
ventral	13	2	15
Total	18	10	28

Appendix table 14 **Mean depolarization response upon LC fiber stimulation in baseline vs. NE-modulated conditions**

Statistical comparison using a Wilcoxon matched-pairs signed rank t-test. N = 10 cells.

	Baseline	NE-modulation
Number of values	8	4
Mean	9,387	7,818
Std. Deviation	8,796	4,909
Std. Error of Mean	3,11	2,454

Wilcoxon matched-pairs signed rank test

P value	0,125
Exact or approximate P value?	Exact
P value summary	ns
Significantly different (P < 0.05)?	No
One- or two-tailed P value?	Two-tailed
Sum of positive, negative ranks	0 , -10
Sum of signed ranks (W)	-10
Number of pairs	4

6.2 Abbreviations

µ	Mean
µg	Microgram
µl	Microliter
µm	Micrometer
µM	Micromolar
AAV	Adeno-associated virus type 2
ACSF	Artificial cerebrospinal fluid
AR	Adrenergic receptor
BF	Basal forebrain
CA1	Cornu ammonis region 1
CA2	Cornu ammonis region 2
CA3	Cornu ammonis region 3
cAMP	Cyclic adenosine monophosphate
ChAT	Choline acetyltransferase
ChR2	Channel Rhodopsin 2
cm	Centimeter
CNS	Central nervous system
cre	Creates-recombination protein
DAG	Diacylglycerol
DNA	Deoxyribonucleic acid
EYFP	Enhanced yellow fluorescent protein
g	Gramm
GABA	γ-aminobutyric-acid
Gal	Galanin
HCF	Hippocampal formation
Hz	Hertz
IP_3	Inositol triphosphate
LC	Locus coeruleus
LFP	Local field potential
loxP sites	Designated cleaving sites
MEA	Microelectrode array
mg	Milligram

min	Minute
mm	Millimeter
MPOA	Medial preoptic area
ms	Millisecond
MSA	Medial septal area
MSDB	Medial septum and the diagonal band of Broca
mW	Milliwatt
NE	Norepinephrine
nm	Nanometer
nM	Nanomolar
NPY	Neuropeptide Y
pA	Picoamperes
PIP_2	Phosphatidylinositol 4,5-biphosphate
PKA	Protein kinase A
PV	Parvalbumin
SD	Standard Deviations
TH1-Cre	Genetically modified mouse line B6.Cg-7630403G23Rik$^{Tg(Th\text{-}cre)1Tmd}$/J
TiN	Titanium nitride
VGluT2	Vesicular glutamate transporter isoform 2
VGluT2-Cre	Genetically modified mouse line Slc17a6 tm2(cre)Lowl /J
WPRE	Woodchuck hepatitis virus posttranscriptional regulatory element

Bibliography

Alreja, M.; Liu, W. (1996): Noradrenaline induces IPSCs in rat medial septal/diagonal band neurons. Involvement of septohippocampal GABAergic neurons. In *The Journal of physiology* 494 (Pt 1), pp. 201–215.

Alsene, Karen M.; Fallace, Katie; Bakshi, Vaishali P. (2010): Ventral striatal noradrenergic mechanisms contribute to sensorimotor gating deficits induced by amphetamine. In *Neuropsychopharmacology : official publication of the American College of Neuropsychopharmacology* 35 (12), pp. 2346–2356. DOI: 10.1038/npp.2010.106.

Anaclet, Christelle; Pedersen, Nigel P.; Ferrari, Loris L.; Venner, Anne; Bass, Caroline E.; Arrigoni, Elda; Fuller, Patrick M. (2015): Basal forebrain control of wakefulness and cortical rhythms. In *Nature communications* 6, p. 8744. DOI: 10.1038/ncomms9744.

Aono, Yuri; Taguchi, Hiroko; Saigusa, Tadashi; Uchida, Takuya; Takada, Koji; Takiguchi, Hatakazu et al. (2015): Simultaneous activation of the α1A-, α1B- and α1D-adrenoceptor subtypes in the nucleus accumbens reduces accumbal dopamine efflux in freely moving rats. In *Behavioural pharmacology* 26 (1-2), pp. 73–80. DOI: 10.1097/FBP.0000000000000113.

Apartis, E.; Poindessous-Jazat, F. R.; Lamour, Y. A.; Bassant, M. H. (1998): Loss of rhythmically bursting neurons in rat medial septum following selective lesion of septohippocampal cholinergic system. In *Journal of neurophysiology* 79 (4), pp. 1633–1642. DOI: 10.1152/jn.1998.79.4.1633.

Arnsten, A. F. (2000): Through the looking glass. Differential noradenergic modulation of prefrontal cortical function. In *Neural plasticity* 7 (1-2), pp. 133–146. DOI: 10.1155/NP.2000.133.

Aston-Jones, G.; Bloom, F. E. (1981): Norepinephrine-containing locus coeruleus neurons in behaving rats exhibit pronounced responses to non-noxious environmental stimuli. In *The Journal of neuroscience : the official journal of the Society for Neuroscience* 1 (8), pp. 887–900.

Aston-Jones, G.; Rajkowski, J.; Cohen, J. (1999): Role of locus coeruleus in attention and behavioral flexibility. In *Biological psychiatry* 46 (9), pp. 1309–1320.

Aston-Jones, G.; Waterhouse, B. (2016): Locus coeruleus. From global projection system to adaptive regulation of behavior. In *Brain research* 1645, pp. 75–78. DOI: 10.1016/j.brainres.2016.03.001.

Aston-Jones, Gary; Cohen, Jonathan D. (2005): An integrative theory of locus coeruleus-norepinephrine function. Adaptive gain and optimal performance. In *Annual review of neuroscience* 28, pp. 403–450. DOI: 10.1146/annurev.neuro.28.061604.135709.

Aston-Jones, Gary; Zhu, Yan; Card, J. Patrick (2004): Numerous GABAergic afferents to locus ceruleus in the pericerulear dendritic zone. Possible interneuronal pool. In *The Journal of neuroscience : the official journal of the Society for Neuroscience* 24 (9), pp. 2313–2321. DOI: 10.1523/JNEUROSCI.5339-03.2004.

Atzori, Marco; Cuevas-Olguin, Roberto; Esquivel-Rendon, Eric; Garcia-Oscos, Francisco; Salgado-Delgado, Roberto C.; Saderi, Nadia et al. (2016): Locus Ceruleus Norepinephrine Release. A Central Regulator of CNS Spatio-Temporal Activation? In *Frontiers in synaptic neuroscience* 8, p. 25. DOI: 10.3389/fnsyn.2016.00025.

Becchetti, Andrea; Gullo, Francesca; Bruno, Giuseppe; Dossi, Elena; Lecchi, Marzia; Wanke, Enzo (2012): Exact distinction of excitatory and inhibitory neurons in neural networks. A study with GFP-GAD67 neurons optically and electrophysiologically recognized on multielectrode arrays. In *Frontiers in neural circuits* 6, p. 63. DOI: 10.3389/fncir.2012.00063.

Bender, Franziska; Gorbati, Maria; Cadavieco, Marta Carus; Denisova, Natalia; Gao, Xiaojie; Holman, Constance et al. (2015): Theta oscillations regulate the speed of locomotion via a hippocampus to lateral septum pathway. In *Nature communications* 6, p. 8521. DOI: 10.1038/ncomms9521.

Berardis, Domenico de; Marini, Stefano; Serroni, Nicola; Iasevoli, Felice; Tomasetti, Carmine; Bartolomeis, Andrea de et al. (2015): Targeting the Noradrenergic System in Posttraumatic Stress Disorder. A Systematic Review and Meta-Analysis of Prazosin Trials. In *Current drug targets* 16 (10), pp. 1094–1106. DOI: 10.2174/1389450116666150506114108.

Berridge, C. W.; Foote, S. L. (1996): Enhancement of behavioral and electroencephalographic indices of waking following stimulation of noradrenergic beta-receptors within the medial septal region of the basal forebrain. In *The Journal of neuroscience : the official journal of the Society for Neuroscience* 16 (21), pp. 6999–7009.

Berridge, C. W.; Isaac, S. O.; España, R. A. (2003): Additive wake-promoting actions of medial basal forebrain noradrenergic alpha1- and beta-receptor stimulation. In *Behavioral neuroscience* 117 (2), pp. 350–359.

Berridge, C. W.; Morris, M. F. (2000): Amphetamine-induced activation of forebrain EEG is prevented by noradrenergic beta-receptor blockade in the halothane-anesthetized rat. In *Psychopharmacology* 148 (3), pp. 307–313. DOI: 10.1007/s002130050055.

Berridge, Craig W.; Schmeichel, Brooke E.; España, Rodrigo A. (2012): Noradrenergic modulation of wakefulness/arousal. In *Sleep medicine reviews* 16, pp. 187–197. DOI: 10.1016/j.smrv.2011.12.003.

Berridge, Craig W.; Waterhouse, Barry D. (2003): The locus coeruleus-noradrenergic system. Modulation of behavioral state and state-dependent cognitive processes. In *Brain research. Brain research reviews* 42 (1), pp. 33–84.

Boehm, S. (1999): Presynaptic alpha2-adrenoceptors control excitatory, but not inhibitory, transmission at rat hippocampal synapses. In *The Journal of physiology* 519 Pt 2, pp. 439–449. DOI: 10.1111/j.1469-7793.1999.0439m.x.

Brazhnik, E. S.; Fox, S. E. (1999): Action potentials and relations to the theta rhythm of medial septal neurons in vivo. In *Experimental brain research* 127 (3), pp. 244–258. DOI: 10.1007/s002210050794.

Broese, M.; Riemann, D.; Hein, L.; Nissen, C. (2012): α-Adrenergic receptor function, arousal and sleep. Mechanisms and therapeutic implications. In *Pharmacopsychiatry* 45 (6), pp. 209–216. DOI: 10.1055/s-0031-1299728.

Buzsáki, G.; Leung, L. W.; Vanderwolf, C. H. (1983): Cellular bases of hippocampal EEG in the behaving rat. In *Brain research* 287 (2), pp. 139–171. DOI: 10.1016/0165-0173(83)90037-1.

Buzsáki, György (1986): Hippocampal sharp waves. Their origin and significance. In *Brain research* 398 (2), pp. 242–252. DOI: 10.1016/0006-8993(86)91483-6.

Buzsáki, György (2002): Theta Oscillations in the Hippocampus. In *Neuron* 33 (3), pp. 325–340. DOI: 10.1016/S0896-6273(02)00586-X.

Buzsáki, György; Anastassiou, Costas A.; Koch, Christof (2012): The origin of extracellular fields and currents--EEG, ECoG, LFP and spikes. In *Nature reviews. Neuroscience* 13, pp. 407–420. DOI: 10.1038/nrn3241.

Carter, Matthew E.; Yizhar, Ofer; Chikahisa, Sachiko; Nguyen, Hieu; Adamantidis, Antoine; Nishino, Seiji et al. (2010): Tuning arousal with optogenetic modulation of locus coeruleus neurons. In *Nature neuroscience* 13, pp. 1526–1533. DOI: 10.1038/nn.2682.

Chandler, Daniel J. (2016): Evidence for a specialized role of the locus coeruleus noradrenergic system in cortical circuitries and behavioral operations. In *Brain research* 1641, pp. 197–206. DOI: 10.1016/j.brainres.2015.11.022.

Chandler, Daniel J.; Gao, Wen-Jun; Waterhouse, Barry D. (2014): Heterogeneous organization of the locus coeruleus projections to prefrontal and motor cortices. In *Proceedings of the National Academy of Sciences of the United States of America* 111, pp. 6816–6821. DOI: 10.1073/pnas.1320827111.

Colom, Luis V.; Castaneda, Maria T.; Reyna, Tania; Hernandez, Sofia; Garrido-Sanabria, Emilio (2005): Characterization of medial septal glutamatergic neurons and their projection to the hippocampus. In *Synapse (New York, N.Y.)* 58 (3), pp. 151–164. DOI: 10.1002/syn.20184.

Coull, J. T. (1994): Pharmacological manipulations of the alpha 2-noradrenergic system. Effects on cognition. In *Drugs & aging* 5 (2), pp. 116–126. DOI: 10.2165/00002512-199405020-00005.

Daaka, Y.; Luttrell, L. M.; Lefkowitz, R. J. (1997): Switching of the coupling of the beta2-adrenergic receptor to different G proteins by protein kinase A. In *Nature* 390 (6655), pp. 88–91. DOI: 10.1038/36362.

Dahlström, A.; Fuxe, Kjell (1964): Evidence for the existance of monoamine-containing neurons in the central nervous system. DEMONSTRATION OF MONOAMINES IN THE CELL BODIES OF BRAIN STEM NEURONS. In *Acta physiologica Scandinavica. Supplementum*, SUPPL 232:1-55.

Dailey, Michael (2002): Optical Imaging of Neural Structure and Physiology. Confocal Fluorescence Microscopy in Live Brain Slices. In : Brain Mapping: The Methods, pp. 49–76.

Delaville, Claire; Deurwaerdère, Philippe de; Benazzouz, Abdelhamid (2011): Noradrenaline and Parkinson's disease. In *Frontiers in systems neuroscience* 5, p. 31. DOI: 10.3389/fnsys.2011.00031.

Devilbiss, David M.; Page, Michelle E.; Waterhouse, Barry D. (2006): Locus ceruleus regulates sensory encoding by neurons and networks in waking animals. In *The Journal of neuroscience : the official journal of the Society for Neuroscience* 26, pp. 9860–9872. DOI: 10.1523/JNEUROSCI.1776-06.2006.

Di Mauro, Michela; Li Volsi, Guido; Licata, Flora (2013): Noradrenergic control of neuronal firing in cerebellar nuclei. Modulation of GABA responses. In *Cerebellum (London, England)* 12 (3), pp. 350–361. DOI: 10.1007/s12311-012-0422-2.

DiNuzzo, Mauro; Mascali, Daniele; Moraschi, Marta; Bussu, Giorgia; Maugeri, Laura; Mangini, Fabio et al. (2019): Brain Networks Underlying Eye's Pupil Dynamics. In *Frontiers in neuroscience* 13, p. 965. DOI: 10.3389/fnins.2019.00965.

Dohlman, H. G.; Thorner, J.; Caron, M. G.; Lefkowitz, R. J. (1991): Model systems for the study of seven-transmembrane-segment receptors. In *Annual review of biochemistry* 60, pp. 653–688. DOI: 10.1146/annurev.bi.60.070191.003253.

Dorn, Gerald W. (2010): Adrenergic signaling polymorphisms and their impact on cardiovascular disease. In *Physiological reviews* 90 (3), pp. 1013–1062. DOI: 10.1152/physrev.00001.2010.

España, Rodrigo A.; Berridge, Craig W. (2006): Organization of noradrenergic efferents to arousal-related basal forebrain structures. In *The Journal of comparative neurology* 496, pp. 668–683. DOI: 10.1002/cne.20946.

Euler, U. vonS. (1946): Sympathin in adrenergic nerve fibres. In *The Journal of physiology* 105, p. 26.

Falck, Bengt; Hillarp, Nils-Åke (1959): On the cellular localization of catechol amines in the brain. In *Acta anatomica* 38, pp. 277–279. DOI: 10.1159/000141530.

Feng, Jiesi; Zhang, Changmei; Lischinsky, Julieta E.; Jing, Miao; Zhou, Jingheng; Wang, Huan et al. (2019): A Genetically Encoded Fluorescent Sensor for Rapid and Specific In Vivo Detection of Norepinephrine. In *Neuron* 102 (4), 745-761.e8. DOI: 10.1016/j.neuron.2019.02.037.

Flicker, C.; Geyer, M. A. (1982): The hippocampus as a possible site of action for increased locomotion during intracerebral infusions of norepinephrine. In *Behavioral and neural biology* 34 (4), pp. 421–426.

Foote, S. L.; Aston-Jones, G.; Bloom, F. E. (1980): Impulse activity of locus coeruleus neurons in awake rats and monkeys is a function of sensory stimulation and arousal. In *Proceedings of the National Academy of Sciences of the United States of America* 77 (5), pp. 3033–3037.

Fuhrmann, Falko; Justus, Daniel; Sosulina, Liudmila; Kaneko, Hiroshi; Beutel, Tatjana; Friedrichs, Detlef et al. (2015): Locomotion, Theta Oscillations, and the Speed-Correlated Firing of Hippocampal Neurons Are Controlled by a Medial Septal Glutamatergic Circuit. In *Neuron* 86, pp. 1253–1264. DOI: 10.1016/j.neuron.2015.05.001.

Fumagalli, Carlo; Maurizi, Niccolò; Marchionni, Niccolò; Fornasari, Diego (2019): β-blockers. Their new life from hypertension to cancer and migraine. In *Pharmacological research*, p. 104587. DOI: 10.1016/j.phrs.2019.104587.

Geisler, Caroline; Robbe, David; Zugaro, Michaël; Sirota, Anton; Buzsáki, György (2007): Hippocampal place cell assemblies are speed-controlled oscillators. In *Proceedings of the National Academy of Sciences of the United States of America* 104 (19), pp. 8149–8154. DOI: 10.1073/pnas.0610121104.

Goulding, Martyn (2009): Circuits controlling vertebrate locomotion. Moving in a new direction. In *Nature reviews. Neuroscience* 10 (7), pp. 507–518. DOI: 10.1038/nrn2608.

Gritti, I.; Henny, P.; Galloni, F.; Mainville, L.; Mariotti, M.; Jones, B. E. (2006): Stereological estimates of the basal forebrain cell population in the rat, including neurons containing choline acetyltransferase, glutamic acid decarboxylase or phosphate-activated glutaminase and colocalizing vesicular glutamate transporters. In *Neuroscience* 143 (4), pp. 1051–1064. DOI: 10.1016/j.neuroscience.2006.09.024.

Gross, G. W.; Rieske, E.; Kreutzberg, G. W.; Meyer, A. (1977): A new fixed-array multi-microelectrode system designed for long-term monitoring of extracellular single unit neuronal activity in vitro. In *Neuroscience letters* 6 (2-3), pp. 101–105. DOI: 10.1016/0304-3940(77)90003-9.

Grzanna, R.; Molliver, M. E. (1980): The locus coeruleus in the rat. An immunohistochemical delineation. In *Neuroscience* 5 (1), pp. 21–40. DOI: 10.1016/0306-4522(80)90068-8.

Haas, H. L.; Schaerer, B.; Vosmansky, M. (1979): A simple perfusion chamber for the study of nervous tissue slices in vitro. In *Journal of neuroscience methods* 1 (4), pp. 323–325. DOI: 10.1016/0165-0270(79)90021-9.

Hagan, J. J.; Salamone, J. D.; Simpson, J.; Iversen, S. D.; Morris, R. G. (1988): Place navigation in rats is impaired by lesions of medial septum and diagonal band but not nucleus basalis magnocellularis. In *Behavioural brain research* 27 (1), pp. 9–20.

Haghdoost-Yazdi, H.; Pasbakhsh, P.; Vatanparast, J.; Rajaei, F.; Behzadi, G. (2009): Topographical and quantitative distribution of the projecting neurons to main divisions of the septal area. In *Neurological research* 31 (5), pp. 503–513. DOI: 10.1179/174313208X353712.

Hangya, Balázs; Borhegyi, Zsolt; Szilágyi, Nóra; Freund, Tamás F.; Varga, Viktor (2009): GABAergic neurons of the medial septum lead the hippocampal network during theta activity. In *The Journal of*

neuroscience : the official journal of the Society for Neuroscience 29, pp. 8094–8102. DOI: 10.1523/JNEUROSCI.5665-08.2009.

Hannes, Christian (2017): Activity patterns in the septal-hippocampal network predict voluntary locomotion. Dissertation. Rheinischen Friedrich-Wilhelms-Universität Bonn, Bonn. Mathematisch-Naturwissenschaftlichen Fakultät.

Herman, Alexander M.; Ortiz-Guzman, Joshua; Kochukov, Mikhail; Herman, Isabella; Quast, Kathleen B.; Patel, Jay M. et al. (2016): A cholinergic basal forebrain feeding circuit modulates appetite suppression. In *Nature* 538 (7624), pp. 253–256. DOI: 10.1038/nature19789.

Holets, V. R.; Hökfelt, T.; Rökaeus, Å.; Terenius, L.; Goldstein, M. (1988): Locus coeruleus neurons in the rat containing neuropeptide Y, tyrosine hydroxylase or galanin and their efferent projections to the spinal cord, cerebral cortex and hypothalamus. In *Neuroscience* 24 (3), pp. 893–906. DOI: 10.1016/0306-4522(88)90076-0.

Holsheimer, J.; Boer, J.; Lopes da Silva, F. H.; van Rotterdam, A. (1982): The double dipole model of theta rhythm generation. Simulation of laminar field potential profiles in dorsal hippocampus of the rat. In *Brain research* 235 (1), pp. 31–50. DOI: 10.1016/0006-8993(82)90194-9.

Horn, Anja K.E. (2005): The reticular formation. In Jean A. Büttner-Ennever (Ed.): Neuroanatomy of the oculomotor system, vol. 151. Updated extended ed. Amsterdam, Oxford: Elsevier (Progress in Brain Research, v. 151), pp. 127–155.

Humpel, C. (2015): Organotypic brain slice cultures. A review. In *Neuroscience* 305, pp. 86–98. DOI: 10.1016/j.neuroscience.2015.07.086.

Hur, Elizabeth E.; Zaborszky, Laszlo (2005): Vglut2 afferents to the medial prefrontal and primary somatosensory cortices. A combined retrograde tracing in situ hybridization study corrected. In *J. Comp. Neurol.* 483 (3), pp. 351–373. DOI: 10.1002/cne.20444.

Ivanov, Anton; Zilberter, Yuri (2011): Critical state of energy metabolism in brain slices. The principal role of oxygen delivery and energy substrates in shaping neuronal activity. In *Frontiers in neuroenergetics* 3, p. 9. DOI: 10.3389/fnene.2011.00009.

Jiménez-Rivera, Carlos A.; Feliu-Mojer, Monica; Vázquez-Torres, Rafael (2006): Alpha-noradrenergic receptors modulate the development and expression of cocaine sensitization. In *Annals of the New York Academy of Sciences* 1074, pp. 390–402. DOI: 10.1196/annals.1369.039.

Joshi, Siddhartha; Li, Yin; Kalwani, Rishi M.; Gold, Joshua I. (2016): Relationships between Pupil Diameter and Neuronal Activity in the Locus Coeruleus, Colliculi, and Cingulate Cortex. In *Neuron* 89 (1), pp. 221–234. DOI: 10.1016/j.neuron.2015.11.028.

Kandel, Eric R.; Schwartz, James H.; Jessell, Thomas; Siegelbaum, Steven A.; Hudspeth, A. J.; Mack, Sarah (Eds.) (2013): Principles of neural science. Fifth edition. New York, Lisbon, London: McGraw-Hill Medical.

Kempadoo, Kimberly A.; Mosharov, Eugene V.; Choi, Se Joon; Sulzer, David; Kandel, Eric R. (2016): Dopamine release from the locus coeruleus to the dorsal hippocampus promotes spatial learning and memory. In *Proceedings of the National Academy of Sciences of the United States of America* 113 (51), pp. 14835–14840. DOI: 10.1073/pnas.1616515114.

Kiss, J.; Maglóczky, Z.; Somogyi, J.; Freund, T. F. (1997): Distribution of calretinin-containing neurons relative to other neurochemically identified cell types in the medial septum of the rat. In *Neuroscience* 78 (2), pp. 399–410.

Kitchigina, V. F.; Kutyreva, E. S.; Sudnitsyn, V. V. (2005): Sensory responses of neurons in the medial septal area in conditions of modulation of theta activity using the alpha-2-adrenoreceptor agonist clonidine. In *Neuroscience and behavioral physiology* 35, pp. 107–116.

Kitchigina, V. F.; Kutyreva, E. V.; Brazhnik, E. S. (2003): Modulation of theta rhythmicity in the medial septal neurons and the hippocampal electroencephalogram in the awake rabbit via actions at noradrenergic alpha2-receptors. In *Neuroscience* 120, pp. 509–521.

Köhler, C.; Chan-Palay, V.; Wu, J. Y. (1984): Septal neurons containing glutamic acid decarboxylase immunoreactivity project to the hippocampal region in the rat brain. In *Anatomy and embryology* 169 (1), pp. 41–44. DOI: 10.1007/bf00300585.

Lein, Ed S.; Hawrylycz, Michael J.; Ao, Nancy; Ayres, Mikael; Bensinger, Amy; Bernard, Amy et al. (2007): Genome-wide atlas of gene expression in the adult mouse brain. In *Nature* 445 (7124), pp. 168–176. DOI: 10.1038/nature05453.

Lewis, P. R.; Shute, C. C. (1967): The cholinergic limbic system. Projections to hippocampal formation, medial cortex, nuclei of the ascending cholinergic reticular system, and the subfornical organ and supra-optic crest. In *Brain : a journal of neurology* 90 (3), pp. 521–540. DOI: 10.1093/brain/90.3.521.

Lippiello, Pellegrino; Hoxha, Eriola; Volpicelli, Floriana; Lo Duca, Giuseppina; Tempia, Filippo; Miniaci, Maria Concetta (2015): Noradrenergic modulation of the parallel fiber-Purkinje cell synapse in mouse cerebellum. In *Neuropharmacology* 89, pp. 33–42. DOI: 10.1016/j.neuropharm.2014.08.016.

Lo, Liching; Anderson, David J. (2011): A Cre-dependent, anterograde transsynaptic viral tracer for mapping output pathways of genetically marked neurons. In *Neuron* 72 (6), pp. 938–950. DOI: 10.1016/j.neuron.2011.12.002.

Loos, Maarten; Koopmans, Bastijn; Aarts, Emmeke; Maroteaux, Gregoire; van der Sluis, Sophie; Verhage, Matthijs; Smit, August B. (2014): Sheltering behavior and locomotor activity in 11 genetically diverse common inbred mouse strains using home-cage monitoring. In *PloS one* 9 (9), e108563. DOI: 10.1371/journal.pone.0108563.

Manns, Ian D.; Lee, Maan Gee; Modirrousta, Mandana; Hou, Yiping P.; Jones, Barbara E. (2003): Alpha 2 adrenergic receptors on GABAergic, putative sleep-promoting basal forebrain neurons. In *Eur J Neurosci* 18 (3), pp. 723–727. DOI: 10.1046/j.1460-9568.2003.02788.x.

Manzanares, G.; Brito-da-Silva, G.; Gandra, P. G. (2018): Voluntary wheel running. Patterns and physiological effects in mice. In *Brazilian journal of medical and biological research = Revista brasileira de pesquisas medicas e biologicas* 52 (1), e7830. DOI: 10.1590/1414-431X20187830.

Mason, S. T.; Fibiger, H. C. (1979): Regional topography within noradrenergic locus coeruleus as revealed by retrograde transport of horseradish peroxidase. In *The Journal of comparative neurology* 187, pp. 703–724. DOI: 10.1002/cne.901870405.

Maura, G.; Gemignani, A.; Raiteri, M. (1985): Alpha 2-adrenoceptors in rat hypothalamus and cerebral cortex. Functional evidence for pharmacologically distinct subpopulations. In *European journal of pharmacology* 116 (3), pp. 335–339. DOI: 10.1016/0014-2999(85)90173-6.

McAinsh, J.; Cruickshank, J. M. (1990): Beta-blockers and central nervous system side effects. In *Pharmacology & therapeutics* 46 (2), pp. 163–197. DOI: 10.1016/0163-7258(90)90092-g.

McBurney-Lin, Jim; Lu, Ju; Zuo, Yi; Yang, Hongdian (2019): Locus coeruleus-norepinephrine modulation of sensory processing and perception. A focused review. In *Neuroscience and biobehavioral reviews* 105, pp. 190–199. DOI: 10.1016/j.neubiorev.2019.06.009.

McCall, Jordan G.; Al-Hasani, Ream; Siuda, Edward R.; Hong, Daniel Y.; Norris, Aaron J.; Ford, Christopher P.; Bruchas, Michael R. (2015): CRH Engagement of the Locus Coeruleus Noradrenergic System Mediates Stress-Induced Anxiety. In *Neuron* 87 (3), pp. 605–620. DOI: 10.1016/j.neuron.2015.07.002.

McCall, Jordan G.; Siuda, Edward R.; Bhatti, Dionnet L.; Lawson, Lamley A.; McElligott, Zoe A.; Stuber, Garret D.; Bruchas, Michael R. (2017): Locus coeruleus to basolateral amygdala noradrenergic projections promote anxiety-like behavior. In *eLife* 6. DOI: 10.7554/eLife.18247.

McKenna, James T.; Yang, Chun; Franciosi, Serena; Winston, Stuart; Abarr, Kathleen K.; Rigby, Matthew S. et al. (2013): Distribution and intrinsic membrane properties of basal forebrain GABAergic and parvalbumin neurons in the mouse. In *The Journal of comparative neurology* 521 (6), pp. 1225–1250. DOI: 10.1002/cne.23290.

McLellan, Micheal A.; Rosenthal, Nadia A.; Pinto, Alexander R. (2017): Cre-loxP-Mediated Recombination. General Principles and Experimental Considerations. In *Current protocols in mouse biology* 7 (1), pp. 1–12. DOI: 10.1002/cpmo.22.

McNaughton, Neil; Ruan, Ming; Woodnorth, Mary-Anne (2006): Restoring theta-like rhythmicity in rats restores initial learning in the Morris water maze. In *Hippocampus* 16 (12), pp. 1102–1110. DOI: 10.1002/hipo.20235.

Mefford, I. N. (1988): Epinephrine in mammalian brain. In *Progress in neuro-psychopharmacology & biological psychiatry* 12 (4), pp. 365–388. DOI: 10.1016/0278-5846(88)90099-1.

Meibach, R. C.; Siegel, A. (1977): Efferent connections of the septal area in the rat. An analysis utilizing retrograde and anterograde transport methods. In *Brain research* 119 (1), pp. 1–20. DOI: 10.1016/0006-8993(77)90088-9.

Meijer, Johanna H.; Robbers, Yuri (2014): Wheel running in the wild. In *Proceedings. Biological sciences* 281 (1786). DOI: 10.1098/rspb.2014.0210.

Milner, T. A.; Lee, A.; Aicher, S. A.; Rosin, D. L. (1998): Hippocampal alpha2a-adrenergic receptors are located predominantly presynaptically but are also found postsynaptically and in selective astrocytes. In *J. Comp. Neurol.* 395 (3), pp. 310–327.

Mogenson, G. J.; Jones, D. L.; Yim, C. Y. (1980): From motivation to action. Functional interface between the limbic system and the motor system. In *Progress in neurobiology* 14, pp. 69–97.

Moises, H. C.; Waterhouse, B. D.; Woodward, D. J. (1983): Locus coeruleus stimulation potentiates local inhibitory processes in rat cerebellum. In *Brain research bulletin* 10 (6), pp. 795–804. DOI: 10.1016/0361-9230(83)90211-3.

Morris, R. G.; Garrud, P.; Rawlins, J. N.; O'Keefe, J. (1982): Place navigation impaired in rats with hippocampal lesions. In *Nature* 297 (5868), pp. 681–683. DOI: 10.1038/297681a0.

Morrow, A. L.; Creese, I. (1986): Characterization of alpha 1-adrenergic receptor subtypes in rat brain. A reevaluation of 3HWB4104 and 3Hprazosin binding. In *Molecular pharmacology* 29 (4), pp. 321–330.

Naegeli, Christoph; Zeffiro, Thomas; Piccirelli, Marco; Jaillard, Assia; Weilenmann, Anina; Hassanpour, Katayun et al. (2018): Locus Coeruleus Activity Mediates Hyperresponsiveness in Posttraumatic Stress Disorder. In *Biological psychiatry* 83 (3), pp. 254–262. DOI: 10.1016/j.biopsych.2017.08.021.

Nagel, Georg; Szellas, Tanjef; Huhn, Wolfram; Kateriya, Suneel; Adeishvili, Nona; Berthold, Peter et al. (2003): Channelrhodopsin-2, a directly light-gated cation-selective membrane channel. In *Proceedings of the National Academy of Sciences of the United States of America* 100 (24), pp. 13940–13945. DOI: 10.1073/pnas.1936192100.

Nam, H.; Kerman, I. A. (2016): Distribution of catecholaminergic presympathetic-premotor neurons in the rat lower brainstem. In *Neuroscience* 324, pp. 430–445. DOI: 10.1016/j.neuroscience.2016.02.066.

Navarro-Castilla, Álvaro; Barja, Isabel; Díaz, Mario (2018): Foraging, feeding, and physiological stress responses of wild wood mice to increased illumination and common genet cues. In *Current zoology* 64 (4), pp. 409–417. DOI: 10.1093/cz/zox048.

Pachitariu, Marius; Steinmetz, Nicholas A.; Kadir, Shabnam N.; Carandini, Matteo; Harris, Kenneth D. (2016): Fast and accurate spike sorting of high-channel count probes with KiloSort. In. Advances in Neural Information Processing Systems, pp. 4448–4456. Available online at http://papers.nips.cc/paper/6326-fast-and-accurate-spike-sorting-of-high-channel-count-probes-with-kilosort.pdf.

Pfaff, Donald; Ribeiro, Ana; Matthews, James; Kow, Lee-Ming (2008): Concepts and mechanisms of generalized central nervous system arousal. In *Annals of the New York Academy of Sciences* 1129, pp. 11–25. DOI: 10.1196/annals.1417.019.

Pickel, V. M.; Segal, M.; Bloom, F. E. (1974): A radioautographic study of the efferent pathways of the nucleus locus coeruleus. In *The Journal of comparative neurology* 155 (1), pp. 15–42. DOI: 10.1002/cne.901550103.

Pudovkina, Olga L.; Cremers, Thomas I. F. H.; Westerink, Ben H. C. (2002): The interaction between the locus coeruleus and dorsal raphe nucleus studied with dual-probe microdialysis. In *European journal of pharmacology* 445 (1-2), pp. 37–42. DOI: 10.1016/s0014-2999(02)01663-1.

Purves, Dale; Augustine, George J. editor; Fitzpatrick, David; Hall, William C.; LaMantia, Anthony-Samuel; White, Leonard E. (2012): Neuroscience. 5th. London: Palgrave Macmillan.

Ramos, Brian P.; Arnsten, Amy F. T. (2007): Adrenergic pharmacology and cognition. Focus on the prefrontal cortex. In *Pharmacology & therapeutics* 113, pp. 523–536. DOI: 10.1016/j.pharmthera.2006.11.006.

Rho, Hee-Jun; Kim, Jae-Hyun; Lee, Seung-Hee (2018): Function of Selective Neuromodulatory Projections in the Mammalian Cerebral Cortex. Comparison Between Cholinergic and Noradrenergic Systems. In *Frontiers in neural circuits* 12, p. 47. DOI: 10.3389/fncir.2018.00047.

Robinson, Jennifer; Manseau, Frédéric; Ducharme, Guillaume; Amilhon, Bénédicte; Vigneault, Erika; El Mestikawy, Salah; Williams, Sylvain (2016): Optogenetic Activation of Septal Glutamatergic Neurons Drive Hippocampal Theta Rhythms. In *The Journal of neuroscience : the official journal of the Society for Neuroscience* 36, pp. 3016–3023. DOI: 10.1523/JNEUROSCI.2141-15.2016.

Rolls, Edmund T. (2015): Limbic systems for emotion and for memory, but no single limbic system. In *Cortex; a journal devoted to the study of the nervous system and behavior* 62, pp. 119–157. DOI: 10.1016/j.cortex.2013.12.005.

Rosin, D. L. (2000): Distribution of alpha 2A- and alpha 2C-adrenergic receptor immunoreactivity in the central nervous system. In *Methods in molecular biology (Clifton, N.J.)* 126, pp. 475–505.

Sara, S. J. (1998): Learning by neurones. Role of attention, reinforcement and behaviour. In *Comptes rendus de l'Academie des sciences. Serie III, Sciences de la vie* 321 (2-3), pp. 193–198. DOI: 10.1016/s0764-4469(97)89821-6.

Sara, Susan J. (2009): The locus coeruleus and noradrenergic modulation of cognition. In *Nature reviews. Neuroscience* 10 (3), pp. 211–223. DOI: 10.1038/nrn2573.

Sarro, G. B. de; Ascioti, C.; Froio, F.; Libri, V.; Nisticò, G. (1987): Evidence that locus coeruleus is the site where clonidine and drugs acting at alpha 1- and alpha 2-adrenoceptors affect sleep and arousal

mechanisms. In *British journal of pharmacology* 90 (4), pp. 675–685. DOI: 10.1111/j.1476-5381.1987.tb11220.x.

Savitt, Joseph M.; Jang, Susie S.; Mu, Weitong; Dawson, Valina L.; Dawson, Ted M. (2005): Bcl-x is required for proper development of the mouse substantia nigra. In *The Journal of neuroscience : the official journal of the Society for Neuroscience* 25 (29), pp. 6721–6728. DOI: 10.1523/JNEUROSCI.0760-05.2005.

Schmidt, Karl T.; Weinshenker, David (2014): Adrenaline rush. The role of adrenergic receptors in stimulant-induced behaviors. In *Molecular pharmacology* 85, pp. 640–650.

Schwarz, Lindsay A.; Luo, Liqun (2015): Organization of the locus coeruleus-norepinephrine system. In *Current biology : CB* 25 (21), R1051-R1056. DOI: 10.1016/j.cub.2015.09.039.

Schwarz, Lindsay A.; Miyamichi, Kazunari; Gao, Xiaojing J.; Beier, Kevin T.; Weissbourd, Brandon; DeLoach, Katherine E. et al. (2015): Viral-genetic tracing of the input-output organization of a central noradrenaline circuit. In *Nature* 524, pp. 88–92. DOI: 10.1038/nature14600.

Segal, D. S.; Mandell, A. J. (1970): Behavioral activation of rats during intraventricular infusion of norepinephrine. In *Proceedings of the National Academy of Sciences of the United States of America* 66 (2), pp. 289–293. DOI: 10.1073/pnas.66.2.289.

Segal, Menahem; Bloom, Floyd E. (1976): The action of norepinephrine in the rat hippocampus. IV. The effects of locus coeruleus stimulation on evoked hippocampal unit activity. In *Brain research* 107 (3), pp. 513–525. DOI: 10.1016/0006-8993(76)90141-4.

Simon, Axelle Pascale; Poindessous-Jazat, Frédérique; Dutar, Patrick; Epelbaum, Jacques; Bassant, Marie-Hélène (2006): Firing properties of anatomically identified neurons in the medial septum of anesthetized and unanesthetized restrained rats. In *The Journal of neuroscience : the official journal of the Society for Neuroscience* 26 (35), pp. 9038–9046. DOI: 10.1523/JNEUROSCI.1401-06.2006.

Simpson, Kimberly L.; Altman, Daniel W.; Wang, Li; Kirifides, Michael L.; Lin, Rick C.-S.; Waterhouse, Barry D. (1997): Lateralization and functional organization of the locus coeruleus projection to the trigeminal somatosensory pathway in rat. In *J. Comp. Neurol.* 385 (1), pp. 135–147. DOI: 10.1002/(SICI)1096-9861(19970818)385:1<135::AID-CNE8>3.0.CO;2-3.

Smith, Caroline C.; Greene, Robert W. (2012): CNS dopamine transmission mediated by noradrenergic innervation. In *The Journal of neuroscience : the official journal of the Society for Neuroscience* 32 (18), pp. 6072–6080. DOI: 10.1523/JNEUROSCI.6486-11.2012.

Snoddy, A. M.; Tessel, R. E. (1985): Prazosin. Effect on psychomotor-stimulant cues and locomotor activity in mice. In *European journal of pharmacology* 116 (3), pp. 221–228.

Sotty, F.; Danik, M.; Manseau, F.; Laplante, F.; Quirion, R.; Williams, S. (2003): Distinct electrophysiological properties of glutamatergic, cholinergic and GABAergic rat septohippocampal neurons. Novel implications for hippocampal rhythmicity. In *The Journal of physiology* 551 (Pt 3), pp. 927–943. DOI: 10.1113/jphysiol.2003.046847.

Stähle, Helmut (2000): A historical perspective. Development of clonidine. In *Best Practice & Research Clinical Anaesthesiology* 14 (2), pp. 237–246. DOI: 10.1053/bean.2000.0079.

Sternberg, N.; Hamilton, D. (1981): Bacteriophage P1 site-specific recombination. I. Recombination between loxP sites. In *Journal of molecular biology* 150 (4), pp. 467–486. DOI: 10.1016/0022-2836(81)90375-2.

Stone, Eric A.; Lin, Yan; Rosengarten, Helen; Kramer, H. Kenneth; Quartermain, David (2003): Emerging evidence for a central epinephrine-innervated alpha 1-adrenergic system that regulates behavioral activation and is impaired in depression. In *Neuropsychopharmacology : official publication of the American College of Neuropsychopharmacology* 28 (8), pp. 1387–1399. DOI: 10.1038/sj.npp.1300222.

Strawn, J. R.; Geracioti, T. D. (2008): Noradrenergic dysfunction and the psychopharmacology of posttraumatic stress disorder. In *Depression and anxiety* 25 (3), pp. 260–271. DOI: 10.1002/da.20292.

Streeter, K. A.; Sunshine, M. D.; Patel, S. R.; Liddell, S. S.; Denholtz, L. E.; Reier, P. J. et al. (2017): Coupling multielectrode array recordings with silver labeling of recording sites to study cervical spinal network connectivity. In *Journal of neurophysiology* 117 (3), pp. 1014–1029. DOI: 10.1152/jn.00638.2016.

Sugisaki, E.; Fukushima, Y.; Tsukada, M.; Aihara, T. (2011): Cholinergic modulation on spike timing-dependent plasticity in hippocampal CA1 network. In *Neuroscience* 192, pp. 91–101. DOI: 10.1016/j.neuroscience.2011.06.064.

Swanson, L. W. (1976): The locus coeruleus. A cytoarchitectonic, golgi and immunohistochemical study in the albino rat. In *Brain research* 110 (1), pp. 39–56. DOI: 10.1016/0006-8993(76)90207-9.

Szabadi, Elemer (2013): Functional neuroanatomy of the central noradrenergic system. In *Journal of psychopharmacology (Oxford, England)* 27, pp. 659–693. DOI: 10.1177/0269881113490326.

T. C. Westfall (2009): Encyclopedia of Neuroscience. Sympathomimetic Drugs and Adrenergic Receptor Antagonists: Academic Press.

Takeuchi, Tomonori; Duszkiewicz, Adrian J.; Sonneborn, Alex; Spooner, Patrick A.; Yamasaki, Miwako; Watanabe, Masahiko et al. (2016): Locus coeruleus and dopaminergic consolidation of everyday memory. In *Nature* 537 (7620), pp. 357–362. DOI: 10.1038/nature19325.

Thomas Jr., C.; SPRINGER, P.; LOEB, G.; BERWALDNETTER, Y.; OKUN, L. (1972): A miniature microelectrode array to monitor the bioelectric activity of cultured cells. In *Experimental Cell Research* 74 (1), pp. 61–66. DOI: 10.1016/0014-4827(72)90481-8.

Totah, Nelson K.; Neves, Ricardo M.; Panzeri, Stefano; Logothetis, Nikos K.; Eschenko, Oxana (2018): The Locus Coeruleus Is a Complex and Differentiated Neuromodulatory System. In *Neuron* 99 (5), 1055-1068.e6. DOI: 10.1016/j.neuron.2018.07.037.

Trillo, Ludwig; Das, Devsmita; Hsieh, Wayne; Medina, Brian; Moghadam, Sarah; Lin, Bill et al. (2013): Ascending monoaminergic systems alterations in Alzheimer's disease. translating basic science into clinical care. In *Neuroscience and biobehavioral reviews* 37, pp. 1363–1379. DOI: 10.1016/j.neubiorev.2013.05.008.

Tsanov, Marian (2015): Septo-hippocampal signal processing. Breaking the code. In *Progress in brain research* 219, pp. 103–120. DOI: 10.1016/bs.pbr.2015.04.002.

Tsuda, K.; Yokoo, H.; Goldstein, M. (1989): Neuropeptide Y and galanin in norepinephrine release in hypothalamic slices. In *Hypertension* 14 (1), pp. 81–86. DOI: 10.1161/01.HYP.14.1.81.

Tye, Kay M.; Prakash, Rohit; Kim, Sung-Yon; Fenno, Lief E.; Grosenick, Logan; Zarabi, Hosniya et al. (2011): Amygdala circuitry mediating reversible and bidirectional control of anxiety. In *Nature* 471 (7338), pp. 358–362. DOI: 10.1038/nature09820.

Uematsu, Akira; Tan, Bao Zhen; Johansen, Joshua P. (2015): Projection specificity in heterogeneous locus coeruleus cell populations. Implications for learning and memory. In *Learning & memory (Cold Spring Harbor, N.Y.)* 22 (9), pp. 444–451. DOI: 10.1101/lm.037283.114.

Uematsu, Akira; Tan, Bao Zhen; Ycu, Edgar A.; Cuevas, Jessica Sulkes; Koivumaa, Jenny; Junyent, Felix et al. (2017): Modular organization of the brainstem noradrenaline system coordinates opposing learning states. In *Nature neuroscience* 20 (11), pp. 1602–1611. DOI: 10.1038/nn.4642.

Urban, Alan; Rancillac, Armelle; Martinez, Lucie; Rossier, Jean (2012): Deciphering the Neuronal Circuitry Controlling Local Blood Flow in the Cerebral Cortex with Optogenetics in PV::Cre Transgenic Mice. In *Frontiers in pharmacology* 3, p. 105. DOI: 10.3389/fphar.2012.00105.

VanderHorst, Veronique G. J. M.; Ulfhake, Brun (2006): The organization of the brainstem and spinal cord of the mouse. Relationships between monoaminergic, cholinergic, and spinal projection systems. In *Journal of Chemical Neuroanatomy* 31 (1), pp. 2–36. DOI: 10.1016/j.jchemneu.2005.08.003.

Vertes, R. P.; Kocsis, B. (1997): Brainstem-diencephalo-septohippocampal systems controlling the theta rhythm of the hippocampus. In *Neuroscience* 81 (4), pp. 893–926. DOI: 10.1016/s0306-4522(97)00239-x.

Villégier, Anne-Sophie; Drouin, Candice; Bizot, Jean-Charles; Marien, Marc; Glowinski, Jacques; Colpaërt, Francis; Tassin, Jean-Pol (2003): Stimulation of postsynaptic alpha1b- and alpha2-adrenergic receptors amplifies dopamine-mediated locomotor activity in both rats and mice. In *Synapse (New York, N.Y.)* 50 (4), pp. 277–284. DOI: 10.1002/syn.10267.

Wallenstein, G. V.; Hasselmo, M. E. (1997): GABAergic modulation of hippocampal population activity. Sequence learning, place field development, and the phase precession effect. In *Journal of neurophysiology* 78 (1), pp. 393–408. DOI: 10.1152/jn.1997.78.1.393.

Warden, Melissa R.; Selimbeyoglu, Aslihan; Mirzabekov, Julie J.; Lo, Maisie; Thompson, Kimberly R.; Kim, Sung-Yon et al. (2012): A prefrontal cortex-brainstem neuronal projection that controls response to behavioural challenge. In *Nature* 492 (7429), pp. 428–432. DOI: 10.1038/nature11617.

Weir, Keiko; Blanquie, Oriane; Kilb, Werner; Luhmann, Heiko J.; Sinning, Anne (2014): Comparison of spike parameters from optically identified GABAergic and glutamatergic neurons in sparse cortical cultures. In *Frontiers in cellular neuroscience* 8, p. 460. DOI: 10.3389/fncel.2014.00460.

Whishaw, I. Q.; Vanderwolf, C. H. (1973): Hippocampal EEG and behavior. Changes in amplitude and frequency of RSA (theta rhythm) associated with spontaneous and learned movement patterns in rats and cats. In *Behavioral biology* 8 (4), pp. 461–484. DOI: 10.1016/s0091-6773(73)80041-0.

White, S. R.; Fung, S. J.; Jackson, D. A.; Imel, K. M. (1996): Serotonin, norepinephrine and associated neuropeptides. Effects on somatic motoneuron excitability. In *Progress in brain research* 107, pp. 183–199. DOI: 10.1016/s0079-6123(08)61865-8.

White, S. R.; Neuman, R. S. (1980): Facilitation of spinal motoneurone excitability by 5-hydroxytryptamine and noradrenaline. In *Brain research* 188 (1), pp. 119–127. DOI: 10.1016/0006-8993(80)90561-2.

Wu, Zheng; Autry, Anita E.; Bergan, Joseph F.; Watabe-Uchida, Mitsuko; Dulac, Catherine G. (2014): Galanin neurons in the medial preoptic area govern parental behaviour. In *Nature* 509 (7500), pp. 325–330. DOI: 10.1038/nature13307.

Yang, Chun; Thankachan, Stephen; McCarley, Robert W.; Brown, Ritchie E. (2017): The menagerie of the basal forebrain. How many (neural) species are there, what do they look like, how do they behave and who talks to whom? In *Current opinion in neurobiology* 44, pp. 159–166. DOI: 10.1016/j.conb.2017.05.004.

Yizhar, Ofer; Fenno, Lief E.; Davidson, Thomas J.; Mogri, Murtaza; Deisseroth, Karl (2011): Optogenetics in neural systems. In *Neuron* 71, pp. 9–34. DOI: 10.1016/j.neuron.2011.06.004.

Zaborszky, Laszlo; Hoemke, L.; Mohlberg, H.; Schleicher, A.; Amunts, K.; Zilles, K. (2008): Stereotaxic probabilistic maps of the magnocellular cell groups in human basal forebrain. In *NeuroImage* 42 (3), pp. 1127–1141. DOI: 10.1016/j.neuroimage.2008.05.055.

Zaborszky, Laszlo; van den Pol, Anthony; Gyengesi, Erika (2012): The Basal Forebrain Cholinergic Projection System in Mice. In Charles Watson, George Paxinos, Luis Puelles (Eds.): The mouse nervous system. 1st ed. London, UK, Waltham, MA, USA: Elsevier/Academic Press, pp. 684–718.

Zant, Janneke C.; Kim, Tae; Prokai, Laszlo; Szarka, Szabolcs; McNally, James; McKenna, James T. et al. (2016): Cholinergic Neurons in the Basal Forebrain Promote Wakefulness by Actions on Neighboring Non-Cholinergic Neurons. An Opto-Dialysis Study. In *The Journal of neuroscience : the official journal of the Society for Neuroscience* 36 (6), pp. 2057–2067. DOI: 10.1523/JNEUROSCI.3318-15.2016.

Zimprich, Annemarie; Garrett, Lillian; Deussing, Jan M.; Wotjak, Carsten T.; Fuchs, Helmut; Gailus-Durner, Valerie et al. (2014): A robust and reliable non-invasive test for stress responsivity in mice. In *Frontiers in behavioral neuroscience* 8, p. 125. DOI: 10.3389/fnbeh.2014.00125.

Zoli, M.; Torri, C.; Ferrari, R.; Jansson, A.; Zini, I.; Fuxe, Kjell; Agnati, L. F. (1998): The emergence of the volume transmission concept. In *Brain research. Brain research reviews* 26 (2-3), pp. 136–147.